Design and Analysis of MEMS Based Electrothermal Mirrors Using Single Material Micro Actuator

Author

Waiqa Amir

00000275640

Co-Supervisor

Dr. Muhammad Mubasher Saleem

Supervisor

Dr. Amir Hamza

DEPARTMENT OF MECHATRONICS ENGINEERING

COLLEGE OF ELECTRICAL & MECHANICAL ENGINEERING NATIONAL UNIVERSITY OF SCIENCES AND TECHNOLOGY

ISLAMABAD

AUGUST 2022

Design and Analysis of MEMS Based Electrothermal Mirrors Using Single Material Micro Actuator

Author
WAIQA AMIR
00000275640

A thesis submitted in partial fulfillment of the requirements for the degree of
MS Mechatronics Engineering

Thesis Supervisor:
DR. AMIR HAMZA

Thesis Supervisor's Signature:

_____

DEPARTMENT OF MECHATRONICS ENGINEERING
COLLEGE OF ELECTRICAL & MECHANICAL ENGINEERING
NATIONAL UNIVERSITY OF SCIENCES AND TECHNOLOGY,
ISLAMABAD
AUGUST 2022

Declaration

I here claim that the research work title "*Design and Analysis of MEMS based Electrothermal Micromirror using single material micro actuators"* is result of my own research. This research work has not submitted in any institution or in any other university for consideration. I have properly mentioned the citations and references that has been used from other's people work and sources.

Signature of Student

Waiqa Amir

00000275640

_____

Signature of Supervisor

Language Correctness Certificate

This thesis has been read by an English expert and is free of typing, syntax, semantic, grammatical, and spelling mistakes. Thesis is also according to the format given by the university.

Signature of Student
Waiqa Amir
00000275640.

Signature of Supervisor
Dr. Amir Hamza

Copyright Statement

Acknowledgements

First and foremost, all the glories and gratitude to ALLAH almighty who shower his blessings on me in completing the requirements of my research and degree as well.

I would also like to pay me regards and gratitude to my supervisor Dr. Amir Hamza head of mechatronics department and my co-supervisor Dr. Muhammad Mubasher Saleem who believed in me and allow me to conduct my thesis. His constant support, technical skills and exceptional knowledge helped me a lot in different levels throughout this journey. He taught me the key principals of research and show me how to present research points as clearly as possible. Learning from both of my supervisors was source of honor and privilege. I would like to pay regards to my committee members as well for their support, suggestions, and feedback.

At the end, special thanks to my parents who invested their time and money in my studies. Their support and motivation play a vital role through this journey. They deserve special gratitude for their prayers and concerns. A special thanks to my husband who is my course mate as well. His guidance and technical knowledge helped me a lot in solving many technical issues during research. His constant check and commitment helped me a lot in completing my work. My heartful gratitude goes to my siblings for theirs support and prayers.

This work is dedicated to my adored parents and beloved husband who always inspired me to do this great accomplishment

Abstract

This work presents the movement of MEMS micromirrors using electrothermal actuation principal. MEMS mirrors specifically micromirrors having thermal actuation have been used in many applications of biomedical for advancing Optical Coherence Tomography. Micromirrors have been designed based on difference in actuation principal techniques like electrostatic, piezo-resistive, and electromagnetic. Those designed based on electrostatic, piezo-resistive, and electromagnetic techniques uses capacitive, resistive, electromagnetic, and electrostatic principles. That's why they have less scope in biomedical applications.

In my thesis work, design of MEMEs electrothermal in plane micro actuator is analyzed for maximμm output results. Target of maximμm displacement and minimμm temperature on plate is achieved by designing different geometries which can be fabricated using SOI MMMPs fabrication process. Analysis and optimization are carried out for electrothermal actuators using ANSYS AIM and DOE process technique. FEM analysis is carried out on the design to measure the performance characteristics of output displacement and plate temperature at simulation level to ensure required and efficient working. Device performance in the presence of temperature is analyzed in detail and hence all the parameters are varied using DOE techniques. Static Experiments have been performed in Minitab software to calculate the input parameters effect on output. This DOE involves placket-Burman analysis, full factorial analysis and regression analysis. The mirror can generate 0.7μm deflection at minimμm voltage of 3.6V. The minimμm temperature at input voltage of 3.6v is 42 ℃ with an input power of 140 mW. Tilt angle of micromirror comes out to be 0.8° at 3.6 V. The simulations are done in ANSYS software.

Key Words: *MEMS, Micromirror, Electrothermal, FEM (Finite element analysis, Full factorial analysis, Regression Analysis, Placket-Burman, Design of Experiments (DOE), ANSYS AIM, Minitab.*

Table of Contents

List of Figures

List of Tables

Acronyms

MEMS	Microelectromechanical Systems
ETA	Electro Thermal Actuator
FEM	Finite Element Method
DOE	Design of Experiments
NIR	Near Infrared Light
MMMPs	Multiuser MEMS

Chapter 1: Introduction

1.1 Introduction to MEMS?

Abbreviation of MEMS is microelectron mechanical systems. The term MEMS were first used in 1987. In Europe and Japan term MEMS is also called microsystems or micromachines. Microelectromechanical systems deal with microscopic mechanical systems and components and their study with electrical circuitry integration. Basic purpose of MEMS is to achieve required functionality in low cost, compact size, and low power consumption of available microscopic level mechanical systems and components integrated with electrical systems The devices that ranges from micrometres to millimetres has been fabricated using different fabrication techniques. The important task that can be tested using this technology are sensing, actuation and control. All devices that range in between 10^6μm are included in MEMS devices. MEMS. Figure 1.1 shows that MEMS technology lies in between nanotechnology and mesoscale technology. Mesoscale devices are visible to human eye but are small. While nano technology is three times smaller than MEMS devices. MEMS provide low power consumption mechanical structures with more sensitivity.

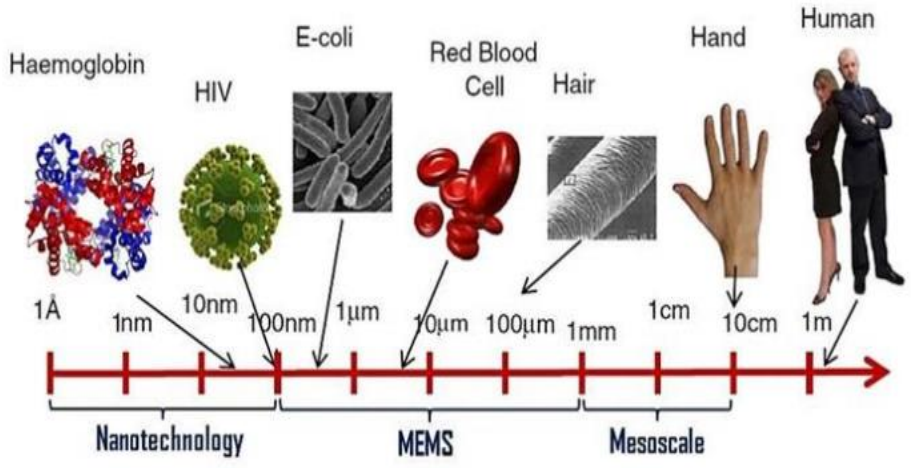

Figure 1.1: Comparison of MEMS devices with nan and mesoscale devices.

In nutshell MEMS technology converts the large-scale mechanical systems into micro level with same sensitivity and other output factors along with integration of electrical circuitry.

1.2 Applications of MEMS

As MEMS devices have compact size with low power consumption benefits, they have vast scope in many fields. Multiple applications of MEMS devices are listed in table mentioned below.

Table 1.1: Application Area of MEMS

Sr. No.	Application Area	Usage
1	Biomedical	MEMS actuators used in medical tools, micromirrors [1] and micro-optics, and detection of glucose in body [2].
2	Market electronics	Projection screen, microphones, pressure sensors, inkjet printer headphones [3].
3	Security	Vibration monitoring, energy harvesting equipment's for army and embedded sensors.
4	Automobile	Temperature and pressure sensors, vehicles tire pressure monitoring [5], measurement of angular and linear position [4].
5	Industrial	Vibration monitoring, detection of earthquake [6].

It can be observed that MEMS devices have been used in almost every field by replacing macro scale devices. MEMS are becoming alternative solution to large scale macro scale devices. Accelerometers, gyroscopes, microgrippers and pressure sensors are the MEMS devices that are in common use.

1.3 Advantages of MEMS

Multiple advantages of MEMS technology are summarised as follows

- MEMS sensors have high sensibility.
- Integration in systems is easy.
- Phenomena of sensing and actuation can be performed at same time.

- Power consumption is very low for operations having high voltages.
- MEMS devices take small space area. It means they are compact in size.
- MEMS devices can be easily integrated with microelectronics systems to obtain micro scale embedded mechatronics systems.
- MEMS switches and actuators have very high frequency attaining properties.
- Scalable in manufacturing with low production cost.

1.4 MEMS Micromirrors

Micromirrors are the optical devices which reflect light over a range of angles within micrometres size range. Reflection angle of micromirror is responsible for rotation of mirror. His reflection angle can be controlled by an actuation principal either statically or dynamically. The actuation mechanism use for micromirror actuation shows multiple diverse response in relation of maximum output displacement, power consumption, size of device, requirement of voltage and fabrication issues as well. Application of micromirrors have number of limitations depending on the actuation technique and application performance. Micromirrors are used in medical applications specially in imaging applications like endoscopic imaging and optical coherence tomography. Beside these mirrors are also used in optical imaging, switching, scanning and microscopic tonometry. Our aim is to design a mirror fulfilling the application limitations of optical coherence tomography.

1.5 Optical Coherence Tomography

Optical coherence tomography is a vivo imaging procedure with high resolution at a range of micrometres. This technique is non-invasive with real time analysis providing high resolution at same time. Key feature of optical coherence tomography is its spatial resolution along with non-invasive technique. It works on basic principle of measuring interaction of reflected light from target area with reference beam. Simple interference principal is used in this application [14].

Function of OCT is in between two arms having two beams of light. Beam splitter is used for splitting one beam into two. The beam passing through the patient arm travels towards the target and other beam moves towards the reference arm for

reaching towards the reference mirror. After reflecting from moveable reference mirror, it moves back towards the beam splitter. Light reflected from target rea is then interacted with the light refracted from reference mirror. Production of interference fringes occurs. Electronic processing and interpretation of these signals are done to find the reflectivity values of target. The value of target is measured as function of depth into body tissues. Changes in the path length of reference mirror causes sweep to the scanning depth. Near infrared light is used in optical coherent tomography because

- It is more coherent
- Focused
- Incoherent temporally to carry various wavelengths.

Detail schematic view of optical coherent tomography is shown in figure 1.2.

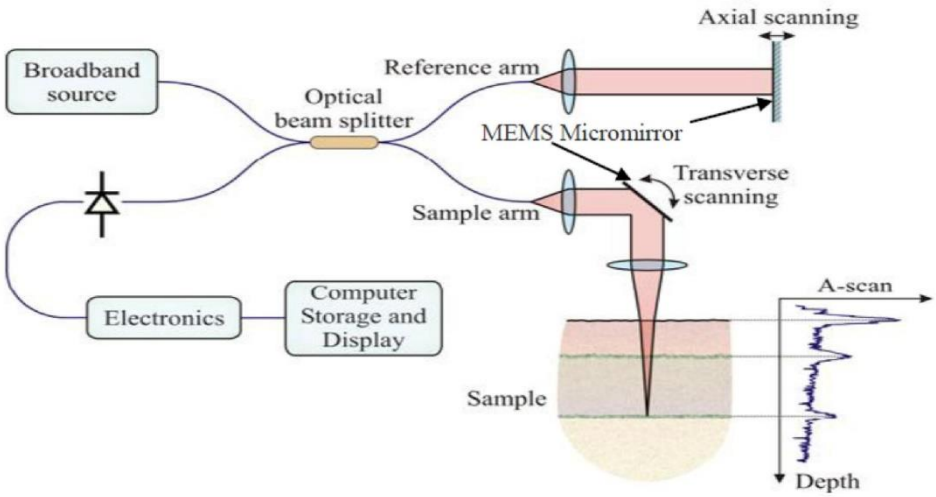

Figure 1.2: Schematic view of Optical Coherence Tomography [14]

Depth of OCT resolution is 0.01mm. Now, the target in this area is to reduce the size of OCT with maximum deflection angle for imaging. In previous work done in MEMS micromirrors, suitable reference mirror is developed which rotate light to scan target tissues of body.

Optimization of MEMS micromirror device is carried out using DOE (design of experiments technique). Our device design is limited to certain input and output parameters. This has been achieved using mathematical model, FEM analysis and measuring both the results to get accuracy. This technique gives accurate results but,

in our case, geometry of micromirror is very complex. In modelling this design many assumptions need to be taken which may results in false results. That's why DOE based optimization is done to optimize the maximum displacement output, input power and minimum temperature at the pate of mirror.

1.6 MEMS Actuators

MEMS actuators are used for actuation of different mechanisms. There are five types of MEMS actuators having different advantages according to output requirements of device. Each actuator has some advantages and some disadvantages. The five actuators used in MEMS are listed below

- Electrothermal Actuators
- Electrostatic Actuators
- Electromagnetic Actuators
- Electrothermal Actuators
- Shape Memory Alloys

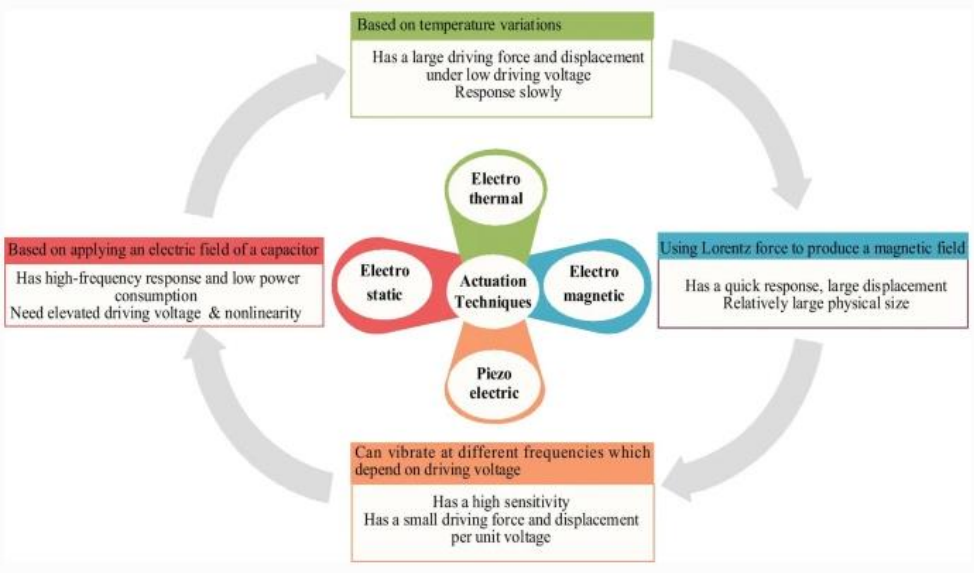

Figure 1.3: Type of MEMS actuation [15].

Electrostatic actuators have fast response, high speed scanning and have low power consumption. Best feature of electrostatic actuator is its low power consμmption. Electrostatic actuation micromirrors contains two types to actuation principal. One is comb drive and other one is parallel plate actuation [7]. Parallel

plate micromirror actuator can be fabricated easily using simple fabrication process but it requires high driving voltage.

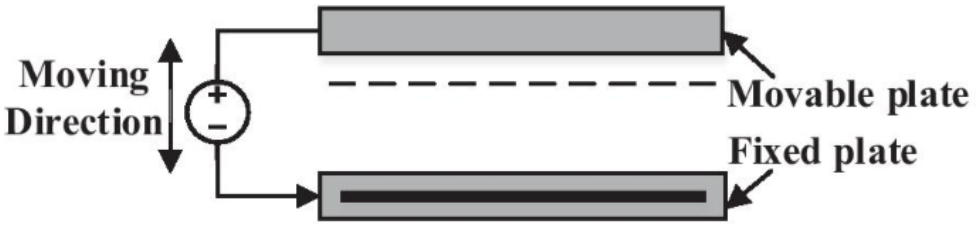

Figure 1.4: Parallel plate actuator [8,9].

This actuator is not recommended due to pull in effect or stiction phenomena. Comb drive actuators operate on low voltage, but they have large operating area which limits its applications in micro mirrors [8,9].

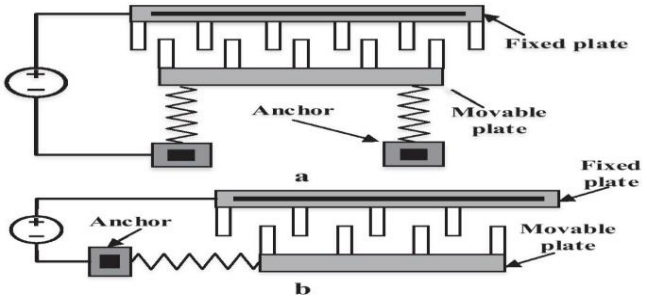

Figure 1.5: Schematic of working of Comb drive actuator [8,9].

Piezoelectric actuators-based mirrors have high response, but their fabrication is a key challenge. They also have large area which limits its applications in MEMS [10,11].

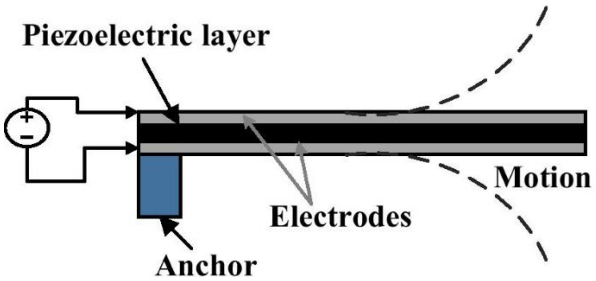

Figure 1.6: Schematic of working of piezoelectric actuator [10,11].

Electromagnetic actuation has low voltage operation but high-power consumption. This action needs an external permanent magnet source for input. External input source makes it performance limited [12]. Electrothermal actuator has large output displacement at low input voltage which makes these actuators valuable

in biomedical applications. Electrothermal actuators expansion depends more on resistivity of material rather than thickness of geometry. High power consumption is a drawback of thermal actuators. Large thermal stress cycles may become a limitation of these actuators. In this work thermal actuation principal is used for micro mirror actuation. There are three types of thermal actuators named as hot and cold arm, bimorph [13], and Chevron (also called as V shape).

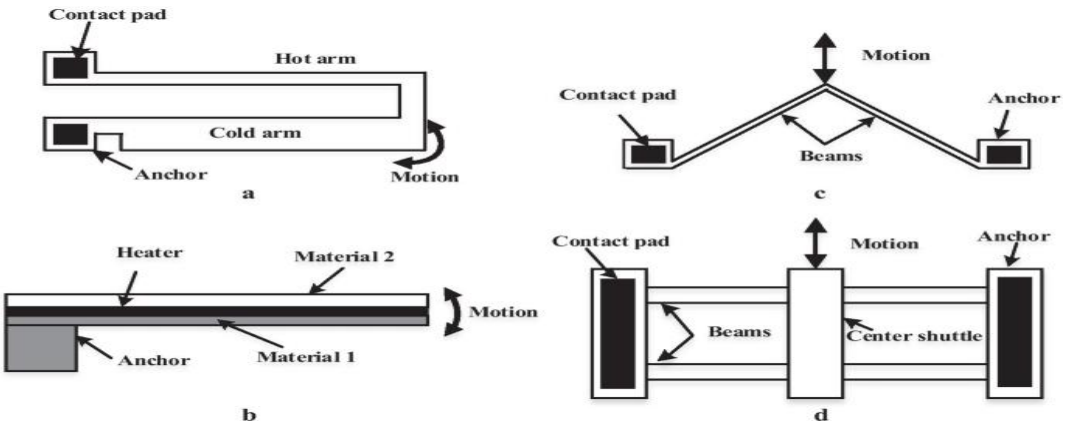

Figure 1.7: Types of thermal actuators [16,17].

1.7 Literature Review

Endoscopic imaging made the non-invasive technique applicable. In early times imaging techniques uses large mechanisms with external motors for movement of reference arm. These external motors limit the speed of scanning. MEMS provide vital solution to these problems by translating mechanical structures at micro levels. Micromirrors plays an important role in OCT probes by providing large deflection range. There are 5 actuators used for actuation principal in micromirrors. Every actuator has its own use along with its drawbacks.

Lorentz forces are used in electromagnetic micromirrors for actuation of mirror. Lorentz forces are achieved by fabrication of coil under mirror surface along with external magnet attached together for generating magnetic field. When current is applied around the coil, magnetic field is induced which force the mirror to move. Position of coil can be replaced by position of external magnet. The force generation will remain the same. Motion of electromagnetic micromirrors can be controlled by controlling the current magnitude [18,20]. Electromagnetic actuators are used in domains where we need more angular displacements usually greater than greater than

15°. Large angular displacement is achieved by applying high currents greater than 100 milli ampere (mA). For applying large currents large chip area is needed which makes these actuators unsuitable for biomedical applications.

An electromagnetic micromirror with 2 degree of freedom is reported in paper [21]. Dimension of electromagnetic micromirror is 3.5mm x 3.5mm. This design can achieve deflection angle of 1.5 al 20-mA current. This actuator can be actuated by attaching an external magnet to the design or by electroplating copper wire. Yalcin kaya et al. presents electromagnetic micromirror whose size is 1.5 mm x 1.5 mm with an optical scan of 60° [21]. A schematic diagram of electromagnetic micromirror is presented in figure below.

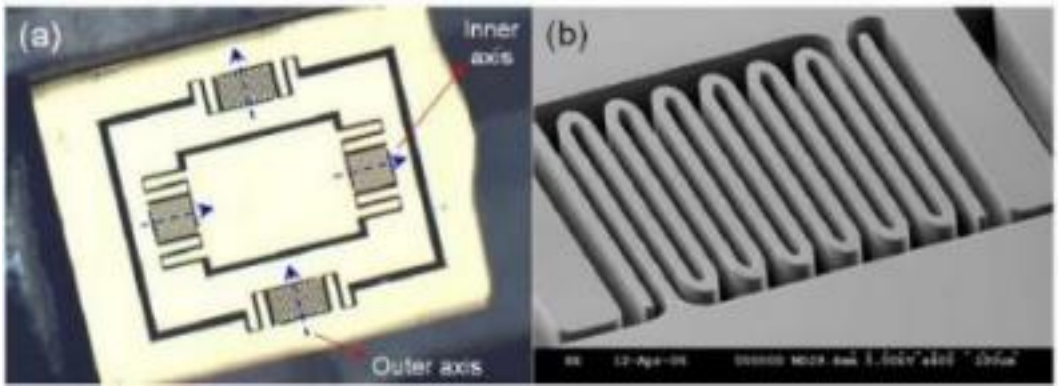

Figure 1.8: Schematic diagram of Electromagnetic actuator [21].

Chuan-Hui Ou et al. [24]. in his paper explains the structure that consists of one pair of outer metallic glass torsion bars connecting the fixed substrate and rotational frame is used for the slow axis scanning. Another pair of inner MG torsion bars connecting the rotational frame and mirror is used for the fast axis scanning which enhance the mechanical strength and changing the stiffness of the micro mirror torsion bar. An electromagnetic actuation solenoid is placed underneath the micro mirror. The diagonally polarized Fe based MG can be actuated in two directions, fast axis, and slow axis, at the same time. An electromagnetic actuation solenoid underneath the micro mirror was used to provide an external actuation magnetic field. The actuation magnetic field is a frequency-dependent magnetic flux and is a composite of two different frequencies to excite the MEMS Fe-based MG micro mirror in dual resonant mode scanning [24].

Fangrong Hua et al. [25] in his paper describes that conventional electrostatically attractive micro-mirror are based on a structure of two parallel plates and a micro mirror placed on actuator plate. The surface of the micro-mirror is supported by a post which is in the center of the actuator plate. L-shaped spring connects the actuator plate to the anchors on each corner of the micro-mirror, the three fixed bottom electrodes are on the substrate. When a voltage of V is applied to the L-shaped spring and the fixed middle bottom electrode which is right below the top while other two bottom electrodes are grounded, symmetrical electric field is produced, and for this reason, the intensity of the electric field on the top surface of the L-shaped spring is larger than that of the corresponding point on the bottom surface.

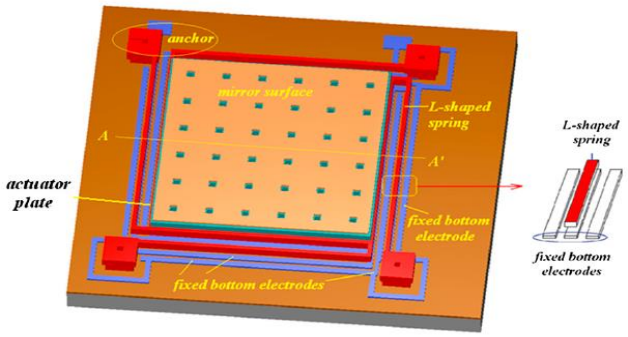

Figure 1.9: Schematic of parallel plate electrostatic actuator [25].

Consequently, the electrostatic force produced on the top surface of the spring is larger than that of the bottom surface. MEMS micro mirror which is driven by electrostatic force. The micro-mirror not only achieves a large stroke at relatively low voltage by eliminating the pull-in effect completely, but also has a higher fill factor of above sixty-five percent through replacing the strait flexure with an L-shaped spring on each side of the micro-mirror [25].

Electrostatic actuators provide low displacement at applied voltages. Electrostatic actuators are divided into two types. One is comb drive and other one is parallel plate actuator. In parallel plate actuator displacement is limited to 1/3 of the output. Stiction phenomena makes it unsuitable for biomedical applications. In comb drive actuation electric combs are attach parallel to each other. They have large displacement on low voltage but have large area. Due to its large size comb drive is not suitable for biomedical applications. Wei Zhang et al. [22] represents in his paper

a unique design of electrothermal actuator with shared movable combs attach with springs. Both horizontal and vertical comb drives are present in this design. The detail view of this design is presented in figure 1.9. SOI based MMMPs fabrication process is used for actuators fabrication along with Gan layer embedded in actuators. When voltage is applied to the actuators through substrate an electrostatic force is generated. This force moves the micro mirror by actuating actuators. Linear relation was found in between input of square voltage and output displacement. Voltage of 300 V produces displacement of ± 17.97 μm and 5.98 μm in vertical and horizontal direction [22].

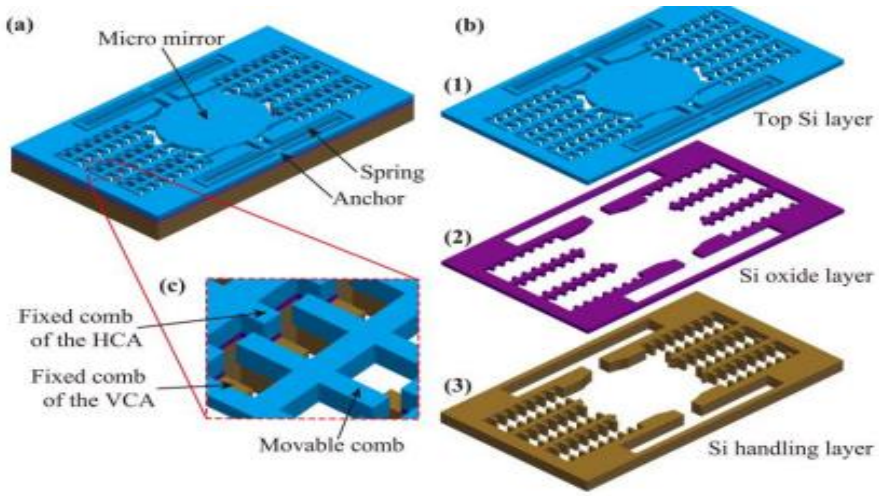

Figure 1.10: (a) schematic structure of electrostatic actuator: (b) layer structure of electrostatic actuator: (c) movable comb drive [22].

Yanjun Fan et al. [23] in his paper represents new design of comb drive actuator. Two structural layers are designed for vertical comb drive one for rotary fingers and the other one for stator fingers. Fabrication is done through one mask lithography. New assembly is deigned to achieve high displacement at low voltage. Mesa wager is stack up with mirror wafer to assembled in vertically comb drive mirror. This design can achieve scan angel of +/- 10.8° with a 95 V sinusoidal signal [23].

JIAN SHAO et al. [26] presents a design that consists of central square mirror plate with 200 μm side length suspended by two L-shaped cantilever beams with one end of each connecting to its two opposite corners. The other ends of these cantilever

beams are connected to the substrate, acting as fixed anchor points. All the structures consist of a silicon layer with 5 μm thickness, onto which a stack layer involving 200 nm Mo (bottom electrode) and 1 μm AlN (piezoelectric layer) is deposited. An additional 200 nm Mo layer is selectively deposited onto the beam regions as the top electrode.

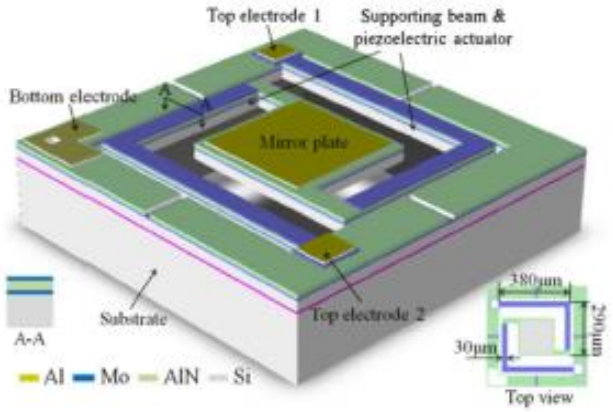

Figure 1.11: Schematic of piezoelectric based actuator [26].

When a voltage is applied between the top and bottom electrodes, the induced stress in the piezoelectric layer will be eventually translated into the out-of-plane deflection of the cantilever beam, thus actuating the mirror movement. If the same voltages are applied onto the two piezoelectric actuators, the micro-mirror plate can be actuated to move with piston type. In comparison, when opposite voltages are applied onto individual actuators, mirror tilt along the diagonal direction can be achieved [26].

Bimorph actuators consists of two material layers which produce expansion due to difference in coefficient of thermal expansion. Multiple structures have been presented in literature for bimorph thermal actuators. Drawback of these actuators is they produce stress during fabrication and misalignment of layers may occur during actuation. Yang et al. mentioned in his paper a tracking positioner with great precision [30]. This tracker is made of doped silicon material. Bimorph actuators are used in this paper. Bimorph with double layer material is presented in Ataka et al. [29] for micro motion vehicles. When voltage is applied across bimorph actuators it increases the temperature of bimorph layers. Increase in temperature id different in different layers because of difference in potential difference. Layer having high CTE value will bend towards the layer having low CTE. Following table represents the

literature review of some bimorph actuators with their displacement, fabrication process, scan angle and structure details.

Table 1.2: Literature review of bimorph actuator

Author	Fabrication Process	Material	Displacement (Vertical / Piston)	Structure	Angle
Lin Liu (2012) [29]	Combination of surface and bulk micromachining	Al/W (Aluminum / Tungsten)	227μm	Curved Concentric Bimorph	11° at 0.6V
Dingkang Wang (2019) [30]	Plasma Enhanced Chemical Vapor Deposition	W/SiO2	Nil	ISC (Invert Series connected) Curling Bimorph	8° at 4.5V
Miguel Lara-Castro (2017) [30]	Sandia Ultra-planar Multi-level MEMS Technology V (SMMMiT V®)	Polysilicon	10.3μm	Two Beam Types (Narrow and wide beams)	Nil
Quentin A. A. Tanguy (2017) [30]	Plasma Enhanced Chemical Vapor Deposition	Al/SiO2	Nil	MISC (Meshed inverted Series connected) Curling Bimorph	22° at 16.5 V

V Merea's et al. [27] paper micro mirror consists of three major components actuator, spring, and mirror plate. The typical mirror is a circular disk of diameter 140 μm, which consists of a thin reflecting material (Al) of 0.9 μm thick and a base plate (Si) of 2 μm thickness. For actuators, Al-Si bimorph are used in the design. The dimensions of the actuator are 64 μm width, 3.1 μm in thickness and 400 μm in length. The actuators generate force and displacement that is translated to the mirror via springs; ultimately resulting into tilting of the mirror plate. The springs also give mechanical cushioning, as well as provide thermal isolation between the actuators and the mirror plate. Thermal based actuation has some limitations that include high

power consumption, low actuation, and material degradation due to large thermal stress cycles. Doesn't operate above 200 because mechanical properties of Al [27].

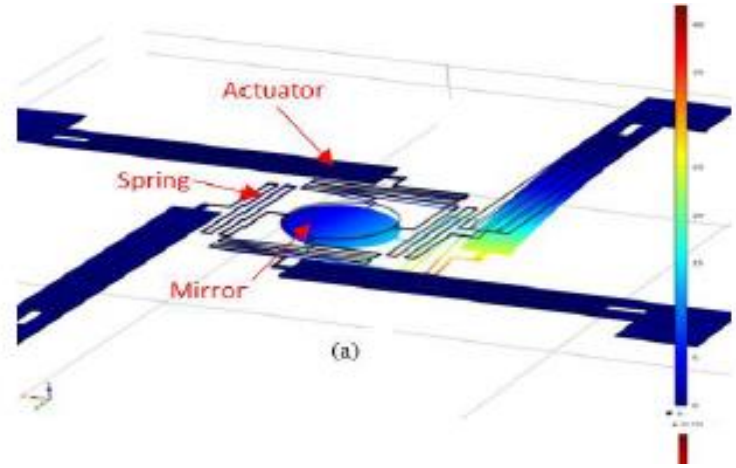

Figure 1.12: Schematic diagram of thermal actuator micromirror [27].

Electrothermal actuators are easy to fabricate as compared to all other mentioned actuators. These actuators can use multiple fabrication materials for fabrication. Just like electrostatic and electromagnetic, electrothermal actuators do not require high voltage and currents for actuation. It should be kept in mind that high temperature should not affect the output plate.

Thermal actuators use principal of thermal expansion for actuation. Hot and cold arm actuators use single material and generates thermal expansion due to difference in geometry shape. Unlike bimorph actuators the hot and cold arm actuators are of same material that can give out of plane displacement. This actuator can overcome the issues comes in bimorph actuators like shear stress, reduced lifetime, and delamination in multiple layers. The out of plane displacement actuator is proposed in [28] with four actuators attach with micromirror at one end and free side on another end. Such micromirrors can be fabricated using single material deposition. Different resistance due to different cross section area of actuator produces different expansion. There is more expansion in hot arm due to less area and high resistivity. Therefore, bending or movement is towards cold arm.

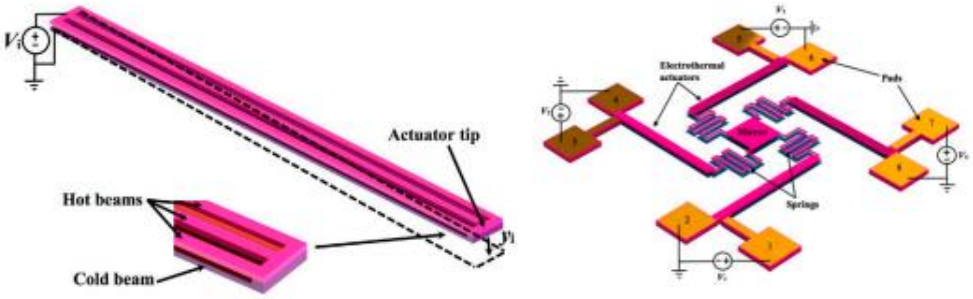

Figure 1.13: Out of plane hot and cold arm actuators [28].

A comparison of multiple thermal actuators is presented in table 3.1. It is clear from this table that versatile work has been done in bimorph actuators. There is less margin in bimorph micromirror actuators. That's why we choose hot and cold arm electrothermal actuators for actuation of micromirrors.

Table 1.3: Comparison of Electrothermal actuators

Actuator	Material	Displacement (µm)	Voltage V	Year
Hot and cold arm	Si	6-7	5	2003
Hot and cold arm	Poly Si	10.3	2.5	2017
Chevron	Si	6-7	4	2010
Bimorph	Cu, W, SiO_2	169	2.3	2015
Bimorph	SiO_2, Pt, Al	621	5.8	2010

1.8 Process of Microfabrication

Multiple fabrication processes are available in market which helps in production of MEMS devices. Different process uses different material based on user's requirement. Type of devices, size of device, cost ratio, and material are the key points on which fabrication process differ.

1.8.1 Metal MUMPs Process

In Metal MUMPs fabrication process electroplating material is used for device fabrication. As In SOIMUMPssilicon is used for whole material fabrication, in this process nickel is used for whole design fabrication. Nickel has high co-efficient of thermal conductivity which results in high temperature. This high temperature may affect the output of device which is not feasible for bio-medical applications.

1.8.2 Poly MUMPs Process

Poly MUMPs is abbreviated as polysilicon multiuser MEMS process. Metal MUMPs is a micromachining process which is used for fabrication of sensors. Eight masks are used for formation of seven layers. Minimum thickness for this fabrication process is 2 μm. Only few MEMS devices have been fabricated through this fabrication process. All the design is fabricated in Polysilicon material. It has high thermal co-efficient but low thermal expansion. It consumes high power that's why it is not useful in biomedical applications.

1.8.3 SOIMUMPs Process

SOIMUMPs is abbreviated as silicon on insulator multi-user MEMS process. It is most used fabrication technique. This technique is commercially common and costs low. As silicon has low thermal expansion and high strength, that's why low displacement is achieved at very high temperatures. The resistivity of silicon can be increased by doing process of n-type and p-type. We use SOIMUMPs fabrication process for fabrication of our device because of it low cost and commercial availability. Silicon used in our case is p-type doped so that resistivity of silicon can be increased.

1.8.4 Limitations of SOIMUMPs

There are multiple limitations of SOIMUMPs process. A list of them is mentioned below

- Thickness Limitation

- Thickness of structures can be 25 μm
- Thickness of structures can be 10 μm

- Width of actuators arm should be greater than 6μm

If width is less than 6μm than it may release from substrate due to undercutting of oxide layer.

If it is necessary to keep width of actuator less than 6μm then in that case maximum Length should be

- 100 μm if the structure is anchored at one end.
- 500 μm if the structure is anchored at two ends.

Chapter 2: Design of Actuators and Micromirror

Designing of Micromirrors is not an easy task as it were on large scale. While designing the mirrors all the fabrication constraints are kept in mind. In our case fabrication limits are micromirrors thickness as well as actuators width. We cannot move beyond 6μm width of actuators and 25 μm thickness of micromirror. As we choose SOIMUMPs process for fabrication so material of actuator and micromirror is silicon. As silicon is an insulator therefore, we use doped silicon for fabrication. We choose SOIMUMPs fabrication process because of it low cost and commercialization.

2.1 Electrothermal Actuators

Electrothermal actuator works on principal of thermal expansion on applied voltage. By applying voltage an increase in temperature causes the material to expand. “Materials expand on heating and shrink on cooling” electrothermal actuators uses this principal. The change in temperature causes to expand the material. We use hot and cold arm actuator in our design. Hot and cold arm expands due to asymmetric heating in actuators arm.

Thermal actuators are divided into two major types. The division of these actuators is based on difference in structure layers and principal of actuation. We use hot and cold arm for actuation. Deflection in hot and cold arm is generated by asymmetric heating. When voltage is applied on actuators end, current passes through anchors and through other terminals. Current density is high in narrow hot arm beam due to which hot arm bends more than cold arm. Silicon based actuators expands as temperature rises.

2.1.1 Design of Flexure

Cold arm movement is due to flexure arm. If the flexure is absent in ETA design than cold arm would be become so stiff for bending. If we increase the temperature difference in between two arms, it will increase the thermal efficiency of ETA actuator. The width of flexure arm should remain thin. The thinner the arm of flexure, the better its deflection performance will be. Thinner flexure will convert

more force generated by hot arm of actuator into deflection of tip. The flexure arms should not be more thin than hot arm of actuator. If they are more thin than hot arm it may heat up more as compared to hot arm of actuator and it will destroy by excessive heat. Length of flexure arm should be sufficiently long enough so that thin arm can bend it elastically. If the length of flexure arm is more than thin arm than it may expand more than thin arm cause issues in desired actuator movement.

2.1.2 Thermal Expansion

Silicon uses joule heating effect for movement and expansion of actuators. Silicon expands as voltages applied. Micromirror deflects due to asymmetric heating of hot and cold arm. As both the arms of actuator are made of same material, the narrow arm has higher electrical resistance as compared to wider arm. When voltage is applies across both ends of actuator, current passes through both arms. Hot arm has high temperature due to its narrow shape. Hot arm in return will expand more than cold arm. The difference of expansion in both arm causes movement of actuators towards cold arm.

Thermal expansion formula is

$$\alpha_L = \frac{1}{L}\frac{dL}{dT} \tag{2.1}$$

Where α_L is thermal expansion, L is the length of object, dL is the change in length and dT is change in temperature.

2.1.3 Ohmic Heating

The power loss in actuation mechanism is also called as ohmic heating. Power loss can be described as

$$P = VI = I^2R \tag{2.2}$$

Where v is the voltage, I represent current, and R is the resistance of geometry. Cross section of geometry having small cross-sectional area will have higher electrical resistance. The difference in different cross sectional area experiences different expansion for multiple parts having same material. When same input of current is applied on small portion area having high electrical resistance, more increase in temperature occurs that will expand. The reason behind its expansion is ohmic

heating. Difference in electric potential applied at substrate anchor points create non uniform electric field. Materials resistivity and current density gives rise to joule heating.

2.1.4 Temperature Distribution

In electrothermal analysis temperature distribution is calculated on entire design including micromirrors and actuators. As the length of actuators is much larger as compared to its cross-section area therefore the geometry can be decomposed into three lines microbeams connected in series with each other. Resistivity of silicon in terms of temperature is given as

$$\rho\,(T) = \rho 0\,[1 + \xi\,(T - Ts)] \tag{2.3}$$

where T is operating temperature of actuators and Ts is the temperature of substrate. We calculate total heat by analyzing the flow of heat in geometry. It is observed that in steady state heat generated in an object is equal to heat dissipation in that object [36].

$$-k_s wh + J^2\,\rho\,whx = -k_s wh\,[\frac{dT}{dx}]_x + Sxw\,\frac{T - Ts}{RT} \tag{2.4}$$

where Ks is the thermal conductivity of silicon and S is the shape factor. J denotes current density and R is the resistance. R is the thermal resistance between silicon structural layer and substrate. Resistance is calculated as

$$R_T = \frac{ta}{Ka} + \frac{ts}{Ks} \tag{2.5}$$

Where ka and ta represents the thickness and thermal coefficient of air. Ts and k_s represents the silicon structural layers thickness and thermal conductivity. Shape factor of geometry is defined as [35]

$$S = \frac{S}{w}\,(\frac{2tv}{h} + 1) + 1 \tag{2.6}$$

Taking limit equal to zero the (2) equation becomes

$$k_s\,[\frac{d2T}{d2x}]\; + J^2\,\rho = \frac{S}{h}\,\frac{T - Ts}{RT} \tag{2.7}$$

By putting equation 4 in equation 5 and solving it by changing it variables temperature distribution on overall geometry is defined by following equations

$$T_h(x) = T_H + c_1\,e^{m_h x} + c_2\,e^{-m_h x} \tag{2.8}$$

$$T_c(x) = T_C + c_3\,e^{m_c x} + c_4\,e^{-m_c x} \tag{2.9}$$

$$T_f(x) = T_F + c_5\,e^{m_f x} + c_6\,e^{-m_f x} \tag{2.10}$$

2.2 Design of Actuator

In this portion detail summary of proposed electrothermal actuator design is given. The material of structure is silicon, and a 2-μm gold structural layer is deposited on micromirror. The actuator has 3 arms. Multiple designs are proposed for actuator on hit and trail basis. Each actuator design has 3 arms. All three arms in all designs are connected by a connector. Some proposed design has two hot and one cold arm, other one has two cold and on hot arm. All the cold arms have flexures which helps in movement of hot arm towards cold arm. All the designs along with their dimensions are discussed below.

2.2.1 Material Selection for ETA

In MEMS technology multiple factors need to be kept in mind while selecting material for any design. In bimorph electrothermal actuators two materials are used having high coefficient of thermal expansion. These two material layers are glued together which causes expansion on heating. The in-plane movement of bimorph actuators causes out of plane deflection. Residual stress during fabrication is major drawback of these actuators. Therefore, we use single material for avoiding these residual stresses during fabrication.

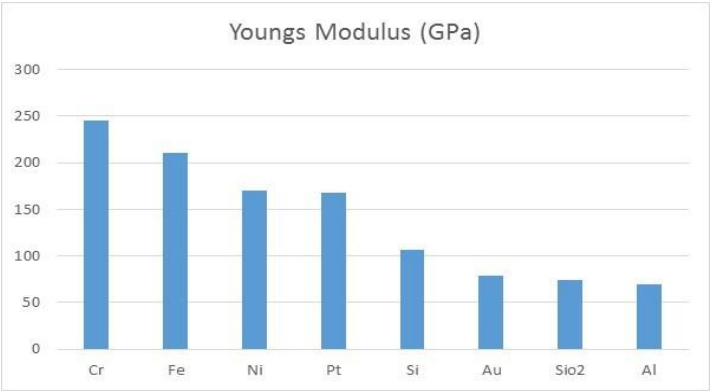

Figure 2.1: Young's Modulus comparison of materials commonly used in MEMS.

The important factors which need to be considered while selecting material is cost consumption, thermal time constant for dynamic analysis, displacement amplitude in static structural analysis, range of temperature ad fabrication limitations. Electrical properties like heat dissipation, conductivity, resistivity also

effects thermal properties. It will in return effects the power consumption of device. There is a trade off in coeffect of thermal expansion and thermal conductivity. Therefore, we will deposit 2-μm gold layer on micromirror along with silicon to make it a suitable pair.

Since silicon is a non-conductor material therefore it is doped with either p type on n type to make it a conductor.

Table 3: Material Properties Comparison

Material Properties	Silicon	Gold
Young's Modulus (Giga Pa)	1.69	70
Poison Ratio	0.27	0.35
Density (kgm^{-3})	2340	19320
Coefficient of Thermal Conductivity	150	300
Coefficient of Thermal Expansion (C^{-1})	4.1852×10^{-6}	14.2×10^{-6}
Isotropic Resistivity (ohm m)	0.00042	—

2.2.2 ETA Design No 1

In this design two cold arms are proposed with one cold arm. This geometry consists of three arms which connected with each other with the help of connectors. Flexures are attached with cold arms. This geometry is replication of previous student design. All the dimensions of this actuators are illustrated in table below

Table 2.1: Dimensions of ETA Design 1

Geometry	**Dimensions (μm)**
Length of Outer Cold Arm	280
Length of Hot Arm	260
Length of Inner Cold Arm	180
Width of Cold Arm	14
Length of Flexure	40
Width of Flexure	6
Width of Hot Arm	6

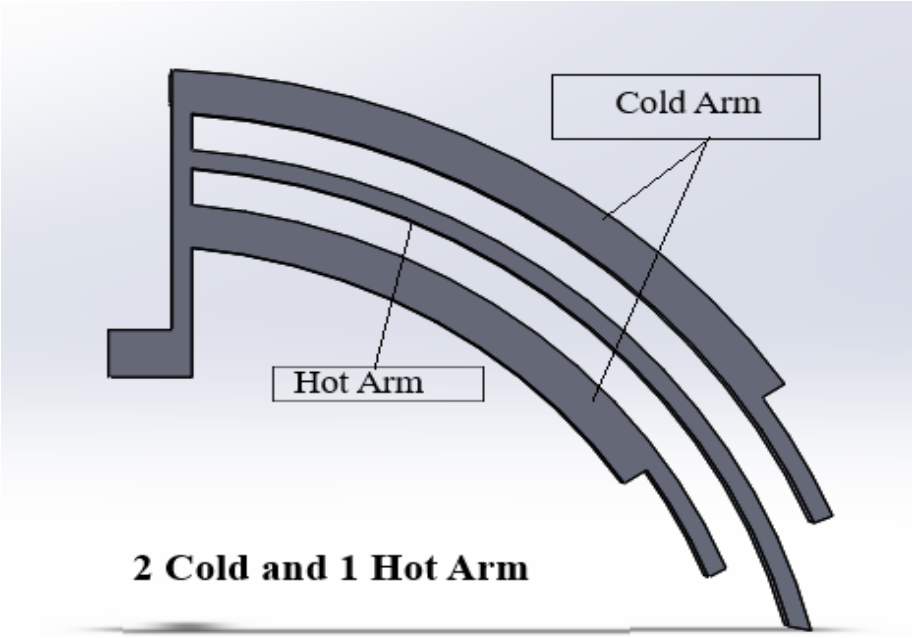

Figure 2.2: Schematic geometry of two cold and one hot arm actuator

2.2.3 ETA Design No 2

In this design two hot arms are proposed with one cold arm. This geometry consists of three arms which connected with each other with the help of connectors. Flexure is attached with cold arms. All the dimensions of this actuators are illustrated in table below

Table 2.2: Dimensions of ETA Design 2

Geometry	Dimensions (μm)
Length of Outer Hot Arm	320
Length of Cold Arm	260
Length of Inner Hot Arm	210
Width of Cold Arm	14
Length of Flexure	40
Width of Flexure	6
Width of Hot Arm	6
Distance b/w Hot and Cold Arm	12

Thickness of all the designs is 25 μm. All actuator has same thickness due to fabrication limitations.

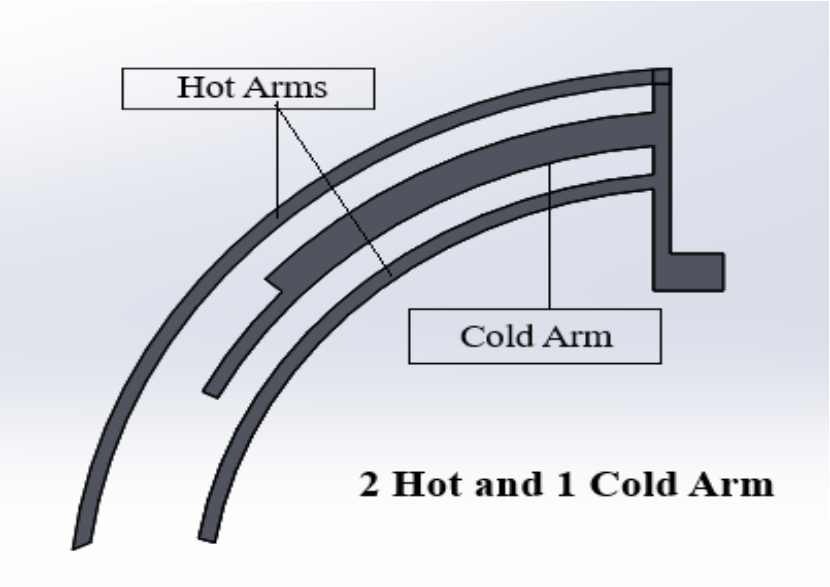

Figure 2.3: Schematic geometry of two hot and one cold arm actuator

2.2.4 ETA Design No 3

In this design two hot arms are proposed with one cold arm. Difference in this design and in previous design is the position of hot arms. In this design two hot arms are at external side and cold arm is in internal side. Design 3 has same dimensions of design 1.

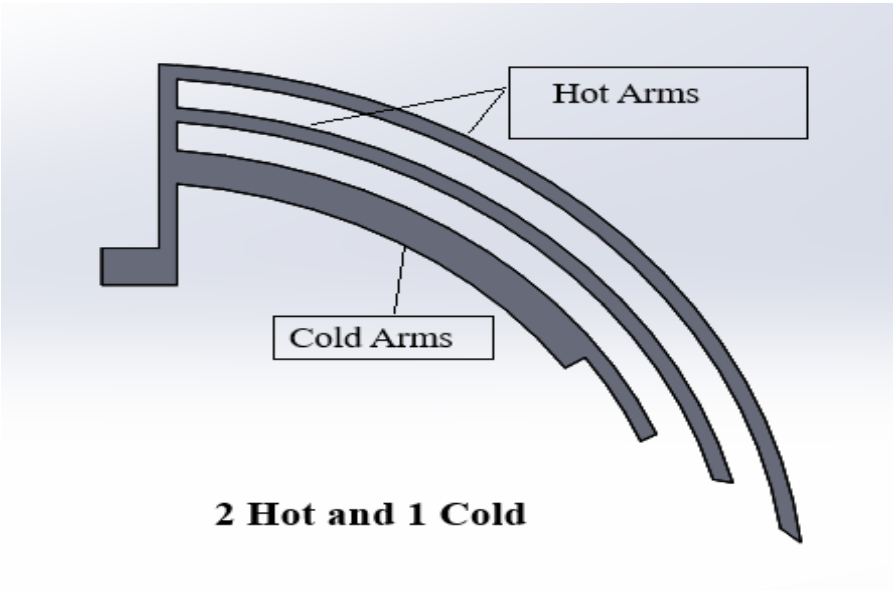

Figure 2.4: Schematic geometry of two outer hot and one cold arm actuator

While in previous design cold arm is proposed in between two hot arms. This geometry consists of three arms which connected with each other with the help of connectors. Flexure is attached with cold arms.

2.2.5 ETA Design No 4

In this design two hot arms are proposed with one cold arm. This design represents unique arrangement of actuator arms. The geometry consists of three arms which connected with each other with the help of connectors. Flexure is attached with cold arms. All the dimensions of this actuators are illustrated in table below

Table 2.3: Dimensions of ETA Design 4

Geometry	Dimensions (µm)
Length of Outer Hot Arm	310
Length of Cold Arm	114
Length of Inner Hot Arm	255
Width of Cold Arm	14
Length of Flexure	85
Width of Flexure	6
Width of Hot Arm	6
Distance b/w Hot Arm	24

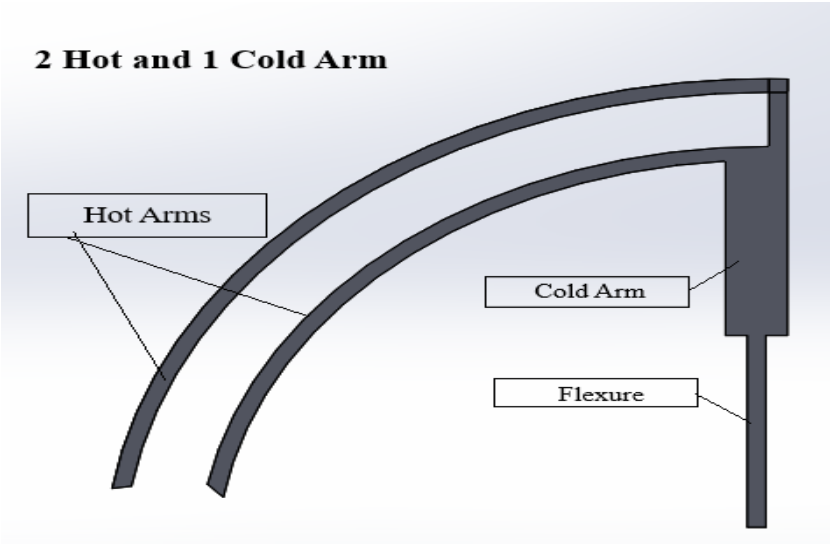

Figure 2.5: Schematic geometry of two hot and one cold arm different actuator

2.3 Design of MEMS Micromirror

In OCT applications, curvature of mirror plays an important role as it reflects light beam and hence it affects the resolution of image. We have designed our mirror by keeping all the important factors in mind. By considering all the important points in mind stress tendency in mirror plate can be reduced. Different materials have different reflectivity. We observed that gold material has good reflectivity of value R= 0.8912 at 0.5876 µm. We deposit 2 µm gold structural layer in our design which makes mirror reasonably reflective. The temperature of actuator must not exceed 1,410 ℃, as silicon has high melting point. The voltage level must keep below 5V. Above 5 V process of electrolysis may occur which may cause problem to thin layered actuator. Our mirror size is 200 × 200 µm. The minimum thickness of micromirror should be kept above 6 µm as per SOIMUMPs fabrication design. So, our mirror thickness is 6 µm.

Multiple types of plates are used for reflection of light. Some of the mirror plates with respect to shape are given below

- Rectangular shaped mirror
- Hexagon shaped mirror
- Square round shaped mirror
- Octagonal shaped mirror
- Diamond shaped mirror
- Circular shaped mirror

We choose circular shape mirror design as it shows better agreement to our design. Another factor for choosing round shape over others is it reduce dynamic deformation.

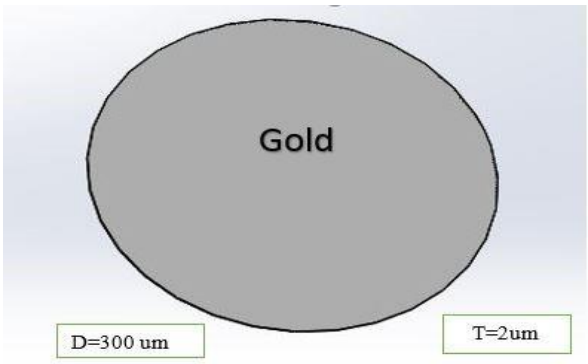

Figure 2.6: A schematic diagram of micromirror.

2.4 Design of Spring

The micromirror plate is attached to actuators with the help of springs. If the actuators are directly attached to micromirror, it will cause an increase in temperature at mirror plate. There should be pace some linkage in between mirror and actuators which translate motion of actuators to mirror. Springs are the best way to translate motion from actuators to micromirrors. Hinges are another option, but it may cause stress at that point. We designed U shaped curved springs which are aligned in concentric circle and are suitable for our design. The schematic diagram of spring is shown in Figure

The mirror plate of 300x300 µm area is attached to four electrothermal actuators through flexural springs. We have made U shaped springs in curved form which make the geometry more concentric. Length and width of spring can be varied according to requirement for best optimal design. The schematic detail of U-shaped spring is expressed in figure 2.9

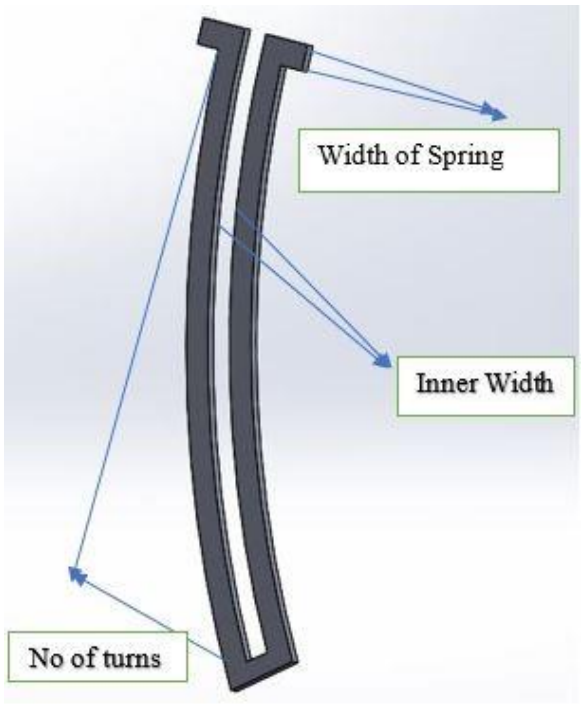

Figure 2.7: Schematic diagram of spring.

It is analysed that stress concentration and changes in stiffness can be caused by changing different parameters of spring [37].

i. An increase in spring thickness causes increase in stiffness along with decrease in stress concentration.
ii. Similarly, an increase in spring length causes an increase in stiffness along with a decrease in stress concentration.
iii. Causing an increase in width of spring both stress and stiffness increases.
iv. An increase in inner diameter of spring causes decrease in both factors.
v. By increasing the number of turns of spring, decrease in both factors occurs.

As the above points shows that no of turns in spring play's vital role in stress concentration as well as in stiffness. Therefore, we use two number of turns as a greater number of turns cause a decrease in both stress concentration and stiffness as well. As whole design is made up of silicon therefore springs material is also made of doped silicon.

2.5 Complete Design Geometry

As this section propose multiple designs for actuators, therefore multiple designs are proposed with micromirror. Analysis will show that which is the most appropriate design. Micromirror and springs dimensions in all designs remains same. There is variation in actuators dimensions and in actuators shape as well. In second last chapter optimization of best design is done based on its parameters.

2.5.1 Concept of Curved Concentric Design

The design of electrothermal actuator is based on curved concentric geometry for better displacement at low voltage. Tilting of mirrors with small side deformations are best solutions or applications where all four actuators need to be actuated at a once. Curved concentric geometry reduces the device size by giving optimal results. In literature a few designs work for in plane movement of mirrors. No single design was found in literature with working phenomena for out of plane movement. This shows the uniqueness of this design.

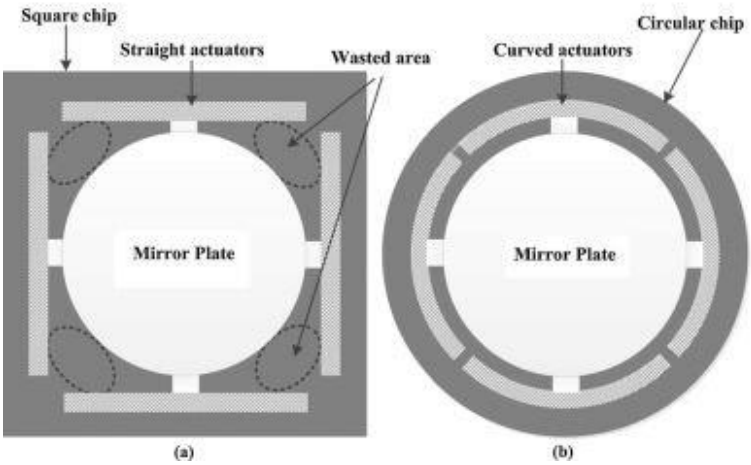

Figure 2.8: (a) Mirror with straight actuators. (b) Mirror with curved actuators [34].

2.5.2 Proposed Design No 1

This design proposes mirror actuation with 2 hot and one cold arm actuator along with springs provide linkage between mirrors and actuators. Thickness of whole design is 25 μm with silicon material.

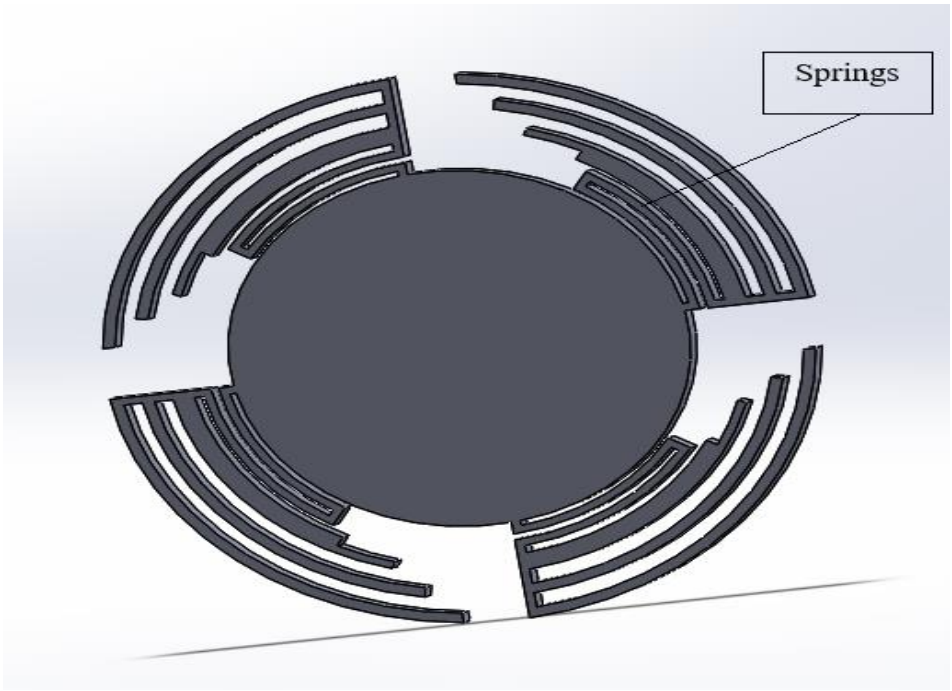

Figure 2.9: Schematic of proposed design 1

2.5.3 Proposed Design No 2

This design proposes mirror actuation with 2 hot and one cold arm actuator along with springs provide linkage between mirrors and actuators. Thickness of

whole design is 25 μm with silicon material. This design in replication of previous student's design expects the thickness of geometry. As in previous work geometry is design according to Poly MMMPs fabrication process but in our case, we design micromirror actuator with SOI MMMPs constraints. According to SOIMMMPs constraints thickness of our design is 25 μm along with width constraints I-e width of all the beams and actuators bars is greater than 6 μm.

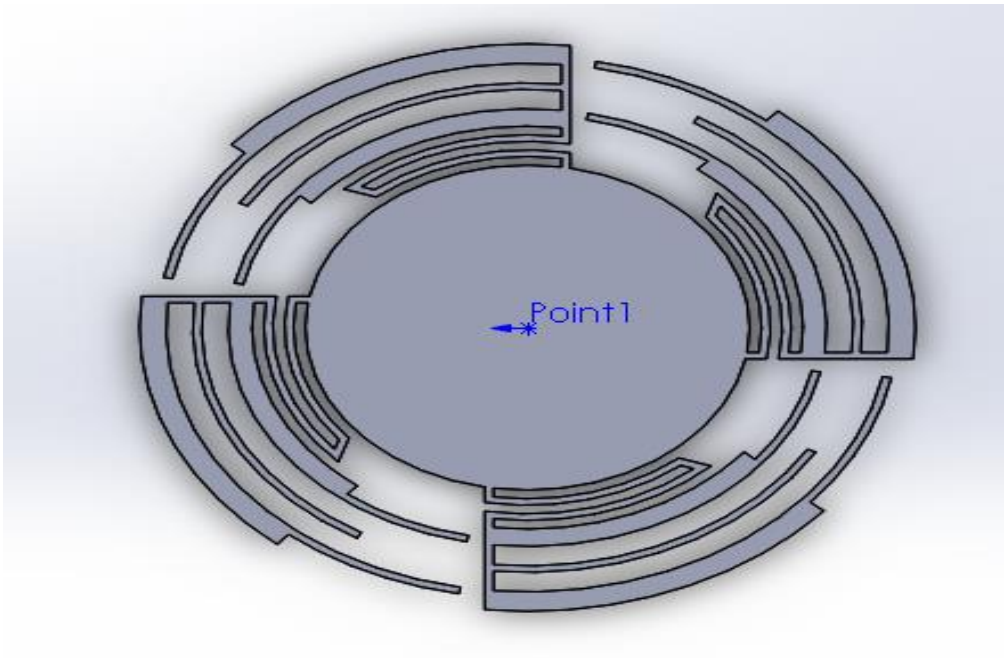

Figure 2.10: Schematic of proposed design 2

2.5.4 Proposed Design No 3

This design proposes mirror actuation with 2 hot and one cold arm actuator along with springs provide linkage between mirrors and actuators. Dimensions of design 3 is like design 1 expect the spring positions. Springs are attached with side of hot arm to translate maximum deflection towards mirror. Thickness of whole design is 25 μm with silicon material. According to SOIMMMPs constraints thickness of our design is 25 μm along with width constraints i-e width of all the beams and actuators bars is greater than 6 μm. As deflection is maximum at actuators left end therefore, we attach spring at that point to get maximum deflection of mirror.

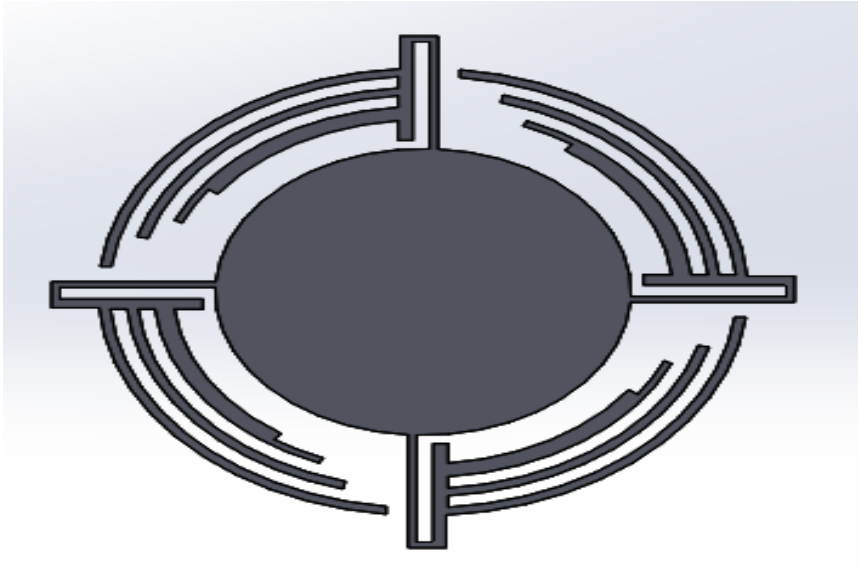

Figure 2.11: Schematic of proposed design 3

2.5.5 Proposed Design No 4

This design proposes mirror actuation with 2 hot and one cold arm actuator along with springs provide linkage between mirrors and actuators. Thickness of whole design is 25 μm with silicon material.

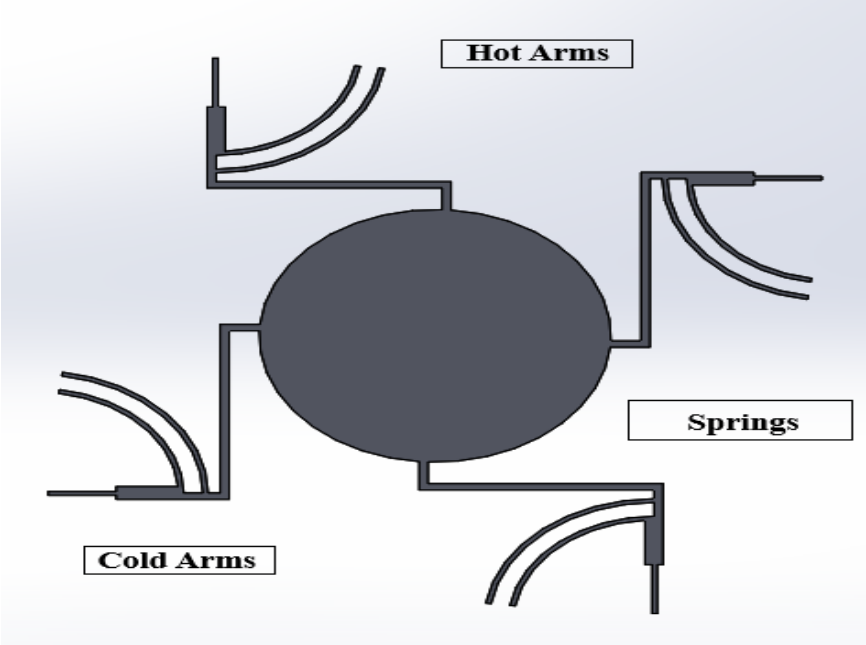

Figure 2.12: Schematic of proposed design 4

Chapter 3: Finite Element Method Based Modelling

Finite element method involves computational analysis of geometries to calculate errors in mathematical models and in physics of geometries. These methods involve structural analysis for stress and displacement calculations, Electrothermal analysis, transient analysis, Thermal electric analysis, and fluid flow analysis.

3.1 FEM based Electro-Thermal and Thermo-Mechanical Analysis

This chapter involves detail discussion of FEM based simulations for proposed designs and actuator designs. FEM is the computational numerical method to solve mathematical and physics of geometries giving optimal answers. The whole geometry is divided into small fine parts called meshing. The FEM analysis solve differential equation for each small part which is known as finite part. After those polynomial solutions of these differential equations are solved. All the results are than sum up to show the errors that will ensure the accuracy of design. A flow chart is presented showing the steps used in ANSYS software for simulations of proposed design.

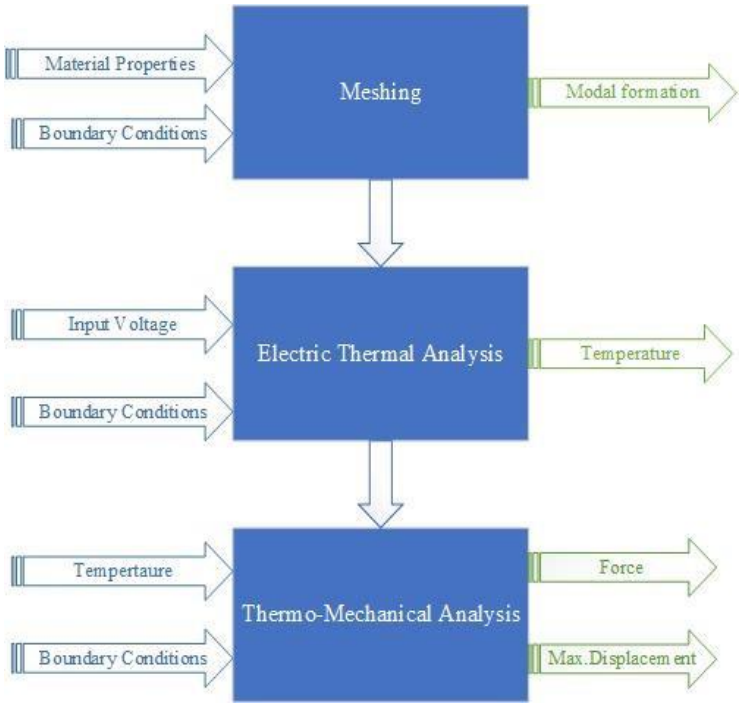

Figure 3.1: The sequential diagram for performing the FEM-based simulations.

In the given flow chart blue arrows on left side of diagram shows input parameters while arrows on right side of diagram shows output parameters. We use ANSYS AIM 17.1 for analysis of actuators and overall designs. All the geometries are made in Solid works 2019. These geometries are than imported in ANSYS for simulations.

3.2 ETA Actuators Analysis

Each design of actuator is analyzed by applying voltages over a range of 0.03V to 5V. We limit the voltage to that point when plate temperature exceeds above 45°C. It means temperature on mirror plate is limitation of our design.

3.2.1 Analysis of ETA Design No 1

Positive voltage is applied on hot arm ends while ground is applied on cold arm ends. Boundary conditions are applied on actuators geometry. In boundary conditions fixed supports are defined and convection is applied. Analysis shows displacement of 0.02 μm in *z* direction with temperature rise of 69° C on plate on applied voltage of 0.3 V.

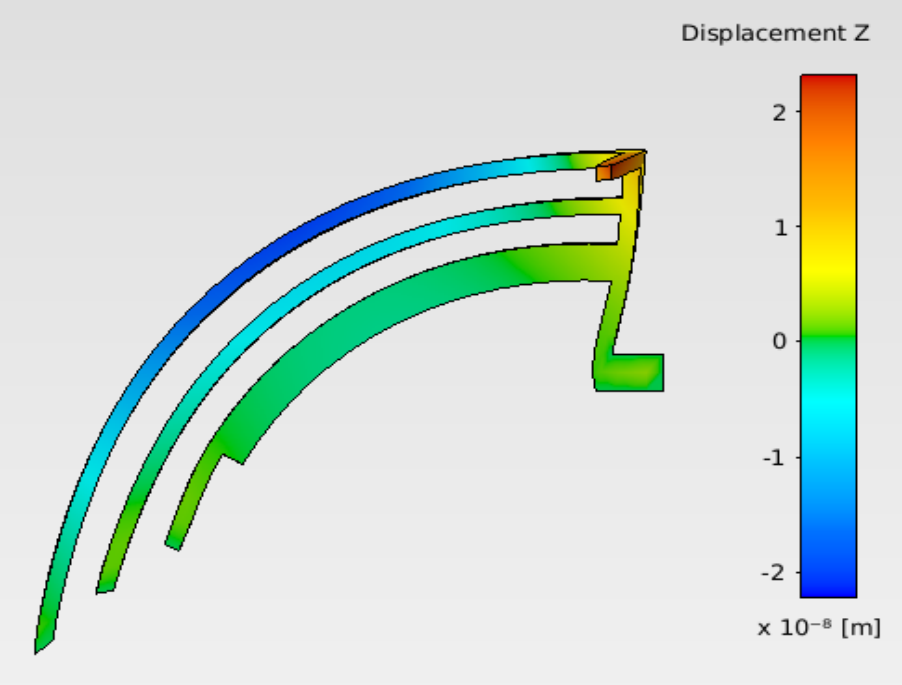

Figure 3.2: Displacement Analysis of ETA design no 1

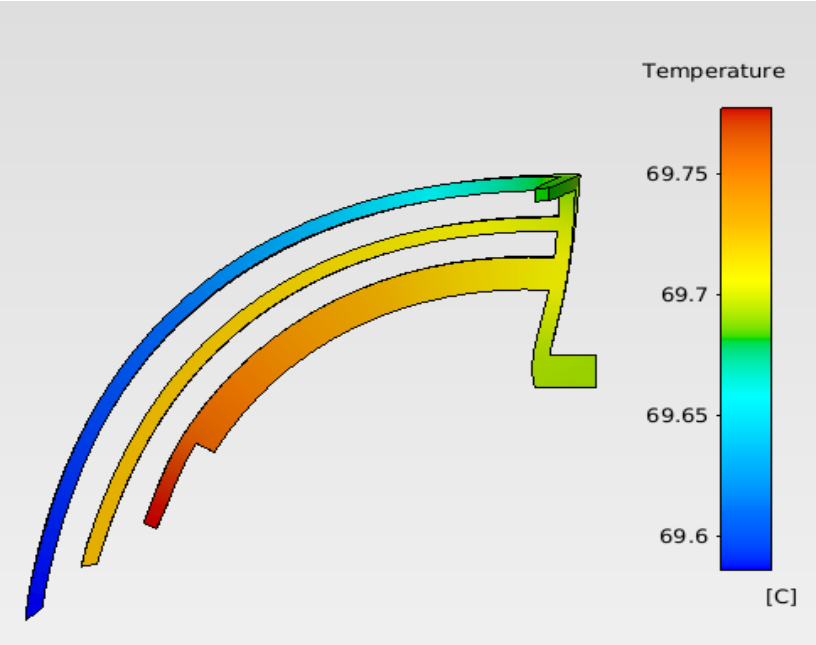

Figure 3.3: Temperature profile of ETA design no 1.

3.2.2 Analysis of ETA Design No

Boundary conditions are applied on actuators geometry. In boundary conditions fixed supports are defined and convection is applied. Analysis shows displacement of 0.028 μm in *z* direction with temperature rise of 59^{o} C on plate on applied voltage of 0.3 V.

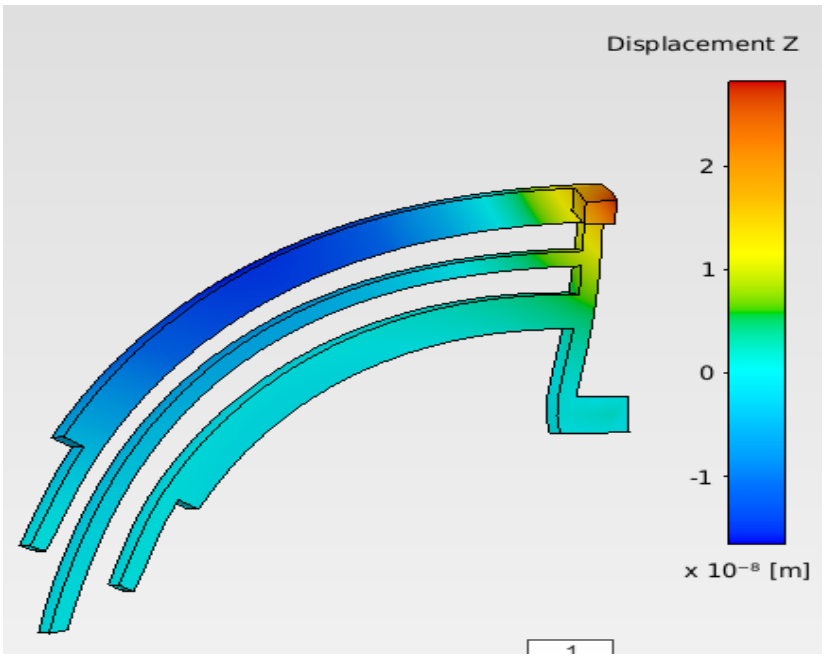

Figure 3.4: Displacement Analysis of ETA design no 2.

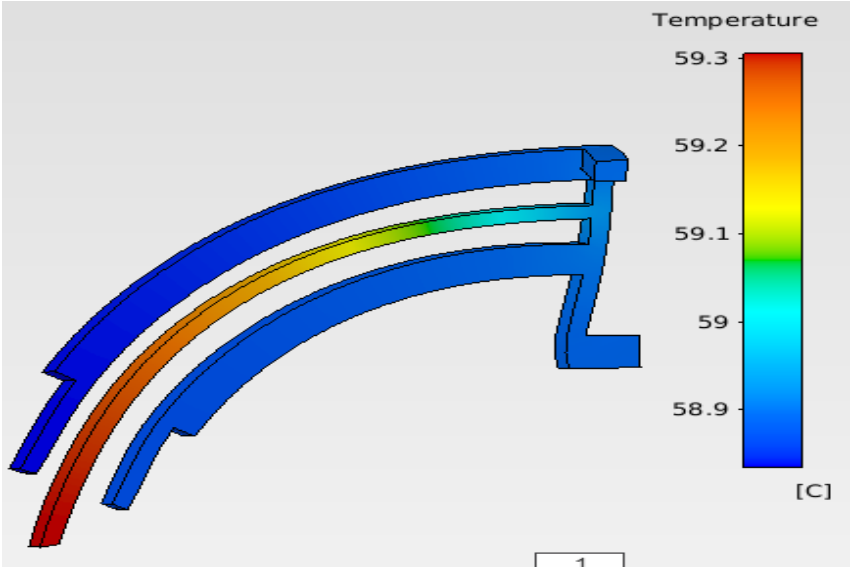

Figure 3.5: Temperature profile of ETA design no 2.

3.2.3 Analysis of ETA Design No 3

In this design positive voltage is applied on hot arm ends while ground is applied on cold arm ends. Boundary conditions are applied on actuators geometry. In boundary conditions fixed supports are defined and convection is applied. Analysis shows displacement of 0.024 μm in *z* direction with temperature rise of 73° C on plate on applied voltage of 0.3 V.

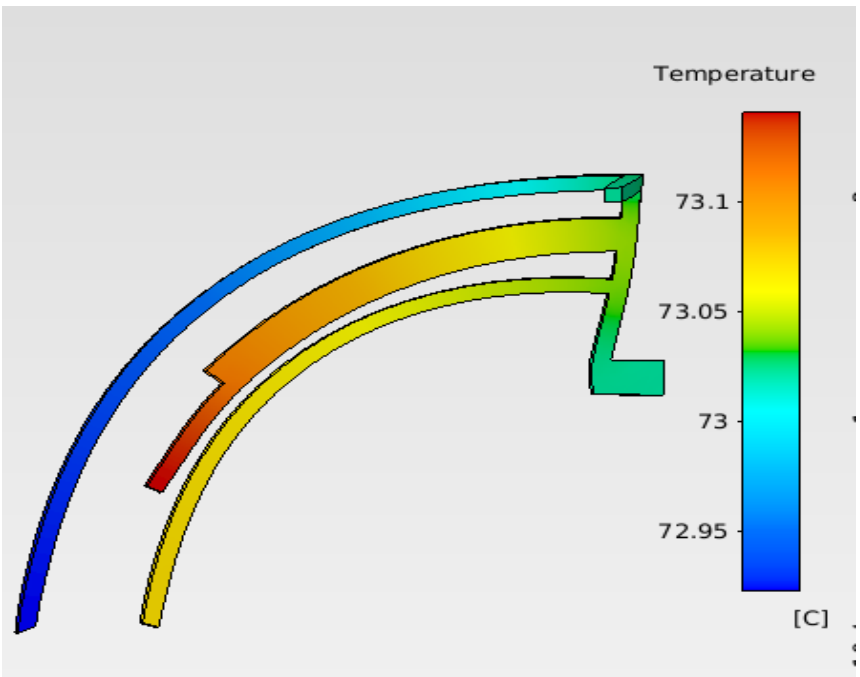

Figure 3.6: Temperature profile of ETA design no 3.

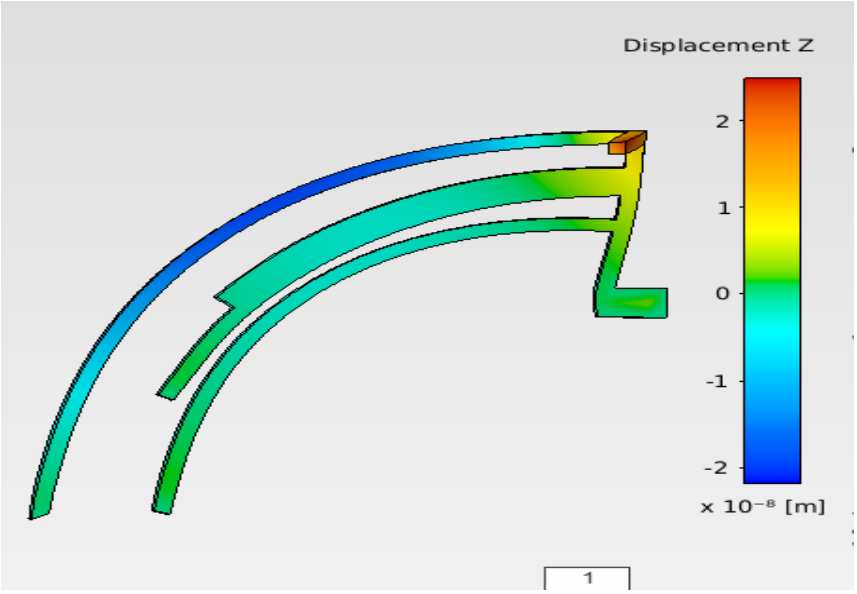

Figure 3.7: Displacement Analysis of ETA design no 3.

3.3 Analysis for Spring Deflection

Stiffness of spring is calculated by static structural analysis in ANSYS. Stiffness is calculated by applying force on one end and calculate stiffness against that force. Static structure analysis shows 416 N/m stiffness against 10 μm of force.

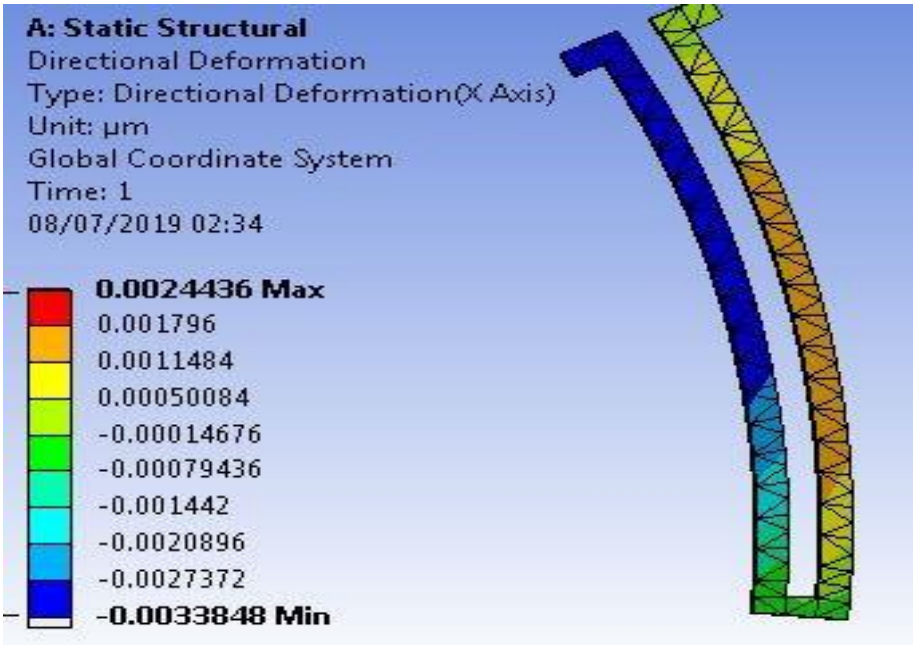

Figure 3.8: Deformation of spring

3.4 Electro-Thermal and Thermo-Mechanical Analysis

In electro thermal analysis, temperature rise on mirror plate is actuated by applying voltages on actuators. Positive voltage is applied on hot arms of actuator while ground is applied on cold arms. As voltage increases current density rises in actuator creating rise in resistivity of material. By increasing the voltage temperature also rises on plate due to deflection of hot and cold arm actuator. The temperature on plate and actuators surface should not rise above 45 degrees Celsius even on application of minimum voltage.

Voltages is applied in electro-thermal analysis to calculate the maximum temperature on plate. The output value of electro thermal analysis is than used as input in thermos-mechanical model to calculate maximum temperature at that temperature through hot and cold shaped actuator.

3.4.1 Analysis for Proposed Design 1

Figure 3.9 shows that maximum displacement of plate is 1.2 nm and maximum temperature on plate actuator is 47° C.

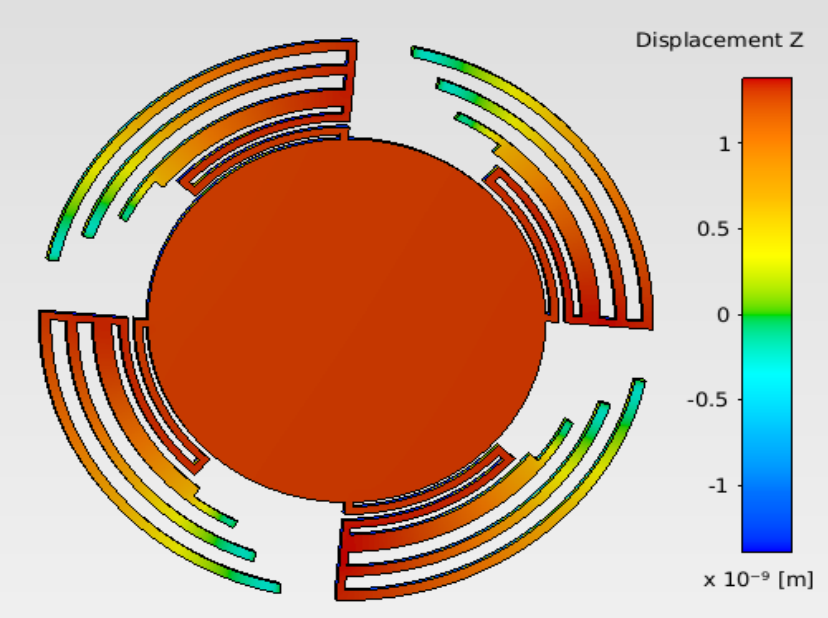

Figure 3.9: Displacement profile of micromirror design 1 on application of voltage

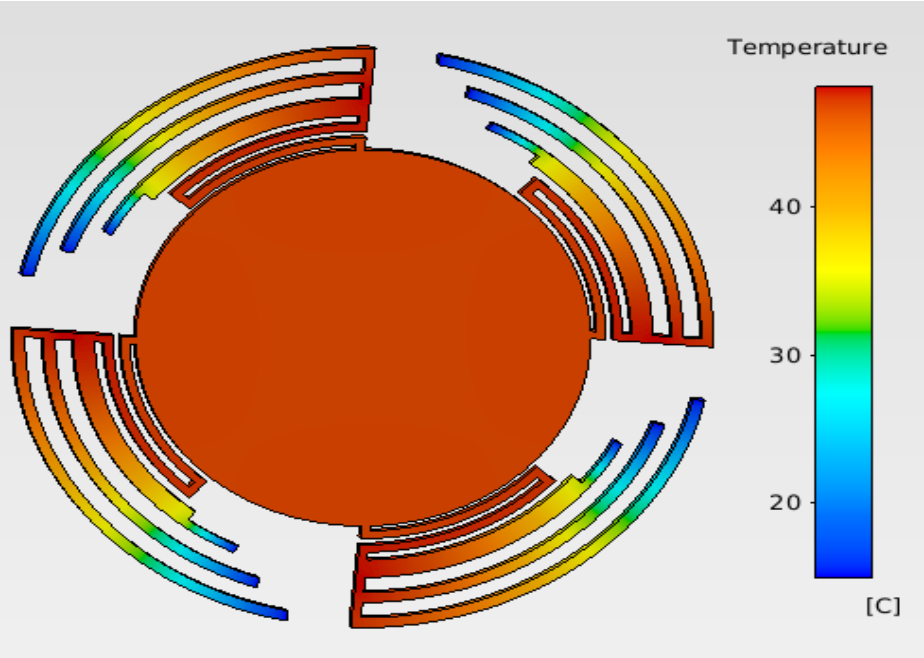

Figure 3.10: Temperature profile of micromirror design 1 on application of voltage

Following figure shows displacement, temperature, and power graphs against same applied voltage in between range of 0.2 V to 3 V. All the graphs are plotted in excel while data is collected by ANSYS simulations.

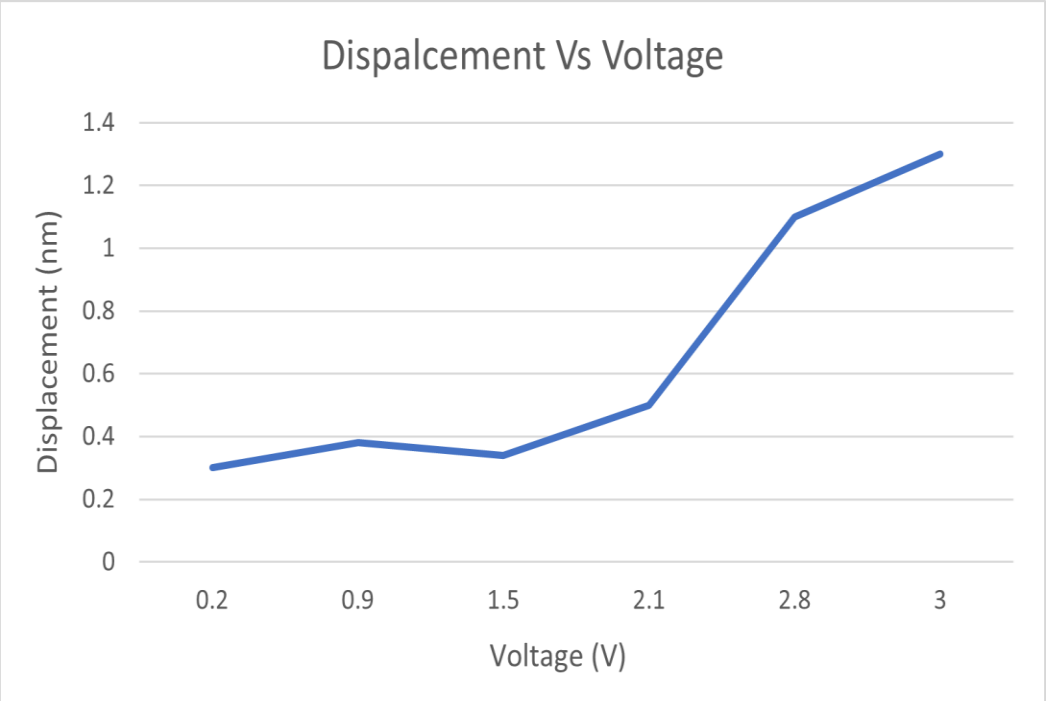

Figure 3.11: Graphical representation of variation of displacement at variation of voltage for design 1.

The usual behavior in Fig.3.11 can be attributed to like error in the boundary conditions and meshing in the simulation software.

Temperature keeps increasing as we increase voltages. We cannot exceed the mirror pate temperature above 45° C.

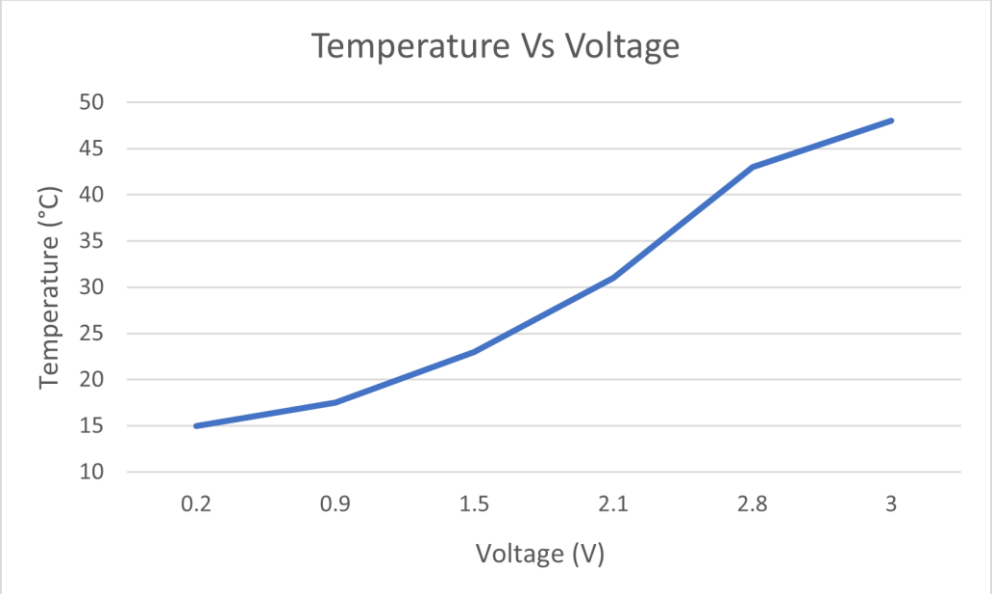

Figure 3.12: Graphical representation of variation of temperature at variation of voltage for design 1.

Power is calculated by measuring current density from ANSYS analysis and multiplying the obtained current density with applied voltage. As increase in power is observed by increasing voltage.

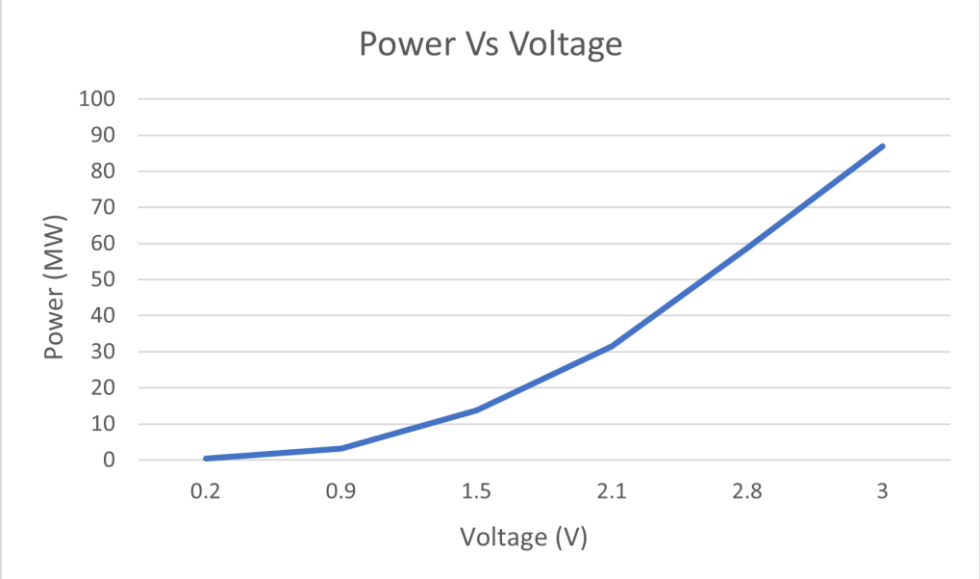

Figure 3.13: Graphical representation of variation of input power at variation of voltage for design 1.

3.4.2 Analysis for Proposed Design 2

The maximum temperature on plate actuator is 42° C on applied voltage of 3.6 V. At this voltage maximum displacement calculated on plate is 9.2 nm.

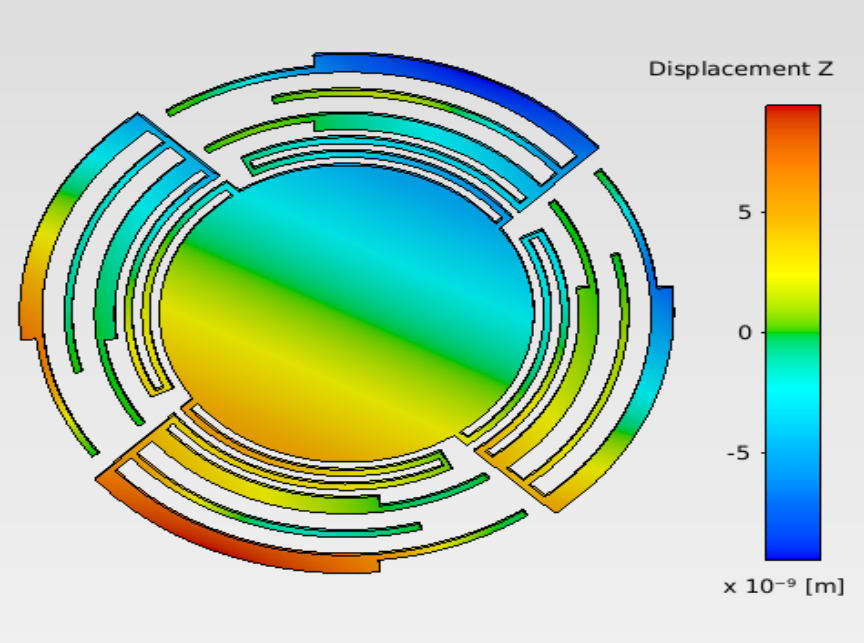

Figure 3.14: Displacement profile of micromirror design 2 on application of voltage

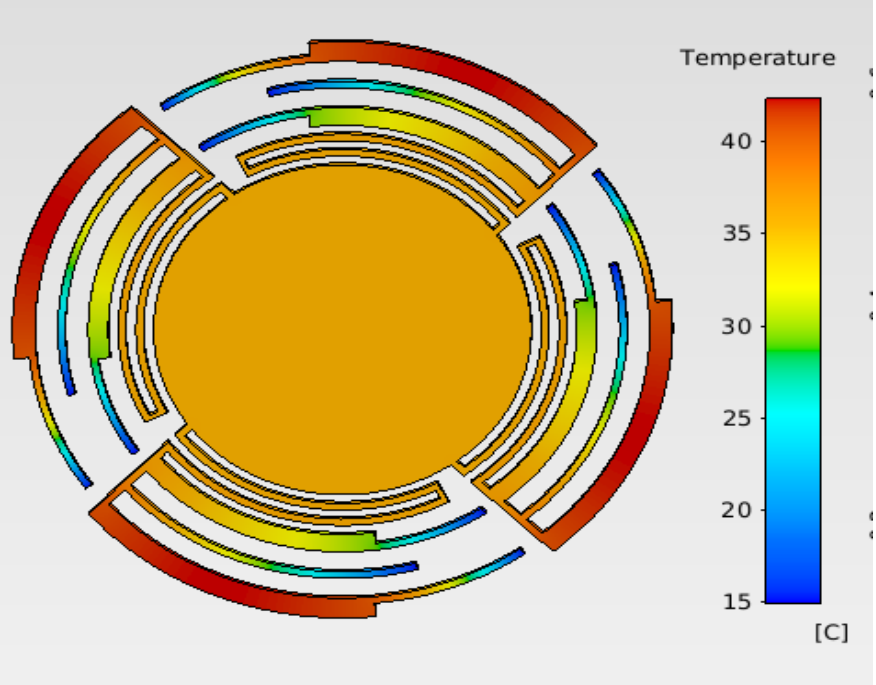

Figure 3.15: Temperature profile of micromirror design 2 on application of voltage

Following figure shows displacement, temperature, and power graphs against same applied voltage in between range of 0.2V to 3V. All the graphs are plotted in excel while data is collected by ANSYS simulations

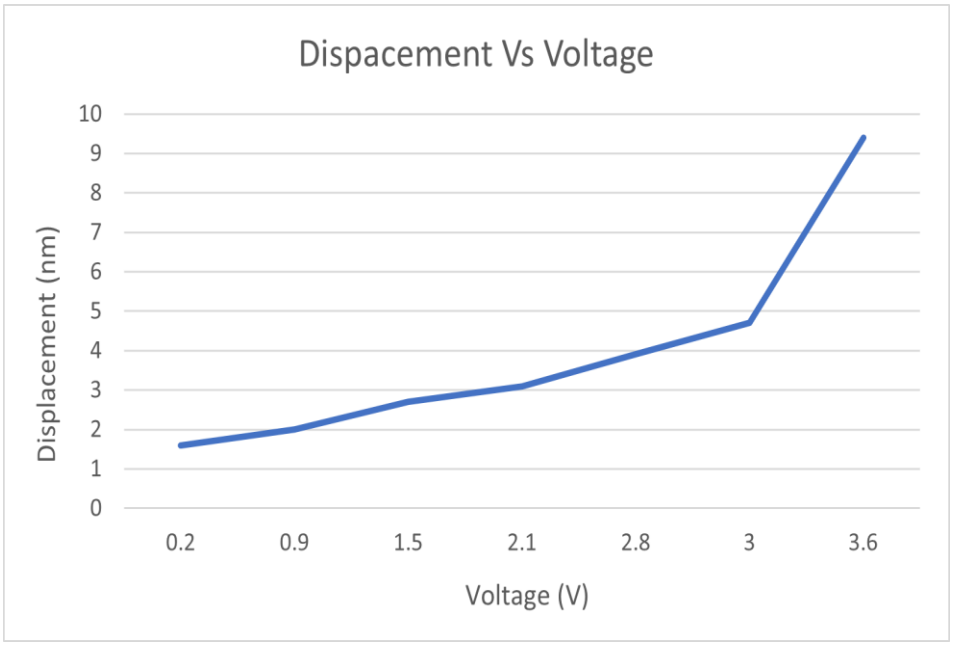

Figure 3.16: Graphical representation of variation of displacement at variation of voltage for design 2.

Temperature keeps increasing as we increase voltages. We cannot exceed the mirror pate temperature above 45°C.

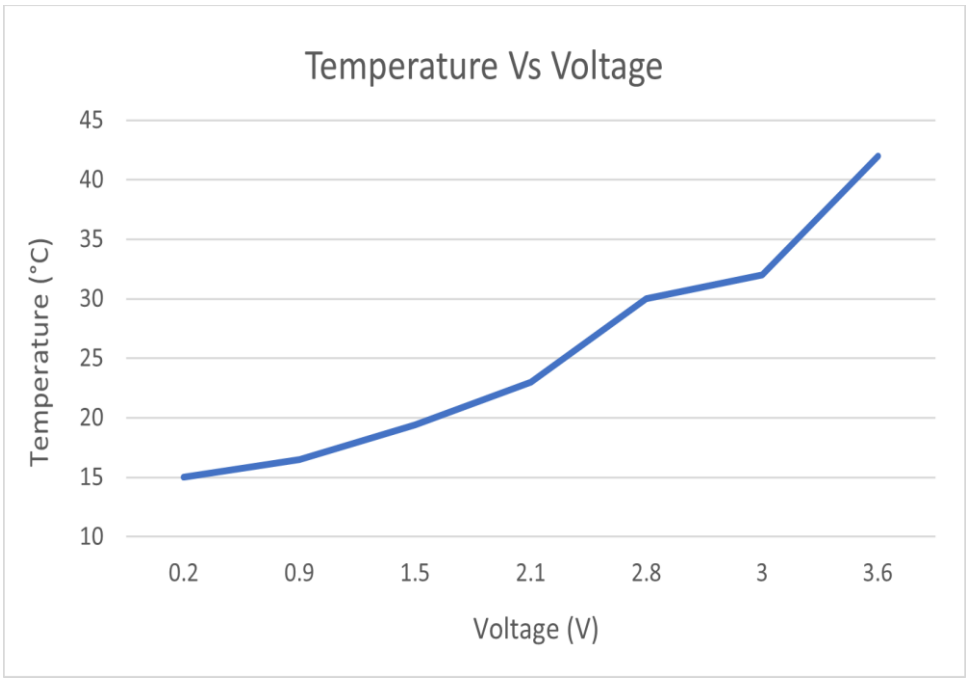

Figure 3.17: Graphical representation of variation of temperature at variation of voltage for design 2.

Power is calculated by measuring current density from ANSYS analysis and multiplying the obtained current density with applied voltage. As increase in power is observed by increasing voltage.

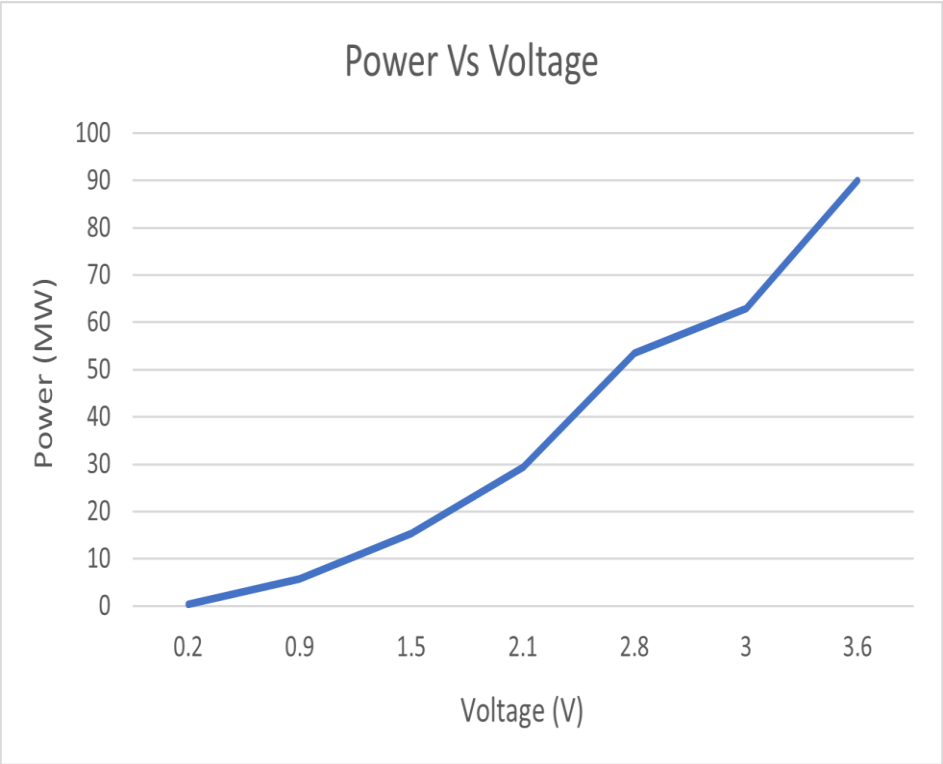

Figure 3.18: Graphical representation of variation of input power at variation of voltage for design 2.

The usual behavior in Fig.3.16 can be attributed to like error in the boundary conditions and meshing in the simulation software.

The usual behavior in Fig.3.17 can be attributed to like error in the boundary conditions and meshing in the simulation software.

The usual behavior in Fig.3.18 can be attributed to like error in the boundary conditions and meshing in the simulation software.

3.4.3 Analysis for Proposed Design 3

The maximum temperature on plate actuator is 45 °C on applied voltage of 3.6V. At this voltage maximum displacement calculated on plate is 0.5 nm.

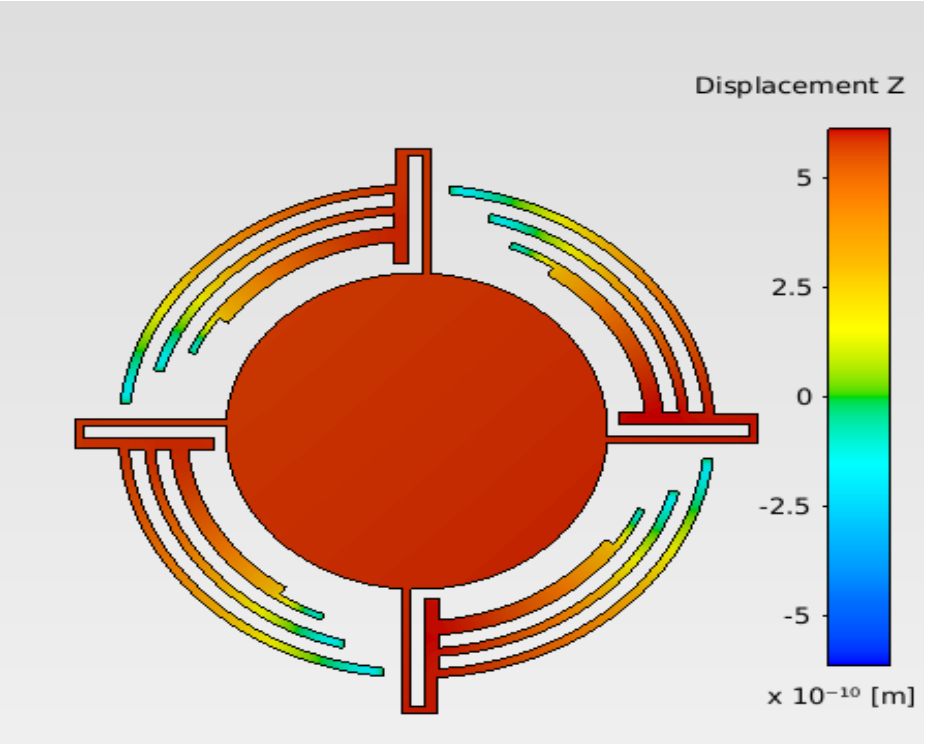

Figure 3.19: Displacement profile of micromirror design 3 on application of voltage

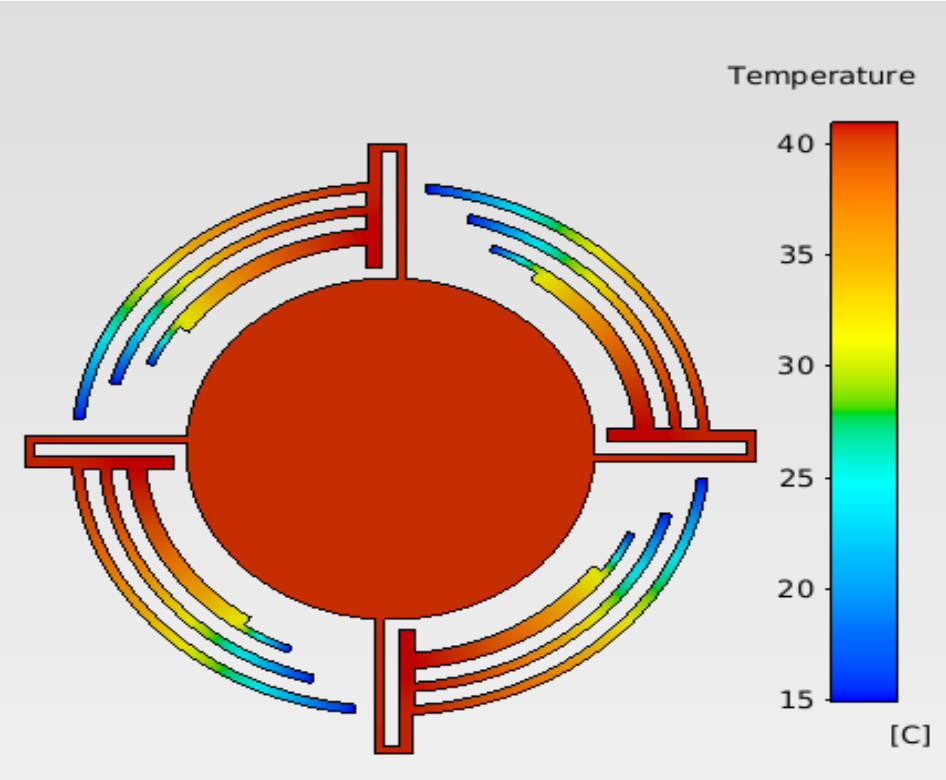

Figure 3.20: Temperature profile of micromirror design 3 on application of voltage

Following figure shows displacement, temperature, and power graphs against same applied voltage in between range of 0.2V to 3V. All the graphs are plotted in excel while data is collected by ANSYS simulations.

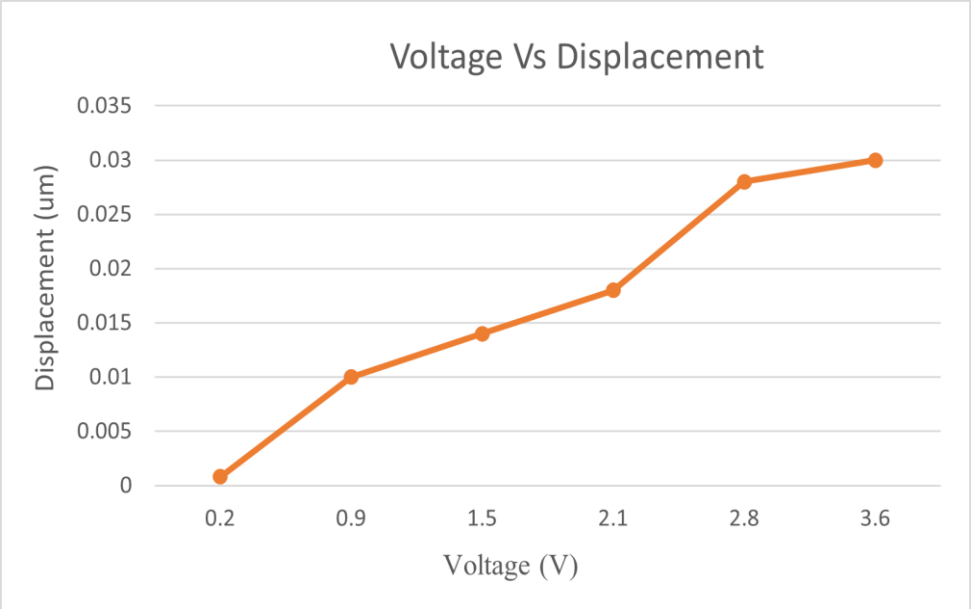

Figure 3.21: Graphical representation of variation of displacement at variation of voltage for design 3.

Temperature keeps increasing as we increase voltages. We cannot exceed the mirror pate temperature above 45°C.

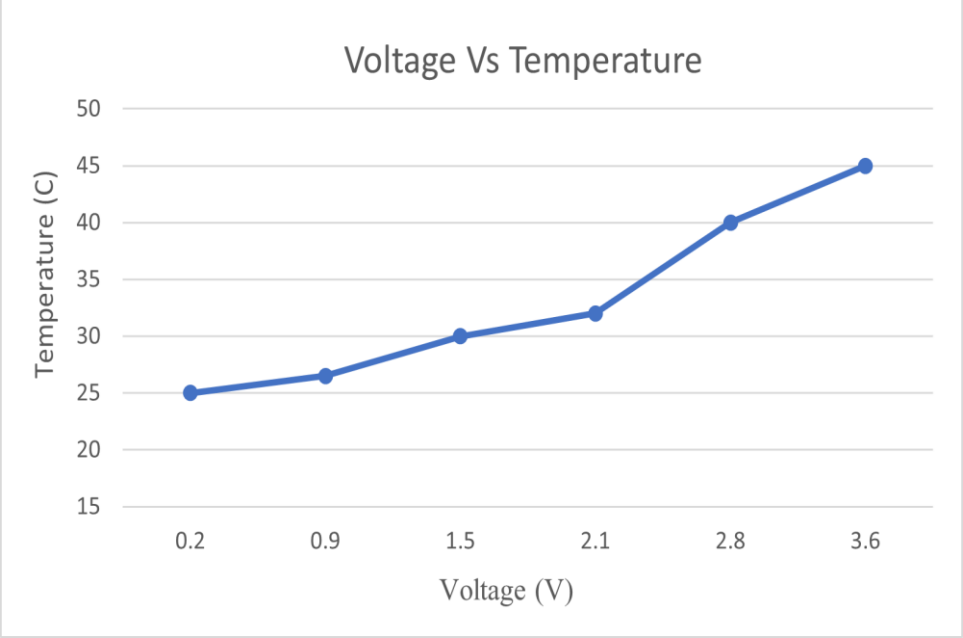

Figure 3.22: Graphical representation of variation of temperature at variation of voltage for design 3.

Power is calculated by measuring current density from ANSYS analysis and multiplying the obtained current density with applied voltage. As increase in power is observed by increasing voltage.

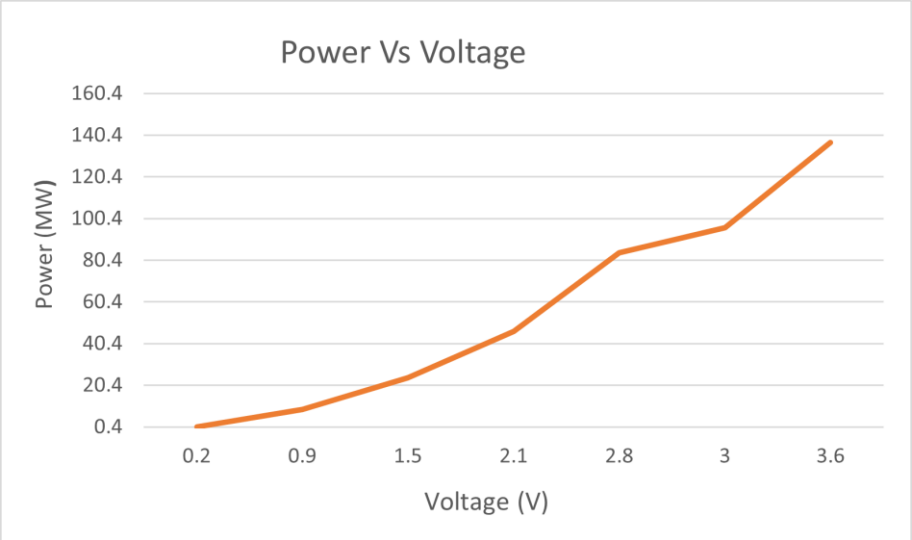

Figure 3.23: Graphical representation of variation of input power at variation of voltage for design 3.

3.4.4 Analysis for Proposed Design 4

The maximum temperature on plate actuator is 42°C on applied voltage of 3.6V. At this voltage maximum displacement calculated on plate is 0.03µm.

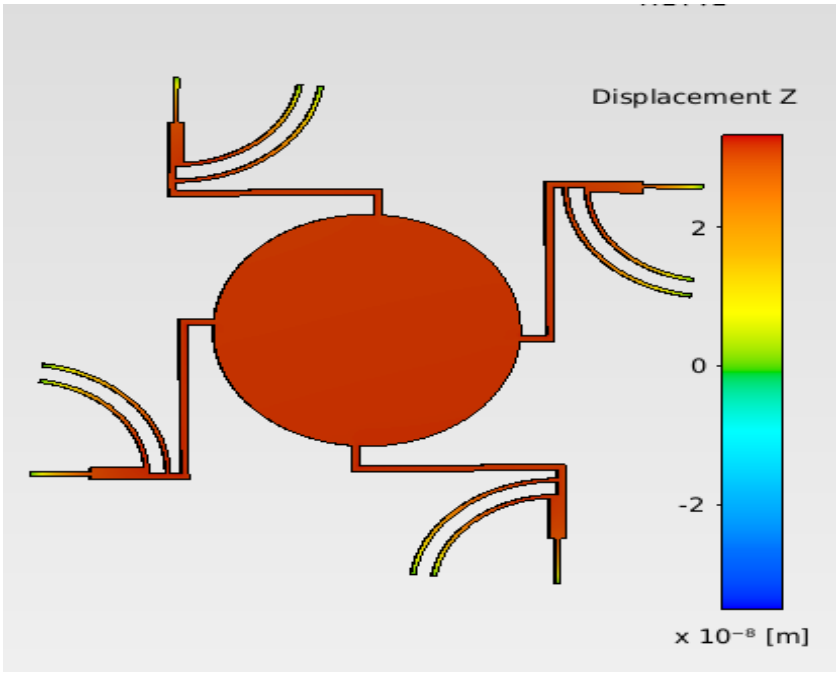

Figure 3.24: Displacement profile of micromirror design 4 on application of voltage

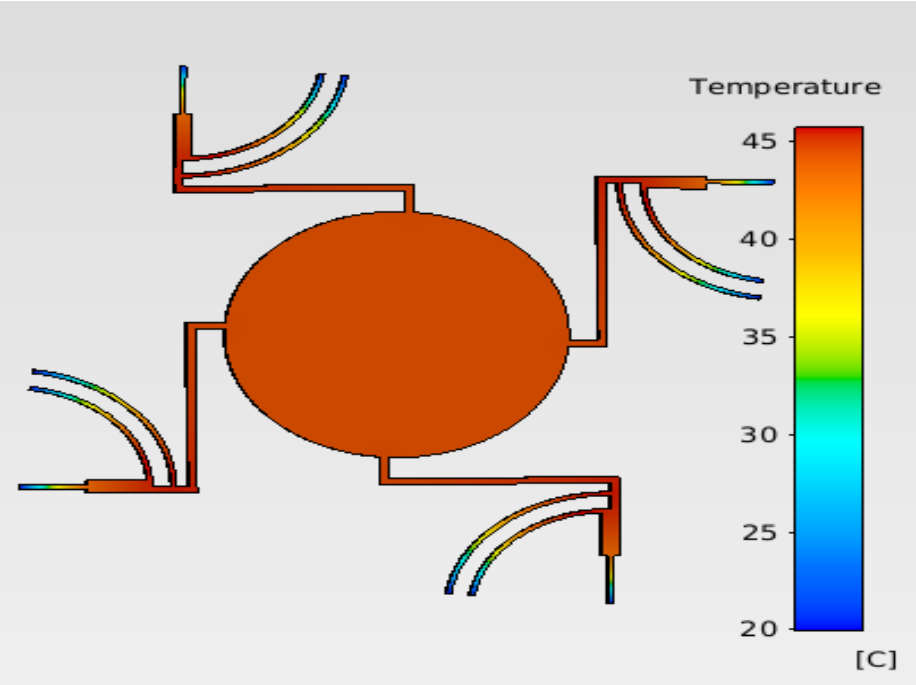

Figure 3.25: Temperature profile of micromirror design 4 on application of voltage

Following figure shows displacement, temperature, and power graphs against same applied voltage in between range of 0.2V to 3V. All the graphs are plotted in excel while data is collected by ANSYS simulations.

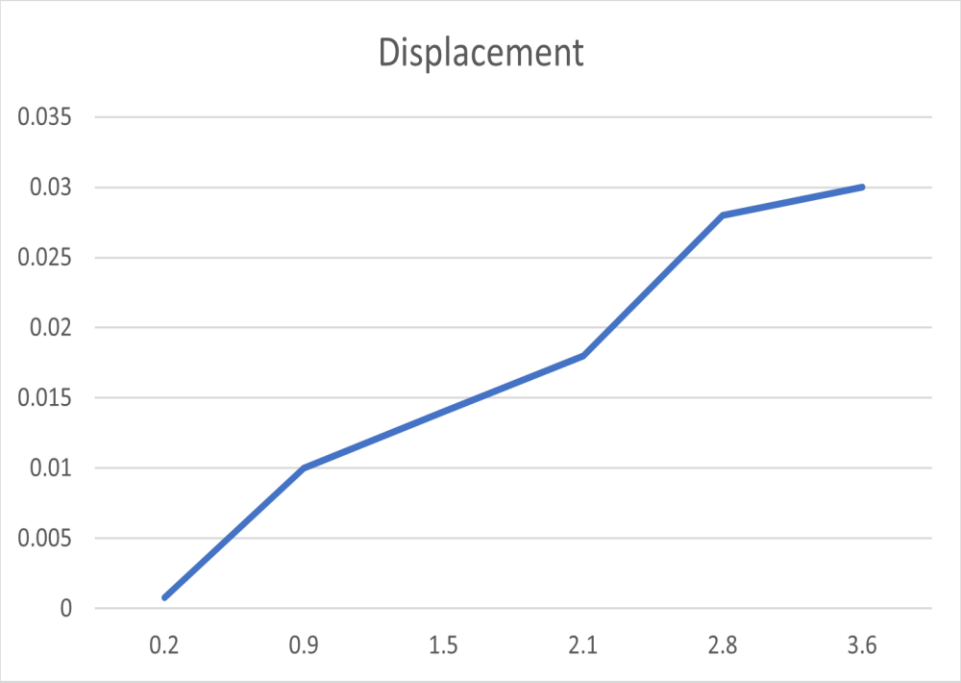

Figure 3.26: Graphical representation of variation of displacement at variation of voltage for design 4.

Temperature keeps increasing as we increase voltages. We cannot exceed the mirror pate temperature above 45°C.

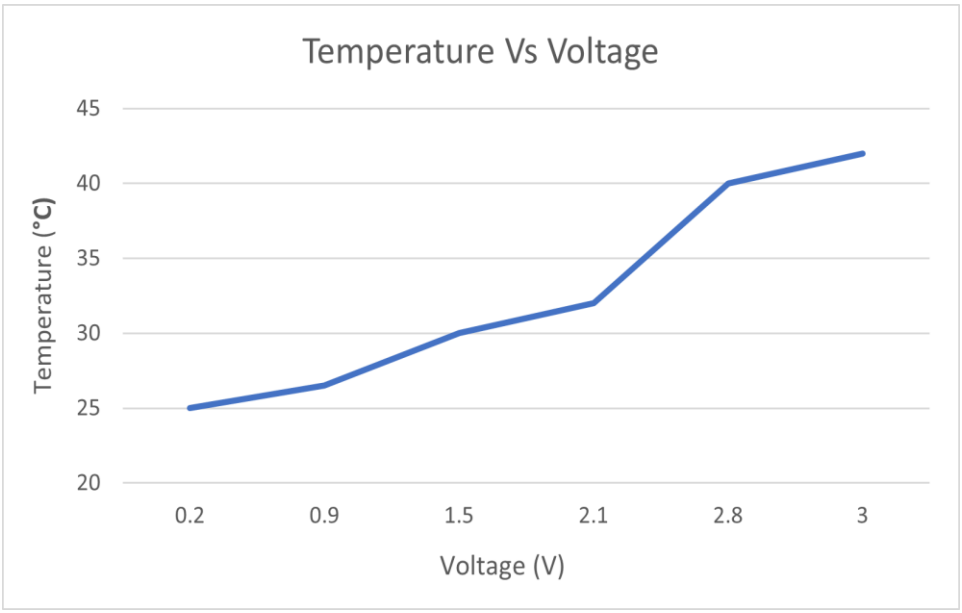

Figure 3.27: Graphical representation of variation of temperature at variation of voltage for design 4.

Power is calculated by measuring current density from ANSYS analysis and multiplying the obtained current density with applied voltage. As increase in power is observed by increasing voltage.

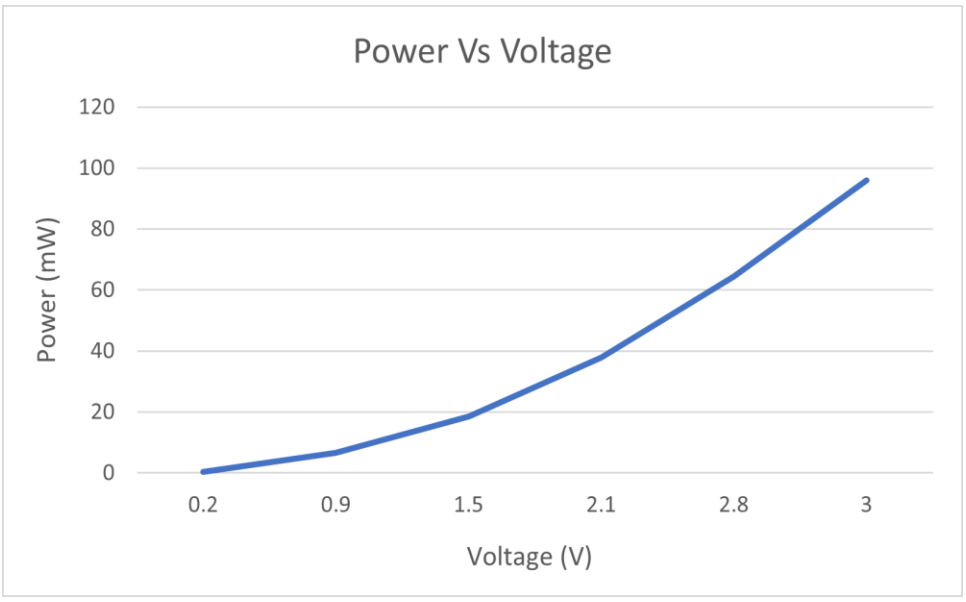

Figure 3.28: Graphical representation of variation of input power at variation of voltage for design 4.

The usual behavior in graphical figures. can be attributed to error in the boundary conditions and meshing in the simulation software.

From above analysis design no 4 gives maximum displacement on applied voltage of 3V. The maximum temperature on plate at this voltage is 42°C. We apply design of experiments technique on design no 4 to calculate the most important input factors which causes significant effects on output results.

Chapter 4: DOE based Optimization of Micromirror

In this Chapter, a comprehensive study of the design parameters is done with design of experiments technique. Design of experiments technique is done for three output parameters. This technique calculates the most effective input parameter which effects the output parameter. The resulted geometry is than modified according to best optimized dimensions for best output results. The flow chat shows the crucial steps that involved in optimization of micromirror design.

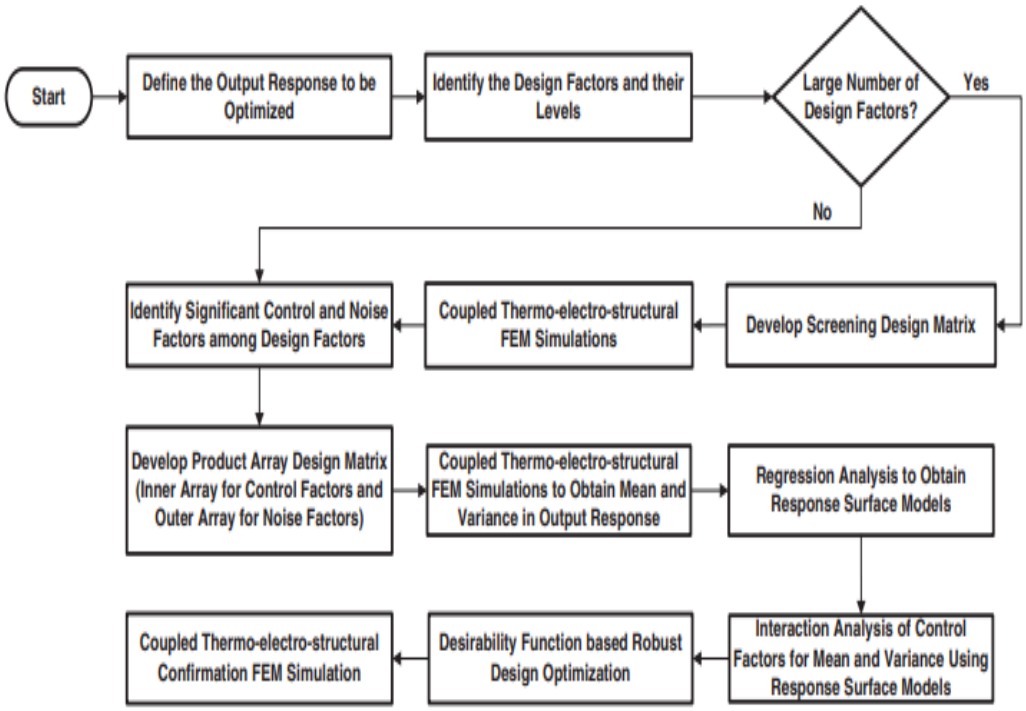

Figure 4.1: Flow chart of DOE based optimization

4.1 Design of Experiments

Design of experiments technique is done for three output parameters. This technique calculates the most effective input parameter which effects the output parameter.

4.1.1 Definitive Screening Design

If we have multiple design factors than their screening is done on manual basis. Select 6 to 7 most crucial parameters that affects the output most. The results

obtain from ANSYS analysis are than further pass-through DOE technique to calculate the optimal value for parameters. By calculating optimal values best resultant geometry is obtained in the end. We calculate design factors which have highest impact on output values. The main goal of DOE technique is to calculate the important parameters to obtain an optimize solution. Important parameters which have hight impact on output responses are mentioned in table below

Table 4.1: Design Parameters with their codes

Code	Design Factors	Units
SL	Spring length	*μm*
SP	Spring width	*μm*
OHL	Outer hot arm length	*μm*
IHL	Inner hot arm length	*μm*
FW	Flexure Width	*μm*
FL	Flexure Length	*μm*
HAW	Hot arm width	*μm*
CAL	Cold arm length	*μm*

The output response for which were calculating input parameters are listed in table below.

Table 4.2: Output Responses with their codes

Code	Output Factors	Units
IP	Input Power	mW
MD	Mirror Displacement	μm
MT	Mirror Temperature	℃

The limitations applied on mirror design should be kept in mind while changing the parameters like width of actuator arms should not get below 6-μm. Thickness of structure should be either 25 μm or 10 μm. Our aim is to achieve maximum displacement, minimum input power and temperature level below 45 degrees.

Following table shows the design factors (Input Factors) along with their low and high values as well.

Table 4.3: Design factors with their low and high values

Code	Design Factors	Low Level	High Level
X_1	Spring length (SL)	240	250
X_2	Outer hot arm length (OHL)	180	190
X_3	Spring width (SP)	8	12
X_4	Inner hot arm length (IHL)	140	144
X_5	Flexure Width (FW)	6	8
X_6	Flexure Length (FL)	75	80
X_7	Hot arm width (HAW)	6	8
X_8	Cold arm length (CAL)	69	71
X_9	Hinge Width (HW)	6	10

The Micromirror design parameters can be observed clearly by the following figure 4.1.

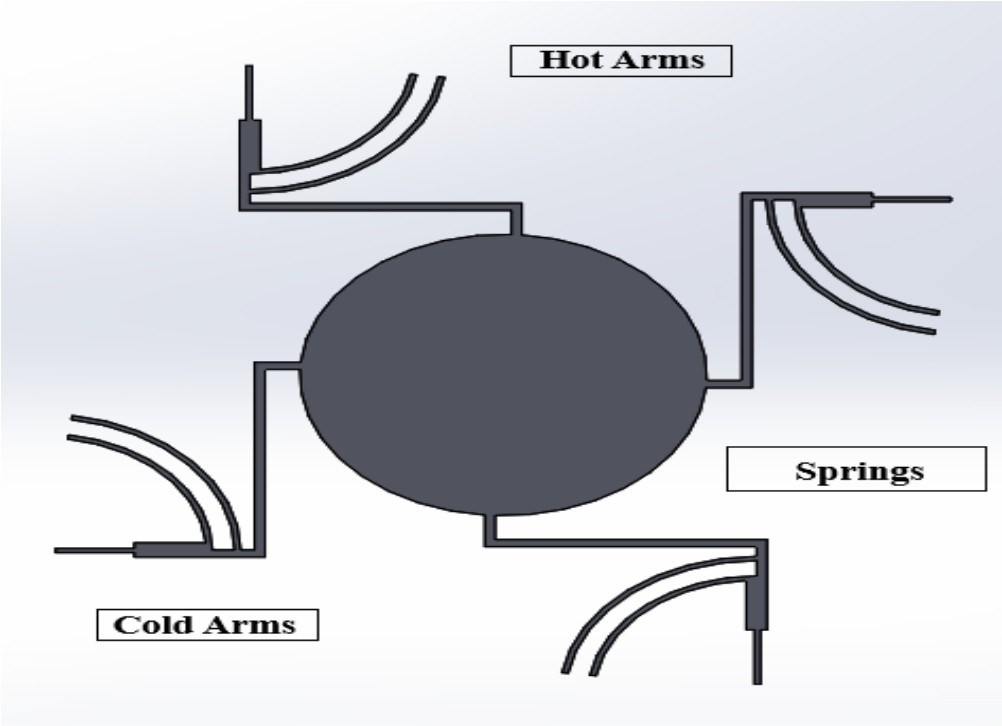

Figure 4.2: Detail diagram of micromirror final design.

4.1.2 Placket Burman Model

Placket Burman model calculates the parameters which are important for experiment. Placket Burman is the most used screen design model. Placket Burman is an experimental technique used to calculate the dependance of independent variable on output. All the input parameters are divided into two values. One high and one low value is assigned to all the parameters by keeping the constraints in mind. This model uses + sign for high values and – sign for low values. This model removes the irrelevant factors such as noise factors from data.

$$Y = \beta_0 + \sum_{i=1}^{i=n} \beta i \, X_{ir} \qquad (4.1)$$

Where Y is the output factor, β_0 is the model intercept and β_I is the linear coefficient. X represents the level of design factor.

Table 4.4: Placket Burman Model

Run	Blk	A	B	C	D	E	F	G	H
1	1	-	+	-	-	-	+	+	+
2	1	-	-	-	+	+	+	-	+
3	1	+	-	-	-	+	+	+	-
4	1	+	-	+	-	-	-	+	+
5	1	-	+	+	-	+	-	-	-
6	1	+	+	-	+	-	-	-	+
7	1	-	+	+	+	-	+	+	-
8	1	+	+	+	-	+	+	-	+
9	1	+	-	+	+	-	+	-	-
10	1	+	+	-	+	+	-	+	-
11	1	-	-	-	-	-	-	-	-
12	1	-	-	+	+	+	-	+	+

The above tables show the total number of runs for all the input parameters. All the parameters are assigned either positive or negative value for 12 runs. Geometry is edit in Solid Works software Analysis in ANSYS is performed to calculate the response of input parameters on desired outputs. Figure 4.3 shows the output value

screen on Placket Burman model designed input parameters. A fixed input voltage of 3V is applied for all simulations.

	C1	C2	C3	C4	C5-T	C6-T	C7-T	C8-T	C9-T	C10-T	C11-T	C12-T
	StdOrder	RunOrder	PtType	Blocks	X1	X2	X3	X4	X5	X6	X7	X8
1	11	1	1	1	240	12	95	140	6	80	8	71
2	9	2	1	1	240	8	95	144	8	80	6	71
3	10	3	1	1	265	8	95	140	8	80	8	69
4	1	4	1	1	265	8	100	140	6	75	8	71
5	3	5	1	1	240	12	100	140	8	75	6	69
6	2	6	1	1	265	12	95	144	6	75	6	71
7	7	7	1	1	240	12	100	144	6	80	8	69
8	6	8	1	1	265	12	100	140	8	80	6	71
9	4	9	1	1	265	8	100	144	6	80	6	69
10	5	10	1	1	265	12	95	144	8	75	8	69
11	12	11	1	1	240	8	95	140	6	75	6	69
12	8	12	1	1	240	8	100	144	8	75	8	71

Figure 4.3: High and low values of placket Burman model.

	C1	C2	C3	C4	C5-T	C6-T	C7-T	C8-T	C9-T	C10-T	C11-T	C12-T	C13	C14	C15	C16
	StdOrder	RunOrder	PtType	Blocks	X1	X2	X3	X4	X5	X6	X7	X8	Displacement	Temperature	FOM	Power
1	12	1	1	1	240	8	180	140	6	75	6	69	0.34	43	0.43	0.45
2	6	2	1	1	250	12	190	140	8	80	6	71	0.76	57	0.57	0.98
3	7	3	1	1	240	12	190	144	6	80	8	69	0.90	98	0.98	0.71
4	3	4	1	1	240	12	190	140	8	75	6	69	0.66	44	0.44	0.31
5	8	5	1	1	240	8	190	144	8	75	8	71	0.87	36	0.35	0.34
6	2	6	1	1	250	12	180	144	6	75	6	71	0.23	27	0.37	0.84
7	10	7	1	1	250	8	180	140	8	80	8	69	0.65	45	0.65	0.15
8	11	8	1	1	240	12	180	140	6	80	8	71	0.89	65	0.98	0.67
9	5	9	1	1	250	12	180	144	8	75	8	69	0.45	23	0.54	0.42
10	9	10	1	1	240	8	180	144	8	80	6	71	0.34	22	0.43	0.70
11	1	11	1	1	250	8	190	140	6	75	8	71	0.76	87	0.76	0.45
12	4	12	1	1	250	8	190	144	6	80	6	69	0.33	54	0.33	0.22

Figure 4.4: Output response value screening of Minitab software

4.1.3 Analysis of Variance

The output results obtained from analysis of ANSYS can be defined by following linear statistical model

$$y_{ij} = u_i + \varepsilon_{ij} \begin{cases} i = 1, 2, 3, \ldots . a \\ j = 1, 2, 3, \ldots . n \end{cases} \qquad (4.2)$$

where y is the response value of ij value, n is the no of times design factors appear in design matrix. The value of P factor should be greater than 0.05 which shows the verification of basic ANNOVA assumptions. Analysis of variance is a design model which counters the input parameters to analyze the effect of design factors on specific output. Overall variation in output response is calculated by total means of variance SS_T. The total mean of variance is a combination of total sum of squares and variable sun of squares.

$$SS_T = SS_A + SS_E \quad (4.3)$$

4.1.3.1 Analysis of displacement

Analysis of variance of displacement shows that SL, SP, IHL and HAW are the most significant factors which causes significant effects on output as their p values are less than 0.05

Table 4.5: Analysis of variance for displacement

Source	DF	Adj SS	Adj MS	F-Value	P-Value
Model	8	0.661867	0.082733	25.07	0.011
Linear	8	0.661867	0.082733	25.07	0.011
X1	1	0.056033	0.056033	16.98	0.026
X2	1	0.030000	0.030000	9.09	0.057
X3	1	0.158700	0.158700	48.09	0.006
X4	1	0.073633	0.073633	22.31	0.018
X5	1	0.006533	0.006533	1.98	0.254
X6	1	0.026133	0.026133	7.92	0.067
X7	1	0.288300	0.288300	87.36	0.003
X8	1	0.022533	0.022533	6.83	0.079
Error	3	0.009900	0.003300		
Total	11	0.671767			

4.1.3.2 Analysis of Temperature

Analysis of variance of displacement shows that SP and FW are the most significant factors which causes significant effects on output as their p values are less than 0.05.

Table 4.6: Analysis of variance for temperature

Source	DF	Adj SS	Adj MS	F-Value	P-Value
Model	8	5842.00	730.25	4.67	0.116
Linear	8	5842.00	730.25	4.67	0.116
X1	1	18.75	18.75	0.12	0.752
X2	1	60.75	60.75	0.39	0.577
X3	1	1900.08	1900.08	12.16	0.040
X4	1	546.75	546.75	3.50	0.158
X5	1	1800.75	1800.75	11.52	0.043
X6	1	546.75	546.75	3.50	0.158
X7	1	954.08	954.08	6.10	0.090
X8	1	14.08	14.08	0.09	0.784
Error	3	468.92	156.31		
Total	11	6310.92			

4.1.3.3 Analysis of Input Power

Analysis of variance of displacement shows that there is no significant effect if input parameter on output as their p values is not than 0.05

Table 4.7: Analysis of variance for power input

Source	DF	Adj SS	Adj MS	F-Value	P-Value
Model	8	0.023600	0.002950	1.74	0.353
Linear	8	0.023600	0.002950	1.74	0.353
X1	1	0.003675	0.003675	2.17	0.238
X2	1	0.000408	0.000408	0.24	0.657
X3	1	0.002408	0.002408	1.42	0.319
X4	1	0.001408	0.001408	0.83	0.429
X5	1	0.005208	0.005208	3.07	0.178
X6	1	0.000208	0.000208	0.12	0.749
X7	1	0.010208	0.010208	6.01	0.091
X8	1	0.000075	0.000075	0.04	0.847
Error	3	0.005092	0.001697		
Total	11	0.028692			

4.1.4 Half Normal and Pareto Plot

Results obtained from ANNOVA are further tested and verified by using half normal and pareto charts. The pareto and half normal charts are used to verify the assumed input parameters with zero error terms. The pareto plot shows the most significant input factors effecting the output in histogram form. It shows ordered frequency for input parameters. Pareto plots differentiates between important input and unimportant factors. Standardization of Displacement

Half normal and pareto charts of displacement shows that SL, SP, IHL and HAW are the most significant factors which causes significant effects on output.

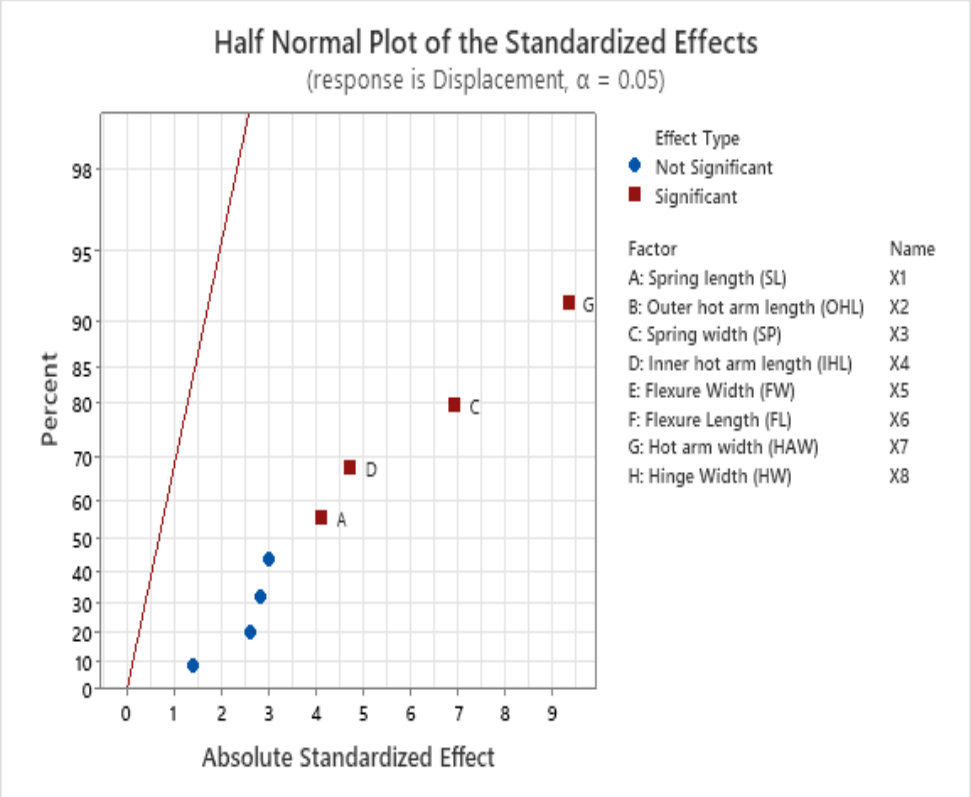

Figure 4.5: Half Normal probability plot showing most significant input factors for displacement.

Pareto plots differentiates between important input and unimportant factors. Pareto chart shows vertical bars with highest value showing most important input factor at highest and other bars with decreasing length. Pareto chart shows similarity with histograms but bins in pareto charts are arranged from high frequency to low frequency.

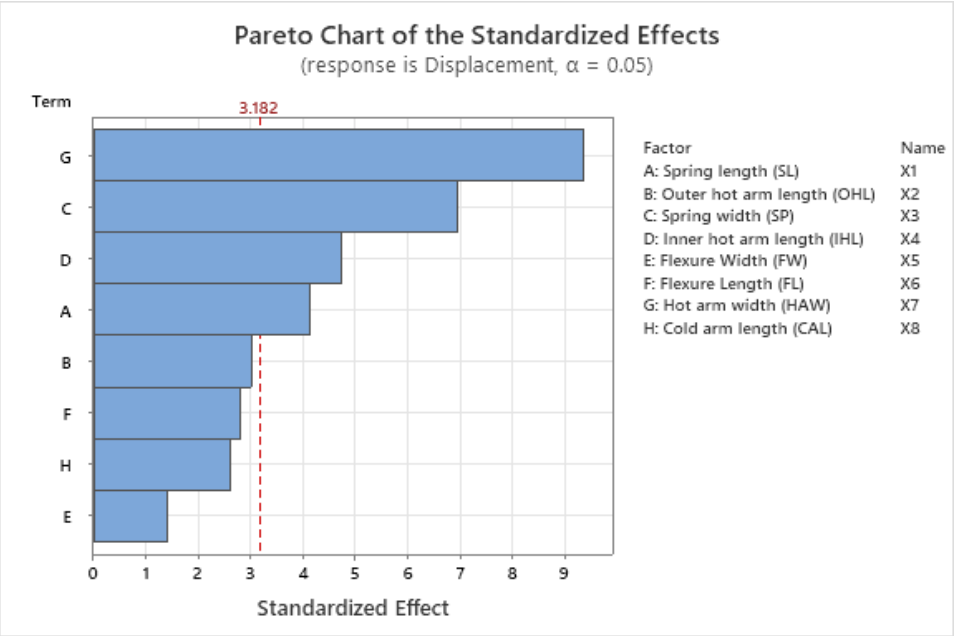

Figure 4.6: Pareto chart showing significant factors for displacement.

4.1.4.1 Standardization of Temperature

Half normal and pareto charts of temperature shows that SP and FW are the most significant factors which causes significant effects on output.

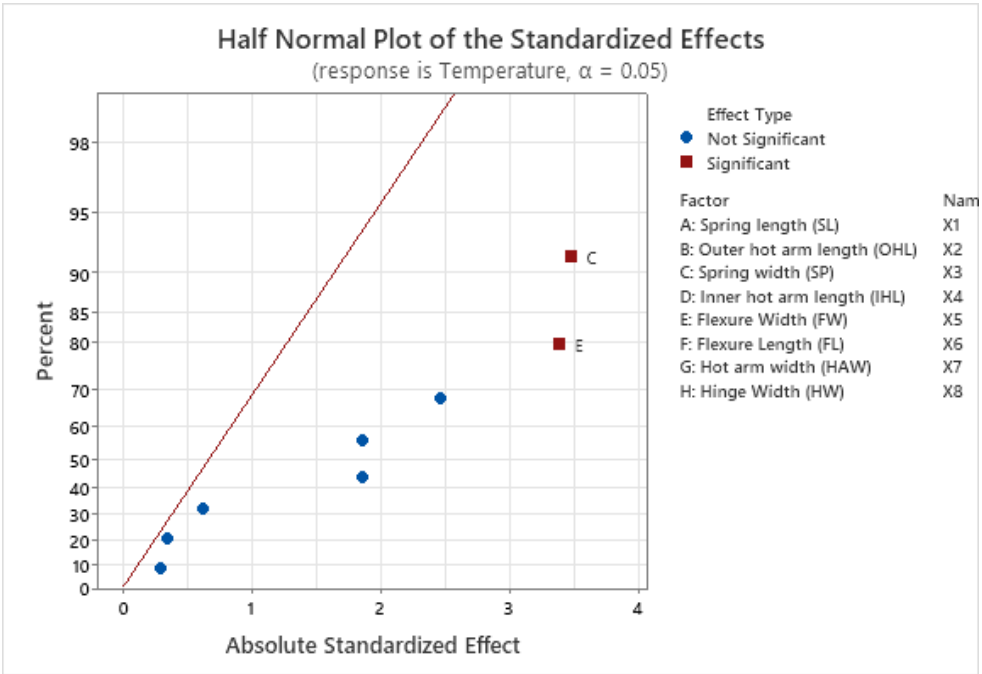

Figure 4.7: Half Normal probability plot showing significant input factors of temperature.

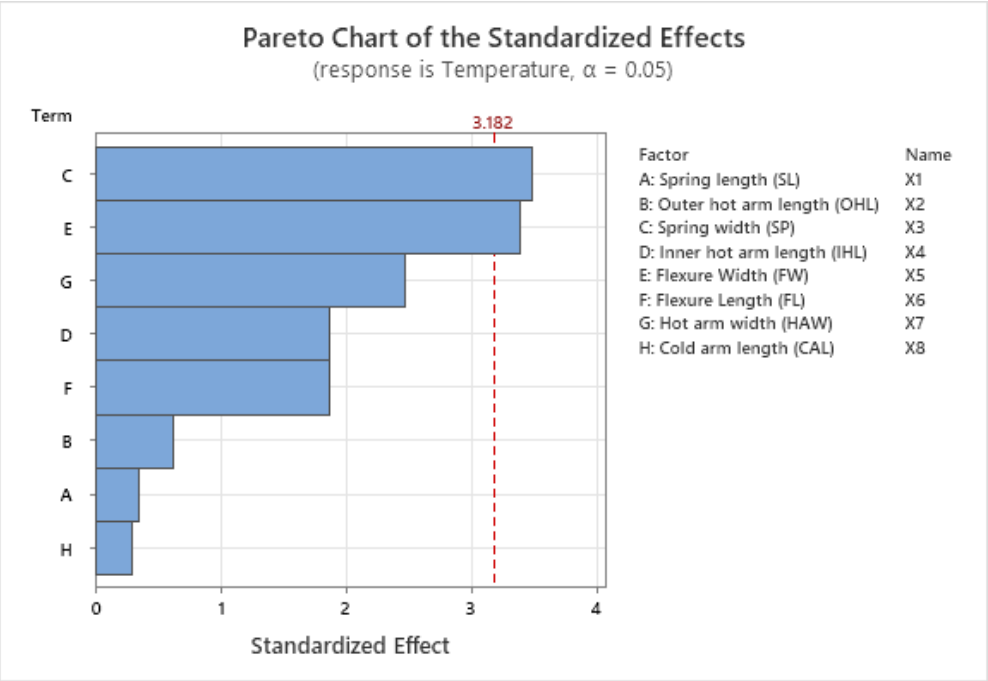

Figure 4.8: Pareto chart showing significant factors for temperature.

4.1.4.2 Standardization of Input Power

Half normal and pareto charts of input power shows that there is no significant factors which causes significant effects on output.

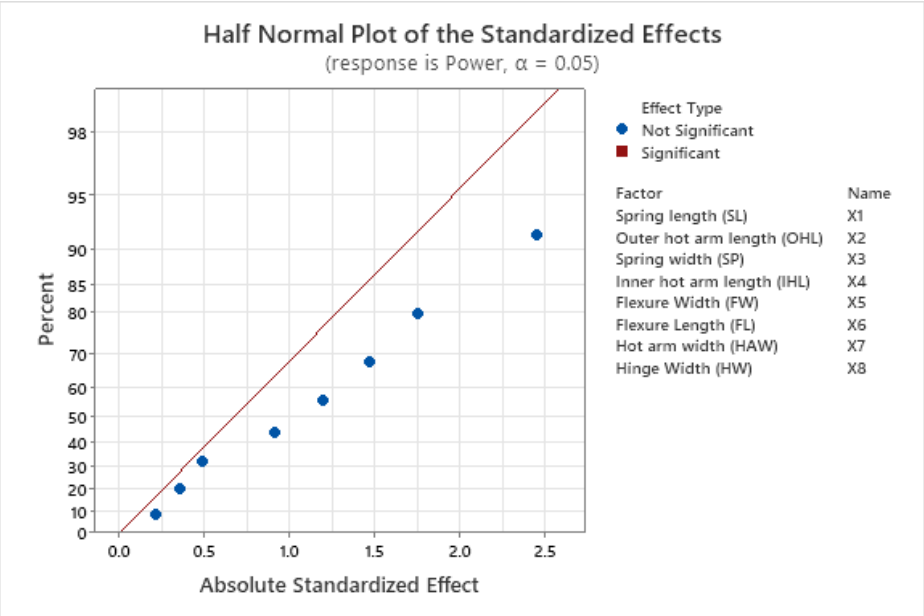

Figure 4.9: Half Normal probability plot showing most significant input factors for input power.

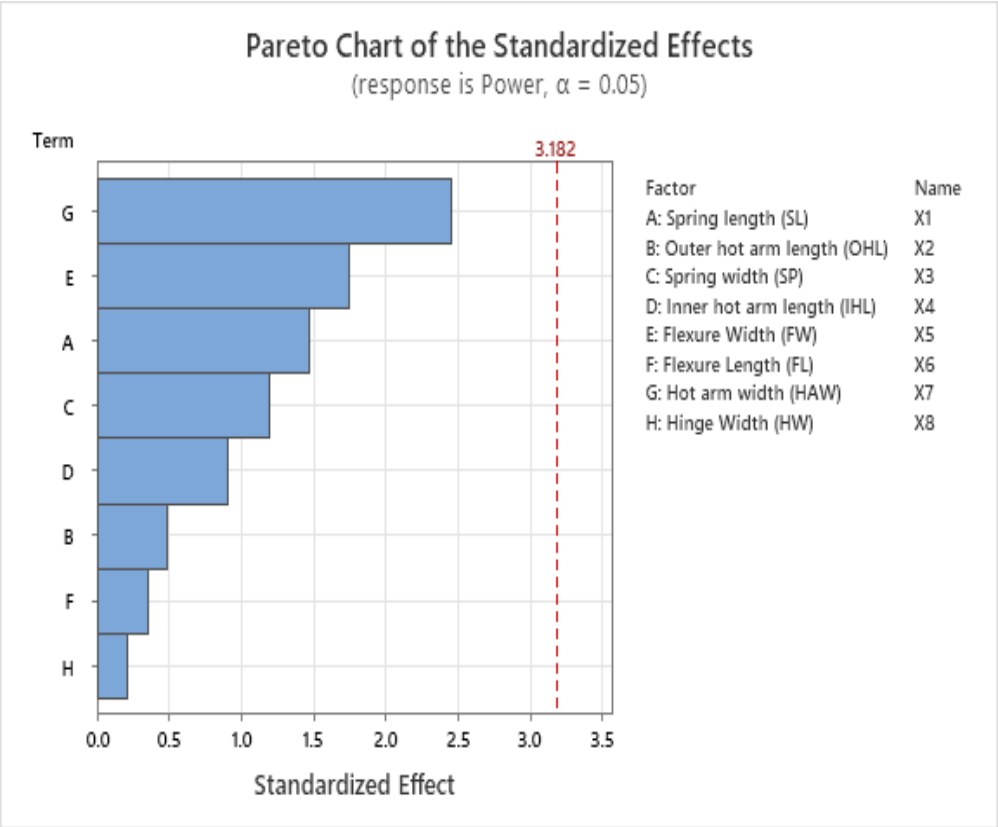

Figure 4.10: Pareto chart showing significant factors for input power.

The usual behavior in graphical figures. Of half normal and pareto analysis of temperature and input power can be attributed to error in the boundary conditions and meshing in the simulation software.

4.1.5 Main Effect Plots

Main effect plot shows the significant value of output factors on every single input point. This plot is usually used to check the strength of experiment. Multiple input parameters effecting output parameter can be calculated by this plot. The graph shows the mean effect of input variable with influence of other variables like error values as well. If the graph shows horizontal line than it means that there is no mean effect and if the graph shows non horizontal line than it means, there is mean effect of parameters. The mean effect is not similar for all factors. Mean effect plots significant input factors that are causing highest impact on output factors. In Minitab software click ANNOVA and select main effect plots for mean calculation. Figure 4.11 shows that spring width, hot arm width, spring width and inner hot arm length causes significant impact on output parameters.

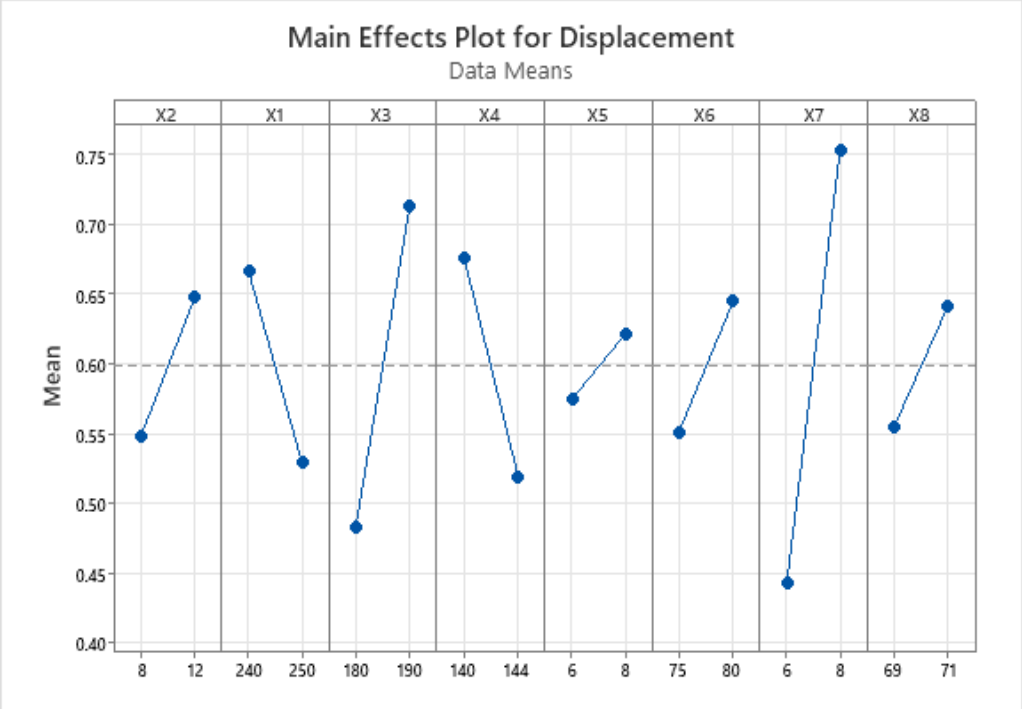

Figure 4.11: Mean effect plot for displacement showing significant input parameters

Similarly figure 4.12 shows that flexure width and spring width causes a significant change in temperature rise in plate.

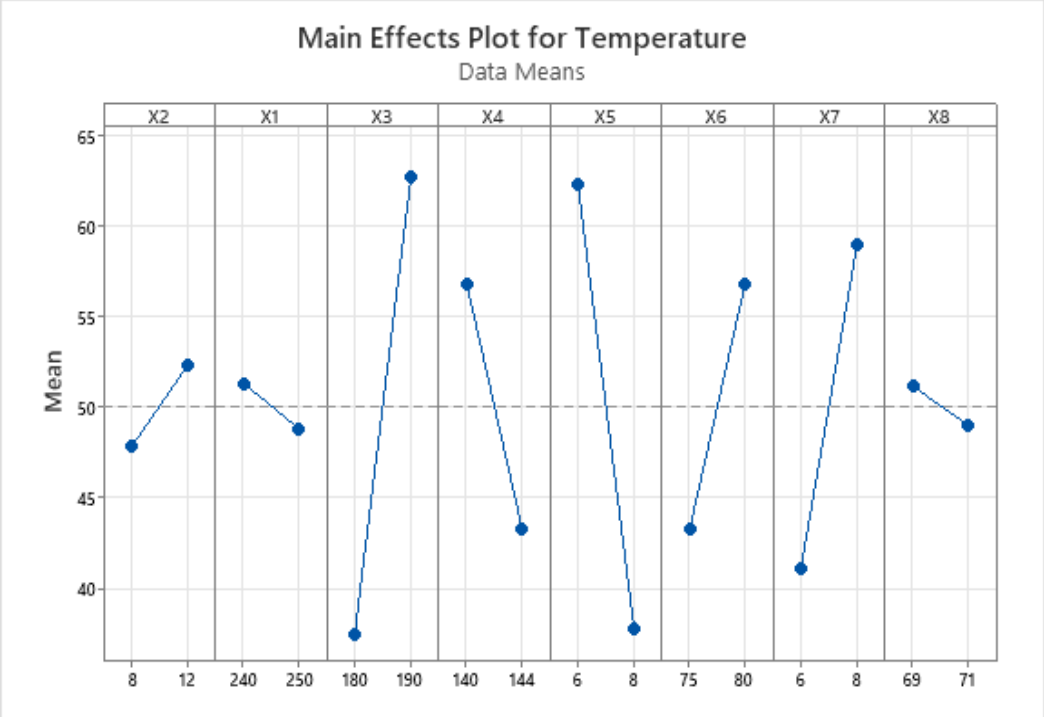

Figure 4.12: Mean effect plot for Temperature showing significant input parameters

Figure 4.13 shows that there is no input parameter which causes significant effect on output parameters.

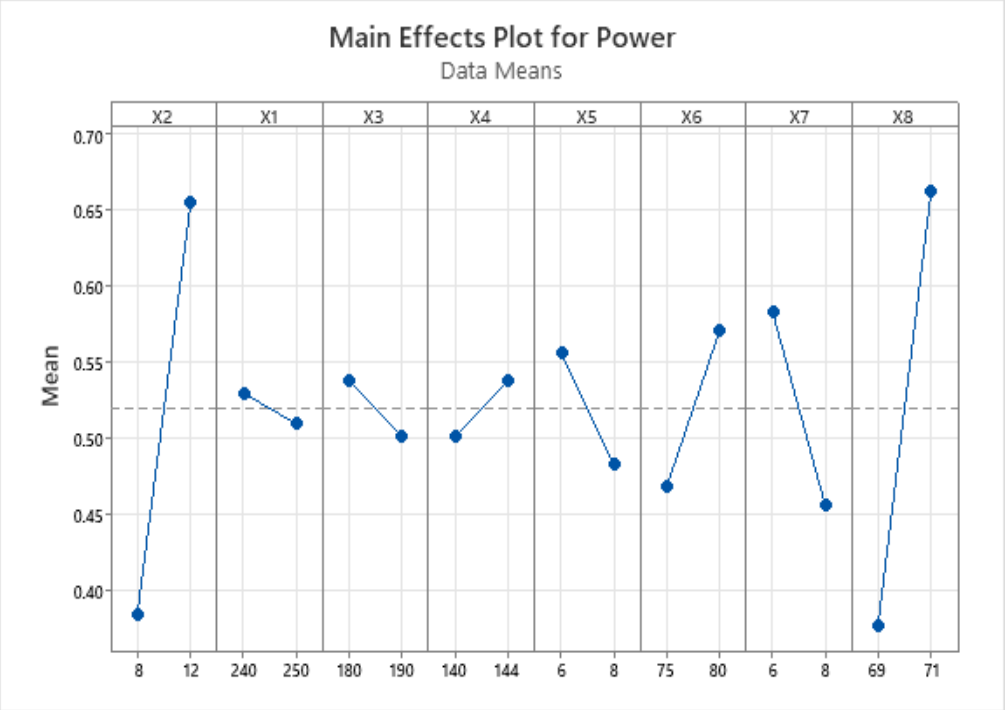

Figure 4.13: Mean effect plot for input power showing significant input parameters

4.2 Optimization by ANSYS

Optimization can be performed by using ANSYS software. ANSYS AIM 17.1 is used for optimization technique of this design. All the input parameters which need to be optimize are parameterize in space claim. After analysis output parameters are also parameterize. Data is entered while changing the input parameters while keeping the constraints in mind. Input values are varied in base points. When we parameterize the input and output values an option of parameterization appears in ANSYS study. By clicking that option parameterization data window will appear. The software will change the geometry according to input data in space claim. Then meshing process occurs and after meshing physics of geometry is solved. Ansys will calculate all the results and show them in table format. We can export the data in excel file to see which input parameters show significant changes in output. All the data is exported in excel file. The first row shows the best optimum values of input

parameters against output i-e maximum displacement, minimum input power and minimum temperature.

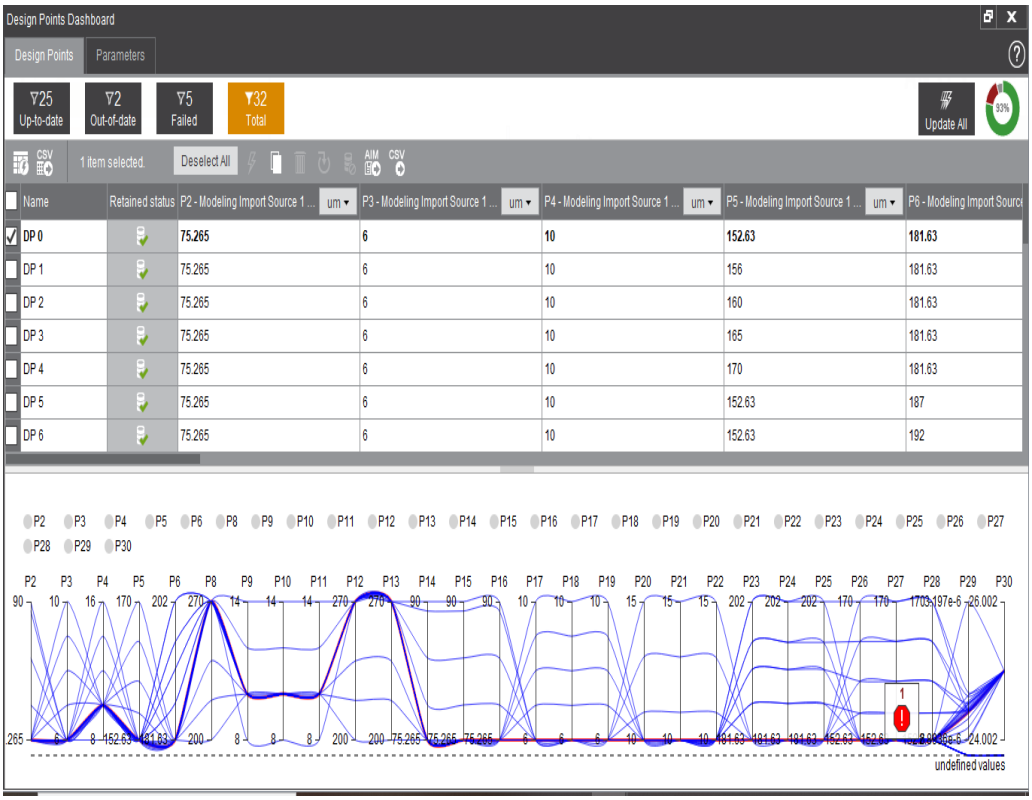

Figure 4.14: Optimization of micromirror using ANSYS.

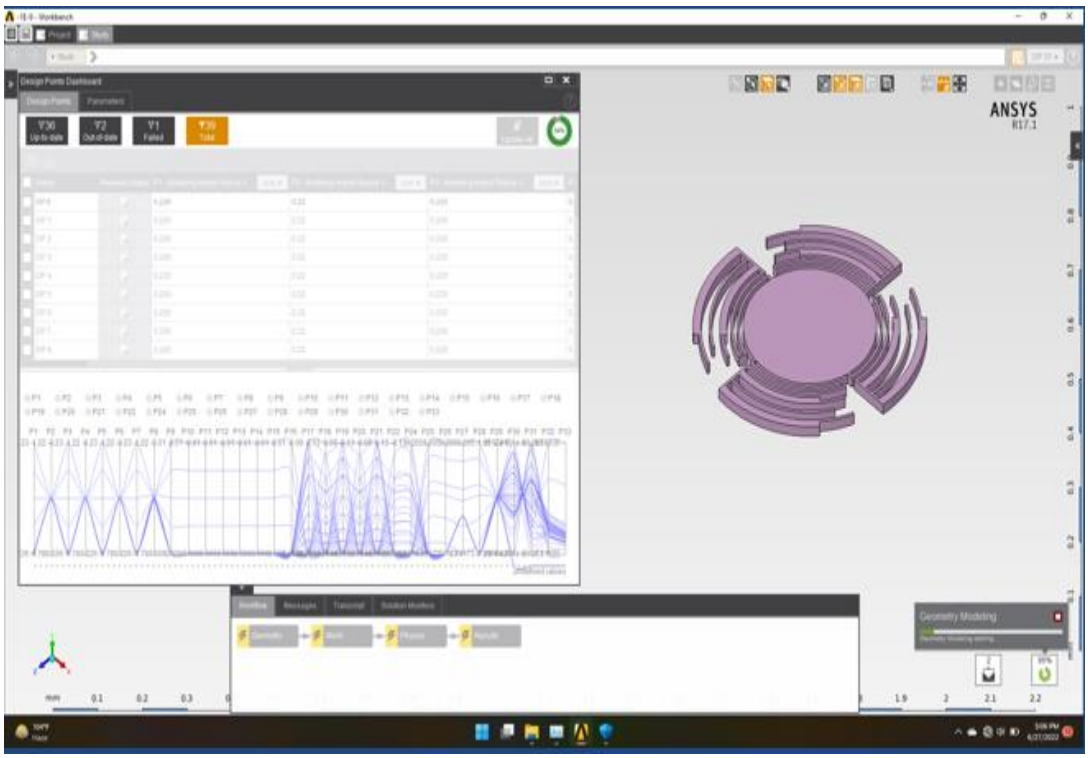

Figure 4.15: ANSYS screen showing optimization process.

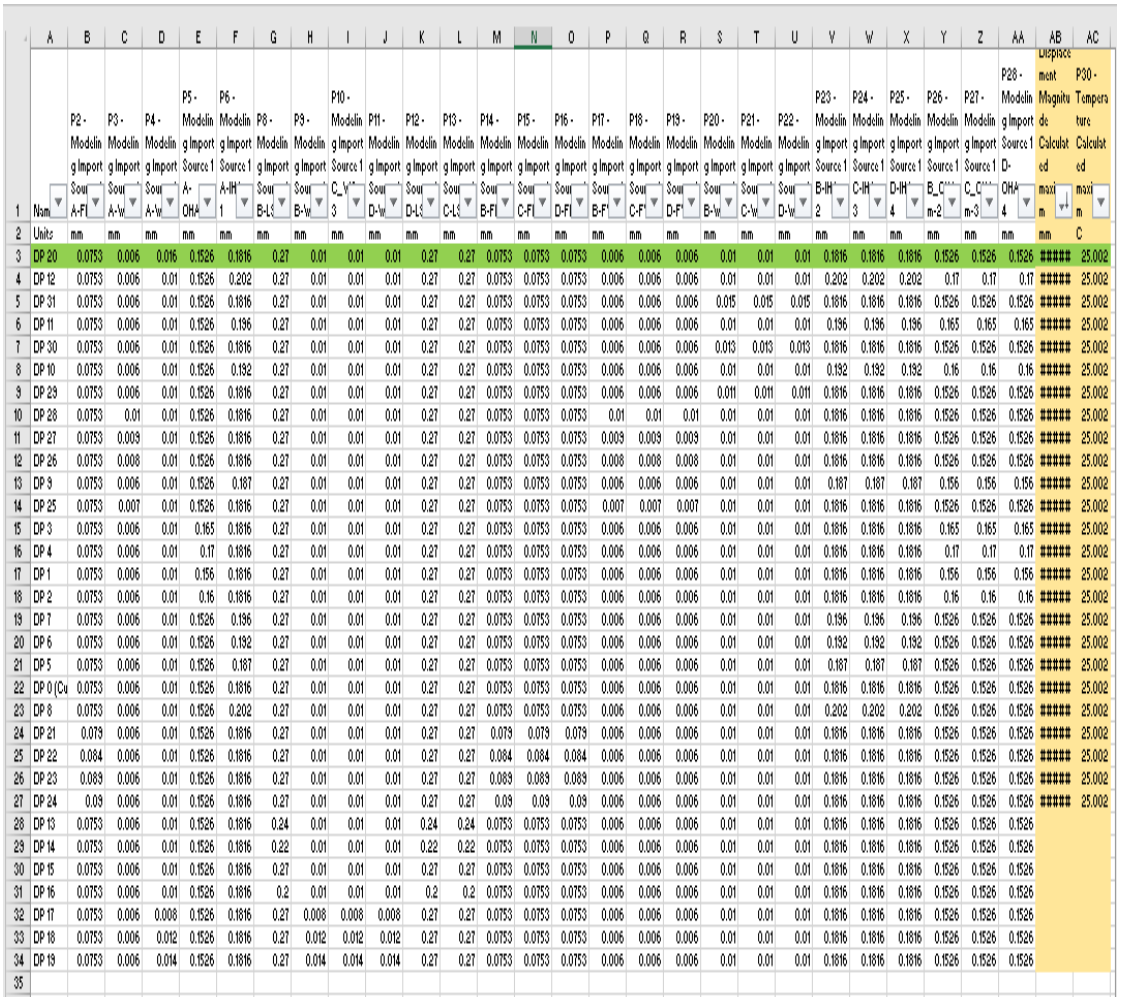

	A	B	C	D	E	F	G	H	I	J	K	L	M	N	O	P	Q	R	S	T	U	V	W	X	Y	Z	AA	AB	AC
1	Nam	P2 - Modelin g Import Sour A-Fl	P3 - Modelin g Import Sour A-W	P4 - Modelin g Import Sour A-W	P5 - Modelin g Import Source 1 A-OHA	P6 - Modelin g Import Source 1 A-IH 1	P8 - Modelin g Import Sour B-L	P9 - Modelin g Import Sour B-W	P10 - Modelin g Import Source 1 C_V 3	P11 - Modelin g Import Sour D-W	P12 - Modelin g Import Sour D-L	P13 - Modelin g Import Sour C-L	P14 - Modelin g Import Sour B-Fl	P15 - Modelin g Import Sour C-Fl	P16 - Modelin g Import Sour D-Fl	P17 - Modelin g Import Sour B-F	P18 - Modelin g Import Sour C-F	P19 - Modelin g Import Sour D-F	P20 - Modelin g Import Sour B-W	P21 - Modelin g Import Sour C-W	P22 - Modelin g Import Sour D-W	P23 - Modelin g Import Source 1 B-IH 2	P24 - Modelin g Import Source 1 C-IH 3	P25 - Modelin g Import Source 1 D-IH 4	P26 - Modelin g Import Source 1 B_C m-2	P27 - Modelin g Import Source 1 C_C m-3	P28 - Modelin g Import Source 1 D-OHA 4	Displace ment Magnitu de Calculat ed maxi m	P30 - Tempera ture Calculat ed maxi m
2	Units	mm	mm	mm	mm	mm	mm	mm	mm	mm	mm	mm	mm	mm	mm	mm	mm	mm	mm	mm	mm	mm	mm	mm	mm	mm	mm	mm	C
3	DP 20	0.0753	0.006	0.016	0.1526	0.1816	0.27	0.01	0.01	0.01	0.27	0.27	0.0753	0.0753	0.0753	0.006	0.006	0.006	0.01	0.01	0.01	0.1816	0.1816	0.1816	0.1526	0.1526	0.1526	#####	25.002
4	DP 12	0.0753	0.006	0.01	0.1526	0.202	0.27	0.01	0.01	0.01	0.27	0.27	0.0753	0.0753	0.0753	0.006	0.006	0.006	0.01	0.01	0.01	0.202	0.202	0.202	0.17	0.17	0.17	#####	25.002
5	DP 31	0.0753	0.006	0.01	0.1526	0.1816	0.27	0.01	0.01	0.01	0.27	0.27	0.0753	0.0753	0.0753	0.006	0.006	0.006	0.015	0.015	0.015	0.1816	0.1816	0.1816	0.1526	0.1526	0.1526	#####	25.002
6	DP 11	0.0753	0.006	0.01	0.1526	0.196	0.27	0.01	0.01	0.01	0.27	0.27	0.0753	0.0753	0.0753	0.006	0.006	0.006	0.01	0.01	0.01	0.196	0.196	0.196	0.165	0.165	0.165	#####	25.002
7	DP 30	0.0753	0.006	0.01	0.1526	0.1816	0.27	0.01	0.01	0.01	0.27	0.27	0.0753	0.0753	0.0753	0.006	0.006	0.006	0.013	0.013	0.013	0.1816	0.1816	0.1816	0.1526	0.1526	0.1526	#####	25.002
8	DP 10	0.0753	0.006	0.01	0.1526	0.192	0.27	0.01	0.01	0.01	0.27	0.27	0.0753	0.0753	0.0753	0.006	0.006	0.006	0.01	0.01	0.01	0.192	0.192	0.192	0.16	0.16	0.16	#####	25.002
9	DP 29	0.0753	0.006	0.01	0.1526	0.1816	0.27	0.01	0.01	0.01	0.27	0.27	0.0753	0.0753	0.0753	0.006	0.006	0.006	0.011	0.011	0.011	0.1816	0.1816	0.1816	0.1526	0.1526	0.1526	#####	25.002
10	DP 28	0.0753	0.01	0.01	0.1526	0.1816	0.27	0.01	0.01	0.01	0.27	0.27	0.0753	0.0753	0.0753	0.01	0.01	0.01	0.01	0.01	0.01	0.1816	0.1816	0.1816	0.1526	0.1526	0.1526	#####	25.002
11	DP 27	0.0753	0.009	0.01	0.1526	0.1816	0.27	0.01	0.01	0.01	0.27	0.27	0.0753	0.0753	0.0753	0.009	0.009	0.009	0.01	0.01	0.01	0.1816	0.1816	0.1816	0.1526	0.1526	0.1526	#####	25.002
12	DP 26	0.0753	0.008	0.01	0.1526	0.1816	0.27	0.01	0.01	0.01	0.27	0.27	0.0753	0.0753	0.0753	0.008	0.008	0.008	0.01	0.01	0.01	0.1816	0.1816	0.1816	0.1526	0.1526	0.1526	#####	25.002
13	DP 9	0.0753	0.006	0.01	0.1526	0.187	0.27	0.01	0.01	0.01	0.27	0.27	0.0753	0.0753	0.0753	0.006	0.006	0.006	0.01	0.01	0.01	0.187	0.187	0.187	0.156	0.156	0.156	#####	25.002
14	DP 25	0.0753	0.007	0.01	0.1526	0.1816	0.27	0.01	0.01	0.01	0.27	0.27	0.0753	0.0753	0.0753	0.007	0.007	0.007	0.01	0.01	0.01	0.1816	0.1816	0.1816	0.1526	0.1526	0.1526	#####	25.002
15	DP 3	0.0753	0.006	0.01	0.165	0.1816	0.27	0.01	0.01	0.01	0.27	0.27	0.0753	0.0753	0.0753	0.006	0.006	0.006	0.01	0.01	0.01	0.1816	0.1816	0.1816	0.165	0.165	0.165	#####	25.002
16	DP 4	0.0753	0.006	0.01	0.17	0.1816	0.27	0.01	0.01	0.01	0.27	0.27	0.0753	0.0753	0.0753	0.006	0.006	0.006	0.01	0.01	0.01	0.1816	0.1816	0.1816	0.17	0.17	0.17	#####	25.002
17	DP 1	0.0753	0.006	0.01	0.156	0.1816	0.27	0.01	0.01	0.01	0.27	0.27	0.0753	0.0753	0.0753	0.006	0.006	0.006	0.01	0.01	0.01	0.1816	0.1816	0.1816	0.156	0.156	0.156	#####	25.002
18	DP 2	0.0753	0.006	0.01	0.16	0.1816	0.27	0.01	0.01	0.01	0.27	0.27	0.0753	0.0753	0.0753	0.006	0.006	0.006	0.01	0.01	0.01	0.1816	0.1816	0.1816	0.16	0.16	0.16	#####	25.002
19	DP 7	0.0753	0.006	0.01	0.1526	0.196	0.27	0.01	0.01	0.01	0.27	0.27	0.0753	0.0753	0.0753	0.006	0.006	0.006	0.01	0.01	0.01	0.196	0.196	0.196	0.1526	0.1526	0.1526	#####	25.002
20	DP 6	0.0753	0.006	0.01	0.1526	0.192	0.27	0.01	0.01	0.01	0.27	0.27	0.0753	0.0753	0.0753	0.006	0.006	0.006	0.01	0.01	0.01	0.192	0.192	0.192	0.1526	0.1526	0.1526	#####	25.002
21	DP 5	0.0753	0.006	0.01	0.1526	0.187	0.27	0.01	0.01	0.01	0.27	0.27	0.0753	0.0753	0.0753	0.006	0.006	0.006	0.01	0.01	0.01	0.187	0.187	0.187	0.1526	0.1526	0.1526	#####	25.002
22	DP 0 (Cu	0.0753	0.006	0.01	0.1526	0.1816	0.27	0.01	0.01	0.01	0.27	0.27	0.0753	0.0753	0.0753	0.006	0.006	0.006	0.01	0.01	0.01	0.1816	0.1816	0.1816	0.1526	0.1526	0.1526	#####	25.002
23	DP 8	0.0753	0.006	0.01	0.1526	0.202	0.27	0.01	0.01	0.01	0.27	0.27	0.0753	0.0753	0.0753	0.006	0.006	0.006	0.01	0.01	0.01	0.202	0.202	0.202	0.1526	0.1526	0.1526	#####	25.002
24	DP 21	0.079	0.006	0.01	0.1526	0.1816	0.27	0.01	0.01	0.01	0.27	0.27	0.079	0.079	0.079	0.006	0.006	0.006	0.01	0.01	0.01	0.1816	0.1816	0.1816	0.1526	0.1526	0.1526	#####	25.002
25	DP 22	0.084	0.006	0.01	0.1526	0.1816	0.27	0.01	0.01	0.01	0.27	0.27	0.084	0.084	0.084	0.006	0.006	0.006	0.01	0.01	0.01	0.1816	0.1816	0.1816	0.1526	0.1526	0.1526	#####	25.002
26	DP 23	0.089	0.006	0.01	0.1526	0.1816	0.27	0.01	0.01	0.01	0.27	0.27	0.089	0.089	0.089	0.006	0.006	0.006	0.01	0.01	0.01	0.1816	0.1816	0.1816	0.1526	0.1526	0.1526	#####	25.002
27	DP 24	0.09	0.006	0.01	0.1526	0.1816	0.27	0.01	0.01	0.01	0.27	0.27	0.09	0.09	0.09	0.006	0.006	0.006	0.01	0.01	0.01	0.1816	0.1816	0.1816	0.1526	0.1526	0.1526	#####	25.002
28	DP 13	0.0753	0.006	0.01	0.1526	0.1816	0.24	0.01	0.01	0.01	0.24	0.24	0.0753	0.0753	0.0753	0.006	0.006	0.006	0.01	0.01	0.01	0.1816	0.1816	0.1816	0.1526	0.1526	0.1526		
29	DP 14	0.0753	0.006	0.01	0.1526	0.1816	0.22	0.01	0.01	0.01	0.22	0.22	0.0753	0.0753	0.0753	0.006	0.006	0.006	0.01	0.01	0.01	0.1816	0.1816	0.1816	0.1526	0.1526	0.1526		
30	DP 15	0.0753	0.006	0.01	0.1526	0.1816	0.27	0.01	0.01	0.01	0.27	0.27	0.0753	0.0753	0.0753	0.006	0.006	0.006	0.01	0.01	0.01	0.1816	0.1816	0.1816	0.1526	0.1526	0.1526		
31	DP 16	0.0753	0.006	0.01	0.1526	0.1816	0.2	0.01	0.01	0.01	0.2	0.2	0.0753	0.0753	0.0753	0.006	0.006	0.006	0.01	0.01	0.01	0.1816	0.1816	0.1816	0.1526	0.1526	0.1526		
32	DP 17	0.0753	0.006	0.008	0.1526	0.1816	0.27	0.008	0.008	0.008	0.27	0.27	0.0753	0.0753	0.0753	0.006	0.006	0.006	0.01	0.01	0.01	0.1816	0.1816	0.1816	0.1526	0.1526	0.1526		
33	DP 18	0.0753	0.006	0.012	0.1526	0.1816	0.27	0.012	0.012	0.012	0.27	0.27	0.0753	0.0753	0.0753	0.006	0.006	0.006	0.01	0.01	0.01	0.1816	0.1816	0.1816	0.1526	0.1526	0.1526		
34	DP 19	0.0753	0.006	0.014	0.1526	0.1816	0.27	0.014	0.014	0.014	0.27	0.27	0.0753	0.0753	0.0753	0.006	0.006	0.006	0.01	0.01	0.01	0.1816	0.1816	0.1816	0.1526	0.1526	0.1526		
35																													

Figure 4.16: Data of ANSYS optimization results showing displacement and temperature values for different input parameters.

4.3 Analysis of Optimized Design

The output values predicted by ANSYS optimization and by Minitab are tested by using FEM analysis-based simulations. The predict alternations of geometry is replaced in Solid Works. All the changes in input parameters are made using solid works software. After changing geometry, ANSYS analysis is performed by setting the same boundary conditions. Set ambient temperature to be 15 °C. Output results obtained from ANSYS simulations shows the deflection of 0.7 µm at input power of 140 mW, while the mirror temperature remains high 22°C from ambient. Analysis of optimize micro mirror design displacement is shown in figure 4.11. While figure 4.12 shows temperature analysis profile. Different graphs are presented showing variations in displacement and temperature at different input

power values. All the graphs are plotted in excel software while analysis is performed in ANSYS.

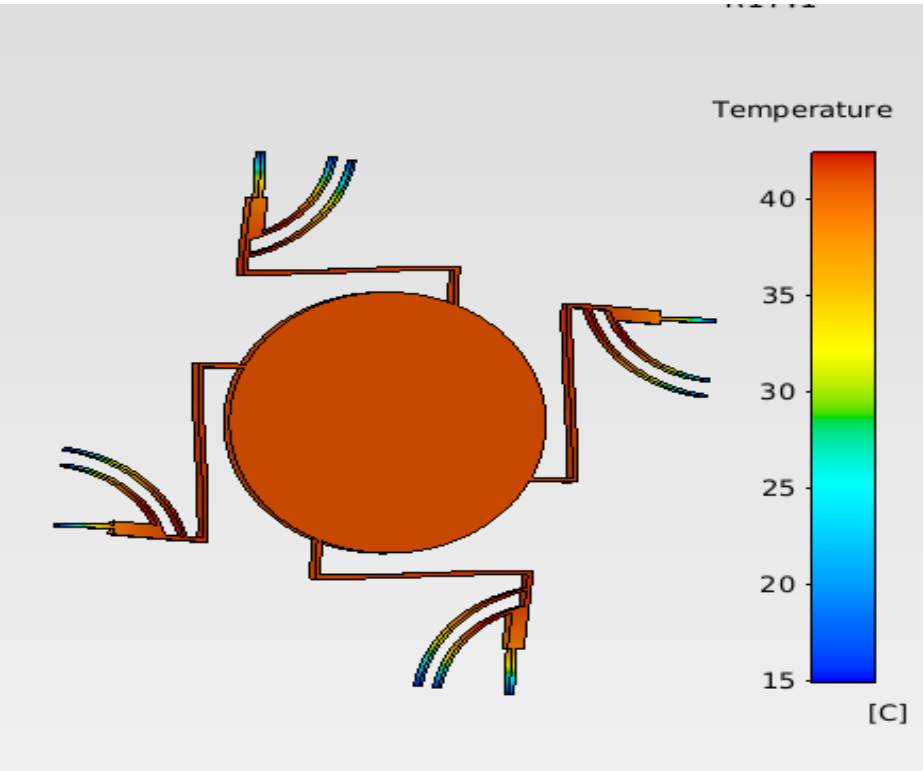

Figure 4.17: Temperature profile of optimized device.

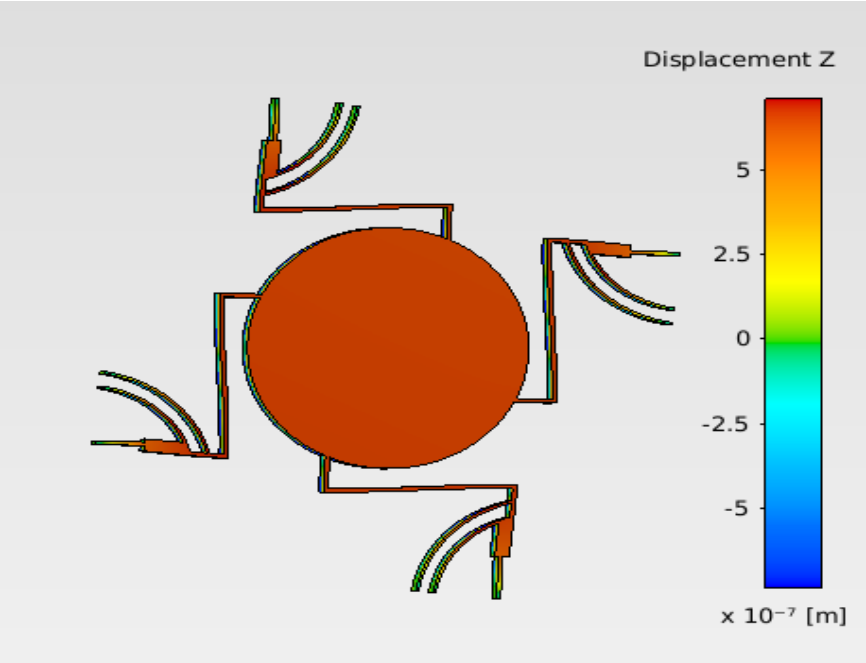

Figure 4.18: Out of plane displacement of optimized device.

Following figure shows displacement, temperature, and power graphs against same applied voltage in between range of 0.2 V to 3.6 V. All the graphs are plotted in excel while data is collected by ANSYS simulations.

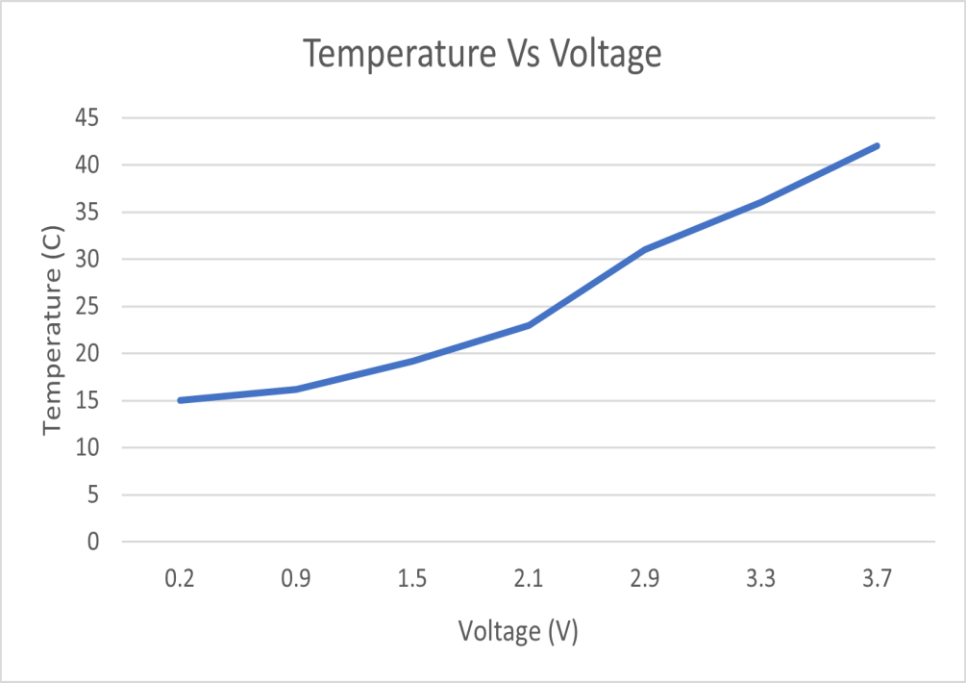

Figure 4.19: Applied voltage vs plate temperature of optimized device.

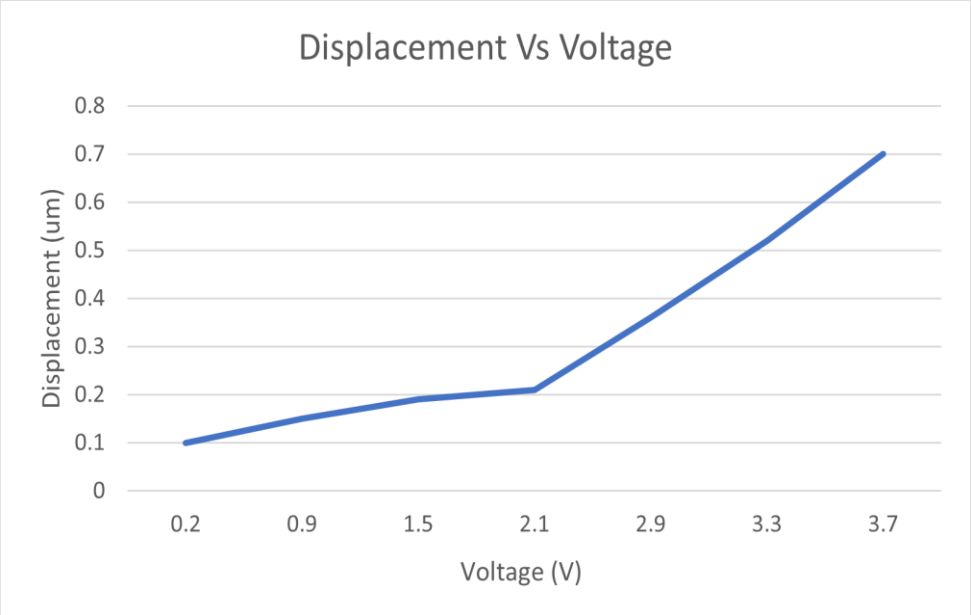

Figure 4.20: Applied voltage vs displacement of optimize design.

4.4 Tilt Angle

Tilt angle is also called as elevation angle. Tilt angle is described as vertical angle of mirror plate. Tilt angle is calculated by right angle triangle. We calculate the right-angle side by ANSYS software, and the base side is known which is 300 μm.

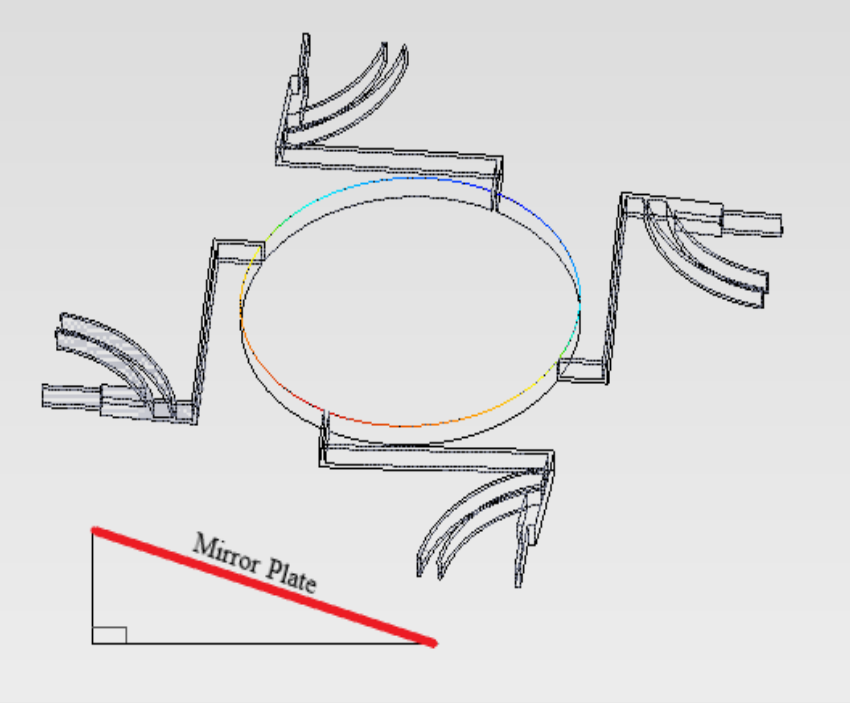

Figure 4.21: Graphical representation of Tilt angle calculations

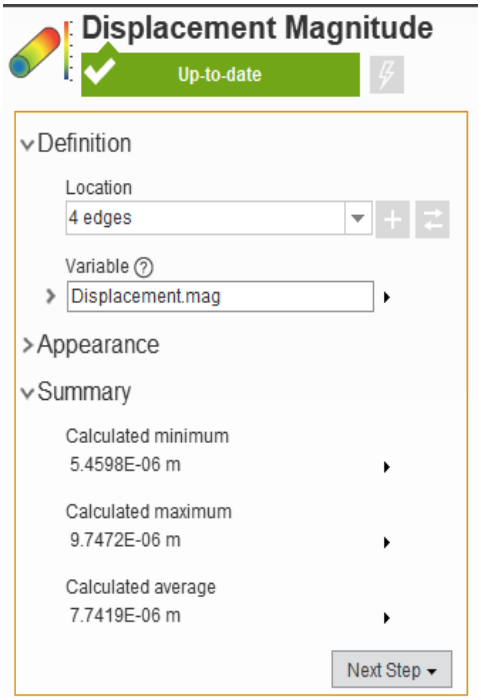

Figure 4.22: Figure shows minimum and maximum displacement of plate.

By Pythagoras Theorem

$$c = \sqrt{a^2 + b^2} \tag{4.4}$$

Given a=4.25 and c=300,

b = 299.96989

$$< a = arcsin(\frac{a}{c}) \tag{4.5}$$

$$< a = \arcsin(\frac{4.25}{299.96})$$

$$< a = 0.812°$$

4.5 Figure of Merit

Figure of merit defines the efficiency of given device. It is the numerical quantity which is based on one or more characteristics of a system which in return measures efficiency as output of that device. By keeping all the constraints and other factors in mind, figure of merit for three output factors is calculated as

$$\text{FOM} = \frac{\text{Displacement (μm)}}{\text{Input Power (mW)} \times \text{Temperature (C)}} \tag{4.6}$$

Following figure shows the figure of merit graph against voltage.

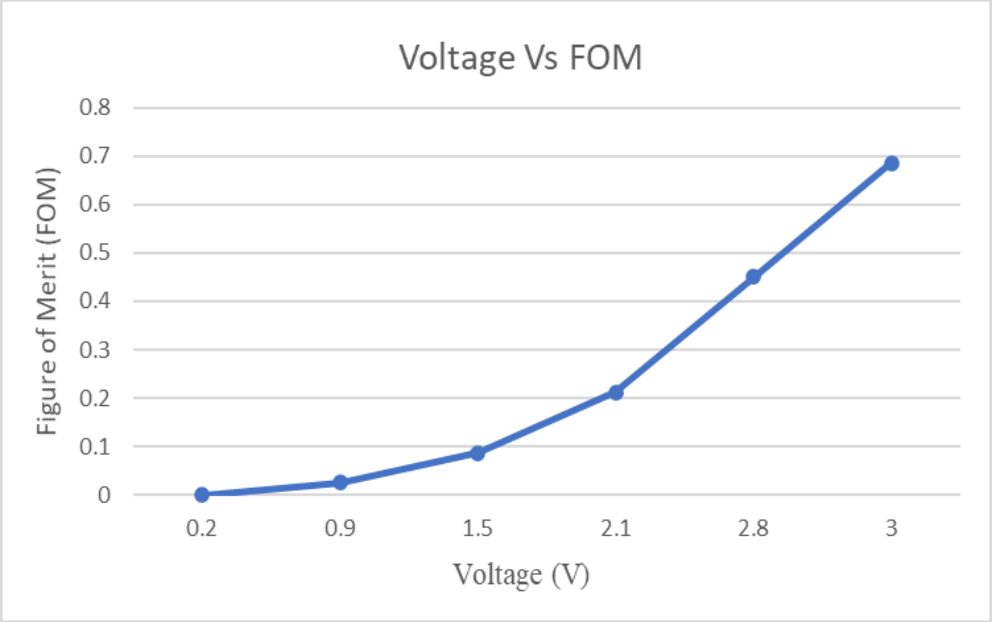

Figure 4.23: Graphical representation of FOM Vs Voltage

The input parameters which need to be maximize are placed in upper side and the parameters which needs to minimize are placed in downside showing inverse relation with FOM. FOM includes all the possible outputs involved in an experiment.

4.6 Comparison with the Literature

The following table represents the output of current designs in comparison with other designs present in literature. The current design for micromirror application is comparable with previous designs present in literature. If compared in terms of size and displacement our design gives more better results. Optimization technique is used to find best optimal solution for output at minimum input power.

Table 4.8: Comparison of current design with literature.

Parameters	This Design	[37]
Dimensions	856 μm × 856 μm	1028 μm × 1028 μm
Displacement	0.7 μm	10.3 μm
Thickness	25 μm	2.25 μm
Temperature	42° C	105° C
Material	Silicon	Polysilicon
Fabrication Process	SOI MUMPS	Sandia Ultra-planar Multi-level MEMS Technology V (SMMMiT)

Chapter 5: Conclusion

In this thesis report, Design and Analysis of MEMS Based Electrothermal Mirrors Using Single Material Micro Actuator is presented. As the name shows, electrothermal actuators are made of single layer of silicon. On application of voltage thermal expansion occurs in electrothermal actuators due to difference in coefficients. This expansion and contraction of actuators moves the mirror plate in tip-tilt or in piston position. The actuators are attached with mirror by flexural springs. Springs are introduced in this design to achieve the maximum deflection and maximum tilt angle. These springs also restricts the high temperature of actuators to reach at mirror plate. Curved geometry is preferred over rectangular geometry due to comparison-based analysis of literature. Multiple designs for micromirror actuation are proposed. After analysis single design was selected due to its large displacement results. Optimization of design is performed using design of experiments technique in Minitab and performing DOE in ANSYS as well. Input parameters are selected and output parameters which need to minimize and maximize are defined. After those changes are made in Solid Works software to change the input parameters according to statistical analysis in Minitab. Simulations are performed in ANSYS workbench to calculate the output parameters at different input parameters. The data of output results are placed in Minitab software. Placket Burman model is used to perform the design of experiments. Pareto and Half Normal Probability plot shows the most significant figures which are affecting output parameters. ANNOVA is used for calculating the mean effect plots. While in ANSYS optimization software itself changes the geometry based on input parameters. Meshing is performed on each design one by one. After meshing physics is performed and results are calculated. All the results are in arranged in table format. The highest row shows the best optimise input parameters giving maximum displacement output at specific voltage. In last a optimise design of micromirror giving maximum displacement at minimum input power is obtained. The mirror can give tip-tilt deflection and in addition piston deflection as well. Final optimise design gives output displacement of 0.7 μm at input power of 140 mW at applied voltage of 3.6V. Tilt angle of 0.8° is achieved at maximum endured temperature of 42°C on micromirror plate.

References

[1] Janak Singh, Terence Gan, Ajay Agarwal, and Saxon Lew, “3D Free-Space Thermally Actuated Micromirror Device,” Sensors and Actuators A: Physical 123 (2005): 468-475.

[2] Xie, Huikai, Yingtian Pan, and Gary K. Fedder, "A SCS CMOS micromirror for optical coherence tomographic imaging," In Micro Electromechanical Systems, 2002. The Fifteenth IEEE International Conference on, IEEE, 2002, pp. 495-498.

[3] Van Kessel, Peter F., Larry J. Hornbeck, Robert E. Meier, and Michael R. Douglass, "A MEMS-based projection display," Proceedings of the IEEE 86, no. 8 (1998): pp. 1687-1704.

[4] Hao, X.; Tanaka, S.; Masuda, A.; Nakamura, J.; Sudoh, K.; Maenaka, K.; Takao, H.; Higuchi, K. Application of silicon on nothing structure for developing a novel capacitive absolute pressure sensor. IEEE Sens. J. **2013**, 14, 808–815.

[5] Bae, B.; Flachsbart, B.R.; Park, K.; Shannon, M.A. Design optimization of a piezoresistive pressure sensor considering the output signal-to-noise ratio. J. Micromech. Microeng. **2004**, 14, 1597–1607.

[6] Sabato, C. Niezrecki and G. Fortino, "Wireless MEMS-based accelerometer sensor boards for structural vibration monitoring: A Review," in *IEEE Sensors Journal*, vol. 17, no. 2, pp. 226-235, 15 Jan.15, 2017, doi: 10.1109/JSEN.2016.2630008.

[7] P. R. Patterson, D. Hah, M. Fujino. W. Piyawattanametha and M. C. Wu, "Scanning micromirrors: an overview," Prac. of SPIE Vol. 5604, 2004, pp. 195-207.

[8] E. M. Abdel-Rahman, M. I. Younis, and A. H. Nayfeh, “Characterization of the mechanical behavior of an electrostaticallyactuated microbeam,” J. Micromech. Microeng., vol. 12, no. 6, pp. 759–766, Nov. 2002.

[9] Alireza Hassanzadeh, “Design considerations for basic MEMS electrostatic actuators”, 978-1-4244-3325-4/09/©2009 IEEE.

[10] N.R. Harris, M. Hill, R. Torah, R. Townsend, S. Beeby, N.M. White, J. Ding," A multilayer thick-film PZT actuator for MEMS applications", Sensors and Actuators A 132 (2006) 311–316.

[11] Isaku Kanno," Piezoelectric MEMS for energy harvesting", Journal of Physics: Conference Series 660 (2015) 012001.

[12] Xingdong Lva, Weiwei Wei, Xu Mao, Yu Chen, Jinling Yang, Fuhua Yanga," A novel MEMS electromagnetic actuator with large displacement", Sensors and Actuators A 221 (2015) 22–28.

[13] Liu, L.; Pal, S.; Xie, H. MEMS mirrors based on a curved concentric electrothermal actuator. Sens. Actuators A Phys. 2012, 188, 349–358.

[14] D. Huang et al., "Optical coherence tomography," (in eng), Science, vol. 254, no. 5035, pp. 1178-81, Nov 22, 1991.

[15] Algamili, A.S., Khir, M.H.M., Dennis, J.O. et al. A Review of Actuation and Sensing Mechanisms in MEMS-Based Sensor Devices. Nanoscale Res Lett 16, 16 (2021).

[16] Huang Q-A, Lee NKS (1999) Analysis and design of polysilicon thermal flexure actuator. J Micromech Microeng 9(1):64

[17] Svili B, Mastropaolo E, Cheung R (2016) Electrothermal actuation of MEMS resonator-based filters with piezoelectric sensing. In: 2016 progress in electromagnetic research symposiμm (PIERS). IEEE, pp 3516–3516.

[18] Ahn, S.H. and Kim, Y.K., 2004. Silicon scanning mirror of two DOF with compensation current routing. Journal of Micromechanics and Microengineering, 14(11), p.1455.

[19] Yang, H.A., Tang, T.L., Lee, S.T. and Fang, W., 2007. A novel coilless scanning mirror using eddy current Lorentz force and magnetostatic force. Journal of microelectromechanical systems, 16(3), pp.511-520.

[20] Yalcinkaya, A.D., Urey, H. and Holmstrom, S., 2007. NiFe plated biaxial MEMS scanner for 2-D imaging. IEEE Photonics Technology Letters, 19(5), pp.330-332.

[21] Yalcinkaya, A.D., Urey, H. and Holmstrom, S., 2007. NiFe plated biaxial MEMS scanner for 2-D imaging. IEEE Photonics Technology Letters, 19(5), pp.330-332.

[22] WEI ZHANG, 1,2 PEI LI, 3 XUEHUA ZHANG, 1,2 YONGJIN WANG, 2 AND FANGREN HU 1,2, 2018 “InGaN/GaN micro mirror with electrostatic comb drive actuation integrated on a patterned silicon-on-insulator wafer” OPTICS EXPRESS 7672

[23] M, Naftali and D. Elata, "Towards a Linear Response of Vertical Comb-Drive Actuators," Technical Report ETR-2004-01. February 2004

[24] Chuan-Hui Ou, Yu-Ching Lin, Yoshiteru Keikoin, Takahito Ono, Masayoshi Esashi4, and Yao-Chuan Tsai1* Two-dimensional MEMS Fe-based metallic glass micromirror driven by an electromagnetic actuator Japanese Journal of Applied Physics 58, SDDL01 (2019)

[25] Fangrong Hua,b, Jun Yao a,*, Chuankai Qiu a, Hao Ren a MEMS micromirror driven by electrostatic force Journal of Electrostatics 68 (2010) 237–242

[26] JIAN SHAO,1 QI LI,1 CHUHUAN FENG,1 WEI LI,1 AND HONGBIN YU1,2, * AlN based piezoelectric micromirror Vol. 43, No. 5 / 1 March 2018 / Optics Letters

[27] V Merea, Vikram Maharshia, Aditia, and Ajay Agarwala, bThermally actuated MEMS micromirror: design aspects (*CSIR-CEERI), Pilani-333031(Raj) India*

[28] Chen, W.-C.; Chu, C.-C.; Hsieh, J.; Fang, W. A reliable single-layer out-of-plane micromachined thermal actuator. Sens. actuators A Phys. 2003, 103, 48–58.

[29] Yang, J.P., Deng, X.C. and Chong, T.C., 2005. An electro-thermal bimorph-based microactuator for precise track-positioning of optical disk drives. Journal of Micromechanics and Microengineering, 15(5), p.958.

[30] Ataka, M., Omodaka, A., Takeshima, N. and Fujita, H., 1993. Fabrication and operation of polyimide bimorph actuators for a ciliary motion system. Journal of Microelectromechanical Systems, 2(4), pp.146-150.

[31] Alissa Potekhina and Changhai Wang"Review of Electrothermal Actuators and Applications" 21 September 2019

[32] Liang Zhou, Xiaoyang Zhang and Huikai Xie "An Electrothermal Cu/W bimorph tip-tilt-piston MEMS mirror with high reliability" published in 14 May 2019.

[33] Liu, R., Wang, H., Li, X., Tang, J., Mao, S. and Ding, G., 2008. Analysis, simulation, and fabrication of MEMS springs for a micro-tensile system. Journal of Micromechanics and Microengineering, 19(1), p.015027.

[34] Liu, L., Pal, S. and Xie, H., 2012. MEMS mirrors based on a curved concentric electrothermal actuator. Sensors and Actuators A: Physical, 188, pp.349-358..

[35] Lin L and Chiao M 1996 Electrothermal response of lineshape microstructures Sensors Actuators A 55 35–41

[36] Comtois J H and Bright V M 1997 Applications for surfacemicromachined polysilicon thermal actuators and arrays Sensors Actuators A 58 19–25

[37] Lara-Castro M, Herrera-Amaya A, Escarola-Rosas MA, Vázquez-Toledo M, López-Huerta F, Aguilera-Cortés LA, Herrera-May AL. Design and modeling of polysilicon electrothermal actuators for a MEMS mirror with low power consμmption. micromachines. 2017; 8(7):203. https://doi.org/10.3390/mi8070203

Completion Certificate

It is certified that the contents of thesis docμment titled "***Design and Analysis of MEMS Based Electrothermal Mirrors Using Single Material Micro Actuator***" submitted by NS Waiqa Amir, Registration No. 00000275640 have been found satisfactory in all respects as per the requirements of Main Office, NUST (Exam branch).

Supervisor:

_____

Dr. Amir Hamza

Date: 4 August 2022